UNIVERSITY OF MANITOBA

LAMINAR FREE CONVECTIVE HEAT TRANSFER FROM AN ISOTHERMAL HORIZONTAL CYLINDER TO WATER NEAR $4^{o}C$

by

Peter J. Weekes

A Thesis

Submitted to the Faculty of Graduate Studies

in Partial Fulfillment of the Requirements for the Degree

of Master of Science

Department of Mechanical Engineering

Winnipeg, Manitoba

August, 1976

"LAMINAR FREE CONVECTIVE HEAT TRANSFER FROM AN ISOTHERMAL HORIZONTAL CYLINDER TO WATER NEAR 4°C"

by

PETER J. WEEKES

A dissertation submitted to the Faculty of Graduate Studies of the University of Manitoba in partial fulfillment of the requirements of the degree of

MASTER OF SCIENCE

ABSTRACT

This thesis is an experimental study of laminar free convective heat transfer from an isothermal cylinder to water near $4^{o}C$. The free convection process in the vicinity of a bulk water temperature of $4^{o}C$ is greatly influenced by the maximum density of water at this temperature. Under certain circumstances, both positive and negative buoyancy forces can exist simultaneously in different parts of the boundary layer. The presence of these two opposing forces complicates both the nature of the flow patterns and the distribution and magnitude of the surface heat fluxes.

Several investigators have studied the general problem of free convection from horizontal cylinders and analytical and empirical models have been constructed to describe this process. Much work has also been done on the melting of ice in different configurations in water near $4^{o}C$, as well as on free convection from vertical flat plates to water in this temperature region. Models have been proposed to describe the nature of the bidirectional flow phenomenon in this area and to locate the boundaries between different flow regions. No such work has been performed for an isothermal horizontal cylinder in water near $4^{o}C$.

The first objective of this experiment was to measure

the local heat fluxes on an isothermal horizontal cylinder in water near $4^{o}C$, for the four different flow regimes which exist in this temperature region. A horizontal cylinder was constructed, with twelve separately controlled heaters mounted around the periphery. By individually adjusting the power to each heater, an isothermal surface could be maintained.

The results of fifty-six tests, performed for a range of surface temperatures from $4.64^{o}C$ to $17.94^{o}C$ and bulk water temperatures from $1.07^{o}C$ to $16.18^{o}C$, verified that the boundaries between different flow regions, defined for a vertical flat plate, applied to the horizontal cylinder problem as well. In addition, the form of the local heat flux distributions, in unidirectional flow regions, coincided with those derived by previous investigators. The nature of the local heat flux distributions in regions of bidirectional flow provided more insight into the complex relationship between the two opposing buoyancy forces in this region.

The second major objective was to try to correlate the average heat transfer results with one or more of the variables of physical importance in the two unidirectional and two bidirectional flow regions. The correlating equations of an earlier experimental investigation were modified to apply to the average heat transfer results from a horizontal cylinder and were fitted to the experimental data of the present work. Although there was a good deal of experimental scatter

in the results, in general, they agreed with the correlations. With the aid of these correlations, accurate estimations of the rates of heat transfer from horizontal cylinders to water can be made in this temperature range.

ACKNOWLEDGEMENTS

I wish to express my profound gratitude to my advisor, Dr. G. K. Yuill for his criticism and guidance throughout the course of this investigation. I am also grateful to the other staff members of the Mechanical Engineering Department as well as to the technical support staff for their assistance and for their many invaluable suggestions and advice.

I would also like to gratefully acknowledge the financial support provided by the Inland Waters Directorate of Environment Canada and by the National Research Council of Canada, which made this study possible.

Finally, I would like to thank my family for their continued encouragement and for their patience during the course of my involvement with this investigation.

TABLE OF CONTENTS

LIST OF FIGURES

LIST OF TABLES

NOMENCLATURE

a	- a constant used by Hermann (Appendix I), dimensionless
A	- constants used by Yuill, $^{o}C^{-1}$ or dimensionless
b	- Langmuir's film diameter, cm.
	- a constant used by Hermann (Appendix I), dimensionless
B	- Langmuir's film thickness for a plane surface, cm.
	- constants used by Yuill, dimensionless, $^{o}C^{-1}$ or $^{o}C^{-2}$
	- buoyancy force per unit mass, cm./sec^2
B^*	- Rice's film thickness for a cylinder, (b-D)/2, cm.
c	- a constant used by Hermann (Appendix I), dimensionless
c_p	- specific heat of a fluid, Joule/gm-^{o}C
C	- various correlating constants, dimensionless
C_I	- a heat transfer constant used in region I, dimensionless
C_{II-N}	- a heat transfer constant used in region II-N, dimensionless
C_{II-S}	- a heat transfer constant used in region II-S, dimensionless
C_{III-IV}	- a heat transfer constant used in regions III and IV, dimensionless
C_i	- a heat transfer constant used in region II-N, dimensionless
C_o	- a heat transfer constant used in region II-S, dimensionless

d - a constant used by Hermann (Appendix I), dimensionless

D - cylinder, wire or sphere diameter, cm.

- constants used by Yuill, dimensionless, $^{o}C^{-1}$ or $^{o}C^{-4}$

$D_{1,2,3}$ - constants in the expression for density (Appendix IV), $^{o}C^{-1,-2,-3}$

E - a constant used by Yuill, $^{o}C^{-1}$

f - Hermann's azimuth function (Appendix I), dimensionless

F - Hermann's azimuth function (Appendix I), dimensionless

- Merk and Prins' azimuth function (Appendix II), dimensionless

- a constant used by Yuill, dimensionless

g - gravitational acceleration, cm/sec^2

- Hermann's azimuth function (Appendix I), dimensionless

g^* - Rayleigh number function (equation 1-22), dimensionless

g_c - gravitational constant, $gm\text{-}cm/N\text{-}sec^2$

g_o - a constant used by Hermann (Appendix I), dimensionless

G - Hermann's azimuth function (Appendix I), dimensionless

- Merk and Prins' azimuth function (Appendix II), dimensionless

- constants used by Yuill, dimensionless, $^{o}C^{-1}$ or $^{o}C^{-3}$

Gr - Grashof number, $g\beta\theta_p D^3/\nu^2$, dimensionless

Gr^* - Grashof number modified by Yuill (equation 1-54 or V-10), dimensionless

Gr' - modified Grashof number used by Dyer, $g\beta\dot{q}D^4/k\nu^2$, dimensionless

- non-Newtonian Grashof number used by Gentry and Wollersheim, $(\rho/\kappa)^2 \cdot D^{n+2} \cdot (g\beta\theta_p)^{2-n}$, dimensionless

h - surface conductance (heat transfer coefficient), $W/cm^2\text{-}^oC$

h_1, h_2, etc. - coefficients used in Merk and Prins' azimuth function (Appendix II), dimensionless

H - Merk and Prins' azimuth function (Appendix II), dimensionless

k - thermal conductivity of fluid, $W/cm\text{-}^oC$

L - length of cylinder or flat plate, cm.

m - an exponent used by Yuill, dimensionless

m_1, m_2 - constants used by Koh, dimensionless

M - Prandtl number function(Appendix II), dimensionless

n - flow behaviour index for non-Newtonian fluids, dimensionless

- an exponent used by Yuill, dimensionless

n_1, n_2 - constants used by Koh and Price, dimensionless

Nu (or $\overline{Nu}$) - average Nusselt number, $\overline{h}D/k$, dimensionless

p - Hermann's velocity function (Appendix I), dimensionless

P - a density function defined by Yuill (Appendix V), dimensionless

$P_{0,1,2,3,4}$ - constants used in the expression for the Prandtl number (Appendix IV), dimensionless, $^oC^{-1,2,3,4}$

Pr - Prandtl number, $\mu c_p/k$, dimensionless

Pr' - Prandtl number for non-Newtonian fluids, $[\rho c_p/k] \cdot [\kappa/\rho]^{2/(n+1)} \cdot D^{(1-n)/(1+n)} \cdot [g\beta\theta_p D]^{3(n-1)/2(n+1)}$, dimensionless

q - Hermann's radial coordinate (Appendix I), dimensionless

$\dot{q}$ - specific heat transfer rate, W/cm^2

Q - a density function defined by Yuill (Appendix V), dimensionless

$\dot{Q}$ - heat transfer rate, Watt

r - radius of cylinder, cm.

Ra - Rayleigh number, Gr:Pr, dimensionless

Re - Reynolds number, uD/ν, dimensionless

R_x - local thermal resistance, $cm^2\text{-}^oC/W$

s - Langmuir's shape factor (equation 1-3), cm.

s_1, s_2, etc. - coefficients in Merk and Prins' sine function (Appendix II), dimensionless

t - Hermann's temperature function (Appendix I), dimensionless

t^* - time required for heated layer to descend (or rise) to level of cylinder (equation 1-46), sec.

T - temperature, ^oC

T_e - equivalent temperature ratio, θ_p/T_∞, dimensionless

u - tangential velocity, cm/sec.

u_1 - Merk and Prins' tangential velocity function (Appendix II), cm/sec.

v - radial velocity, cm/sec.

$V_{1,2,3}$ - constants used in the expression for dynamic viscosity (Appendix IV), $^oC^{-1,-2,-3}$

W - width of tank in the plane normal to the longitudinal axis of the cylinder (Figure 4b), cm.

x - tangential coordinate, cm.

y - radial coordinate, cm.

Y - distance from the centerline of the cylinder to the free surface (Figure 4b), cm.

Z - Yuill's buoyancy function, α - 0.02825, dimensionless

GREEK SYMBOLS

α - thermal diffusivity of fluid, cm^2/sec.

- Yuill's buoyancy function (Appendix V), dimensionless

β - thermal expansion coefficient, $^oC^{-1}$

γ - a constant used by Hermann (Appendix I), dimensionless

- Yuill's angle of rotation, radians

δ - boundary layer thickness, cm.

ε - a constant used by Hermann (Appendix I), dimensionless

ζ - stream function, dimensionless

η - radial coordinate, dimensionless

θ - temperature difference, $T - T_\infty$, ^oC

κ - specific heat ratio for a gas, dimensionless

- consistency index for non-Newtonian fluids, $gm/cm\text{-}sec^{2-n}$

λ - mean free path of a gas, cm.

μ - dynamic (or absolute) viscosity, gm/cm-sec.

ν - kinematic viscosity of a fluid, cm^2/sec.

ξ - tangential coordinate, x/r, dimensionless

- angle, degrees

ρ - density, gm/cm^3

σ - root mean square deviation, varying dimensions

- accommodation coefficient for a gas, dimensionless

Σ - non-dimensional point in the boundary layer where $\rho = \rho_\infty$, dimensionless

τ - shear stress, N/cm^2

- temperature function, θ/θ_p, dimensionless

ϕ - Langmuir's conductivity function (equation 1-2), W/cm.

- Yuill's temperature function, ^oC

Φ - Madden and Piret's heat transfer function (equation 1-25), dimensionless

ψ - stream function, cm^2/sec.

ω - Hermann's tangential coordinate (Appendix I), dimensionless

Ω - point in the boundary layer where $\rho = \rho_\infty$, cm.

SUBSCRIPTS AND SUPERSCRIPTS

crit. - at the point of transition to turbulence

D - evaluated for a cylinder of diameter D

f - evaluated at the film temperature

i	- evaluated at the film temperature of the inner boundary layer(or ΔT across inner boundary layer)
k	- evaluated at the absolute temperature (^{o}K)
L	- evaluated for a plate of length L
o	- evaluated at the film temperature of the outer boundary layer(or ΔT across outer boundary layer)
	- evaluated at $\xi = 0$
p	- evaluated at the surface temperature(except c_p)
r	- evaluated using r (instead of D)
x	- evaluated using x (instead of D or L)
δ	- evaluated using δ (instead of x or D or L)
η	- differentiation with respect to η
ξ	- differentiation with respect to ξ
Σ	- evaluated at $\eta = \Sigma$
Ω	- evaluated at $y = \Omega$
∞	- evaluated at the temperature of the bulk fluid
$\bar{}$	- average value of a property
'	- denotes differentiation (except for Gr'and Pr')

CHAPTER 1

INTRODUCTION

1.1 Introduction to the Problem

The density of most fluids decreases with temperature in a linear manner. However, four fluids, water, antimony, gallium and bismuth exhibit a density anomaly. They all possess a maximum density at some temperature above their freezing points. In the particular case of water, which is the most abundant liquid on this planet, the maximum density occurs at $4^{o}C$.

Fluid flows which are primarily a result of forced convection are not affected to any great extent by this density phenomenon, since density gradients are relatively unimportant. Free convective flows are initiated and maintained by density differences within the fluid. Hence, the peculiar density distribution of water is bound to have a significant effect both on the nature of the flow pattern and on the magnitude of the free convection heat transfer in this region.

The temperature at which the maximum density occurs may not, at first, seem to be significant but it must be remembered that in moderate to high latitudes, all natural bodies of water pass through this temperature twice yearly. With the advent of arctic and sub-arctic resource develop-

ment, any process which occurs in a body of water may be close to this temperature for the entire year. For example, heat transfer from heated underwater pipelines will be greatly influenced by this phenomenon. Since the horizontal cylinder is a common engineering configuration, it is important to increase our knowledge of various aspects of free convection heat transfer from isothermal horizontal cylinders to water near $4^{o}C$.

1.2 Description of the Phenomenon

The effect of the density gradient on the flow regimes about a flat plate has been studied previously. Vanier [43] solved the differential equations for the flow field in the regions where similarity solutions were valid. Yuill [48] extended this analysis both analytically and experimentally to include the entire range of temperatures. The flow field around a horizontal cylinder was not expected to be radically different, especially for a large radius cylinder.

The map of different modes of free convective flow, shown in Figure 1, resulted from these analyses. It clearly shows regions of pure downflow, bidirectional flow and pure upflow. With the bulk temperature at $0^{o}C$, the zones may be physically interpreted as follows. For a surface temperature between $0^{o}C$ and $8^{o}C$, the heated fluid in the boundary layer

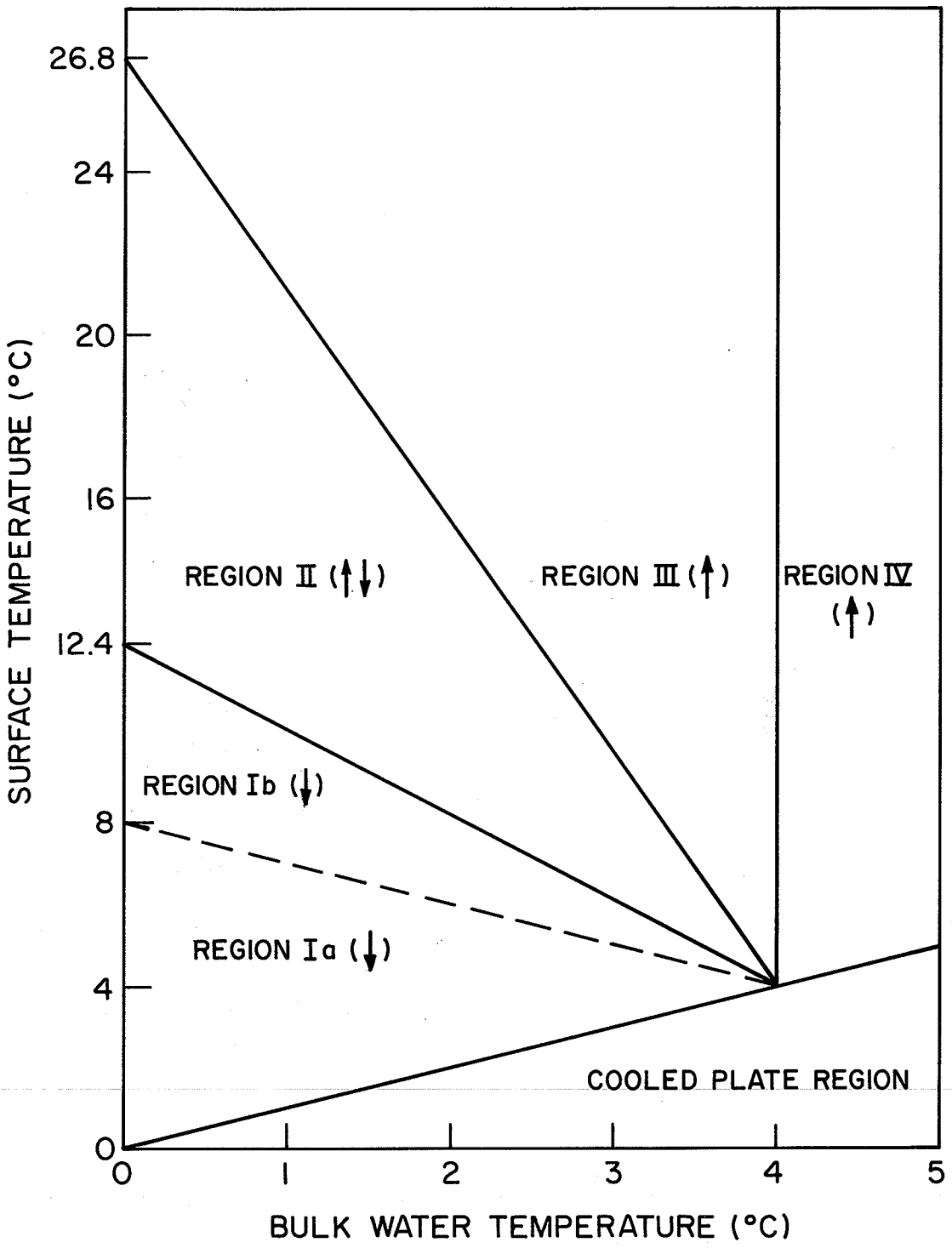

Fig. 1. Map of Free Convection Zones in Low Temperature Water.

is denser than the bulk fluid and descends. Between $8^{o}C$ and $12.4^{o}C$, the fluid adjacent to the surface is lighter than the bulk fluid but the net motion is still downward since the shear stress exerted by the outer part of the boundary layer is enough to overcome the difference in density. At $12.4^{o}C$, the velocity gradient at the surface is zero, which means that the buoyancy and shear forces are balanced. At temperatures between $12.4^{o}C$ and $26.8^{o}C$, bidirectional flow will occur; upflow near the surface and downflow towards the outer edge of the boundary layer. The relative magnitude of these two regions change as the temperature increases. At temperatures above $26.8^{o}C$, the inner upward flowing part of the boundary layer predominates. The shear force it exerts on the heavy outer part of the boundary layer is great enough so that the flow is purely upward above this point. At bulk temperatures above $0^{o}C$, the transition points between flow regimes wil change but the same general behaviour persists. Naturally, at bulk temperatures above $4^{o}C$, in the heated plate region, the flow will be purely upward, since the boundary layer must, by definition, be lighter than the bulk fluid.

1.3 Review of Previous Work

1.3.1 Free Convection From Horizontal Cylinders

The first analytic investigation of heat transfer from horizontal cylinders was carried out by Langmuir [22] in 1912. By studying free convective heat transfer from high temperature wires to different gases, he concluded that the dominant heat transfer mechanism was radial conduction through a stationary layer, or film, surrounding the wire. This he deduced from the fact that in gases, even at high temperatures, the velocity of the gas was very small while the thermal conductivity became appreciable. As a verification of this hypothesis, he presented the results of his experiments which showed that the heat loss was independent of the orientation of the wire, which would not have been the case if most of the heat was being carried away by convective currents. The analytic solution of this problem then became:

$$\dot{Q} = \text{heat transfer rate}$$

$$= s(\phi_p - \phi_\infty) \quad \text{.....(1-1)}$$

where ϕ = conductivity function

$$= \int_0^T k \cdot dT \quad \text{.....(1-2)}$$

s = shape factor

$$= 2\pi L/\ln(b/D) \quad \text{.....(1-3)}$$

$$\text{and } b \cdot \ln(b/D) = 2B \quad \ldots\ldots\ldots\ldots\ldots\ldots\ldots\ldots (1\text{-}4)$$

The subscripts p and ∞ referred to the conductivity function evaluated at the surface and bulk water temperatures respectively, k was the thermal conductivity of the fluid, L was the cylinder length, D was the cylinder diameter and b was Langmuir's film thickness for a cylinder. B was the equivalent film thickness for a plane surface and was constant for a specific gas. For air at room temperature and pressure, Langmuir found B = 0.43.

Davis [4], in the early 1920's, looked at the problem from a dimensional analysis point of view. He utilized Boussinesq's hypothesis which stated that:

$$\dot{q}D/k\theta_p = F(g\beta\theta_p D^3 \rho^2 c_p^2/k^2) \cdot f(\rho c_p \nu/k) \quad \ldots\ldots (1\text{-}5)$$

where $\dot{q}$ was the heat transfer rate per unit area, θ_p was the difference between the surface and bulk water temperatures, g was the acceleration of gravity, β was the thermal expansion coefficient of the fluid, ρ was the density of the fluid, c_p was the specific heat of the fluid and ν was the kinematic viscosity of the fluid. He dropped the second function, assuming that the Prandtl number, $\rho c_p \nu/k$, was constant for all fluids and experimentally determined the following relationship:

$$\dot{q}D/k\theta_p = C\cdot(Gr\cdot Pr^2)^{0.233} \quad \text{.....(1-6)}$$

where Gr was the Grashof number, $g\beta\theta_p D^3/\nu^2$ and Pr was the Prandtl number, $\mu c_p/k$. Davis [5] later discovered that omitting this function was not valid, especially for fluids, and so determined that:

$$\dot{q}D/k\theta_p = F(Gr\cdot Pr) \quad \text{.....(1-7)}$$

Around the same period of time, Rice [32] combined Langmuir's film theory with Davis' dimensional analysis to find a relationship for B^*, the film thickness for cylinders:

$$B^* = 3.4(\mu/\rho)^{1/2}\cdot(D/g)^{1/4} \quad \text{.....(1-8)}$$

where μ was the dynamic viscosity of the fluid . The constants and exponents were determined experimentally. He found that for long cylinders and very large film thicknesses:

$$s = 2\pi L/\ln(2B^*/D + 1) \quad \text{.....(1-9)}$$

He also found that for large cylinders with comparatively small film thicknesses:

$$s = \pi DL/B^* \quad \text{.....(1-10)}$$

The experimental results of Langmuir (air), Ayrton and Kilgour (air), Kennelly (air), Petavel (air, hydrogen, oxygen and carbon dioxide) and Davis (toluene, carbon tetrachloride, anilene, olive oil and glycerine) were in good agreement with equations (1-8) and (1-9).

The theory was later extended by Rice [33] to take into account the variation of the convective heat losses at low temperatures with the 5/4 power of the temperature difference, by including β and θ_p in the dimensional analysis of the expression for the film thickness:

$$B^*/D = 2.12(Gr \cdot Pr)^{-1/4} \quad \text{.....(1-11)}$$

Up until this point in time, all of the work on free convection from horizontal cylinders had either been confined to empirical correlations of experimental data or to very simplified theoretical considerations. No attempt had been made to solve the full Navier-Stokes equations because of their extreme complexity . A major breakthrough in the analytic investigation of the free convective flow phenomenon came in 1930, when Schmidt and Beckmann [38] first suggested applying the approximations of boundary layer theory to simplify the full Navier-Stokes equations. The

resulting partial differential equations were transformed by Pohlhausen [30], for a vertical flat surface, into ordinary differential equations with one independent variable. To solve these equations, five boundary conditions were required, three at the surface and two at the freestream. The convergence of the solution, however, was much too slow and so Pohlhausen used Schmidt and Beckmann's experimental results for air, to obtain two more boundary conditions at the wall. His results were therefore restricted to air.

Jodlbauer [19], three years later, extensively measured the temperature and velocity fields around heated pipes and compared his results with the theory of similarity of flow fields, discussed by Davis and also by Schmidt and Beckmann for the flat plate. This data has been used by many people, since that time, as a check against theoretical predictions.

The most extensive work on this subject was performed by Hermann [18] in 1936. He transformed the partial differential equations into ones which were identical to those solved by Pohlhausen for a vertical flat plate (Appendix I). The transformation used by Hermann was not exactly correct and as a result, his azimuth functions, $f(\xi)$ and $g(\xi)$, were overdetermined (i.e. three equations in two unknowns). However, his results compared quite favorably with those of

Jodlbauer [19]. They were:

$$u(x,y) = \text{tangential velocity}$$
$$= (\nu/r).(Gr/8)^{1/2} f(\xi)g(\xi)p'(q) \ldots (1\text{-}12)$$

$$\theta(x,y) = T - T_\infty$$
$$= \theta_p . t(q) \ldots\ldots\ldots\ldots\ldots\ldots (1\text{-}13)$$

$$h(x) = \text{local heat transfer coefficient}$$
$$= -(k/r).(Gr/8)^{1/4} g(\xi)t'(0) \ldots\ldots (1\text{-}14)$$

$$Nu(x) = \text{local Nusselt number}$$
$$= -2(Gr/8)^{1/4} g(\xi)t'(0) \ldots\ldots\ldots (1\text{-}15)$$

$$\overline{Nu} = \text{average Nusselt number}$$
$$= \overline{h}D/k$$
$$= -2(Gr/8)^{1/4} . \overline{g} . t'(0) \ldots\ldots\ldots\ldots (1\text{-}16)$$

x was the tangential coordinate, y was the radial coordinate, r was the radius of the cylinder, T was the temperature, T_∞ was the bulk water temperature and ξ, q, t(q), $f(\xi)$ and $g(\xi)$ are defined in Appendix I. Hermann graphically integrated $g(\xi)$ and found that $\overline{g} = 0.616$. Using Pohlhausen's results for air (Pr = 0.733), t'(0) = -0.508 and:

$$\overline{Nu} = 0.372(Gr)^{1/4} \quad \text{.....(1-17)}$$

He compared the solutions for a horizontal cylinder and for a flat plate and found that:

1) if $Gr_D = Gr_L$ (i.e. D = L)
   then $\overline{Nu}_D = 0.777\ \overline{Nu}_L$ .....(1-18)
2) if $\overline{h}_D = \overline{h}_L$
   then L = 2.76 D .....(1-19)

Also of interest was Hermann's work on the transition to turbulence in free convective flow over a horizontal cylinder. He found that the critical Reynolds number, based on the boundary layer thickness, $Re_{\delta,crit.} = 285$ for a cylinder, which is considerably less than the critical Reynolds number for forced convection. Using this number and his theoretically derived formula:

$$Re_\delta(\xi) = 0.357\ Gr^{1/4}.f(\xi) \quad \text{.....(1-20)}$$

a formula for the critical Grashof number and the position of the onset of turbulence was determined:

$$Gr_{crit.} = [800/f(\xi_{crit.})]^4 \quad \text{.....(1-21)}$$

For $Gr < 3.5 \times 10^8$, the flow was laminar over the entire cylinder. At $Gr \simeq 3.5 \times 10^8$, turbulence appeared at $\xi = \pi$ (the top of the cylinder). At $Gr \simeq 3 \times 10^9$, the flow was turbulent from $\xi = \pi/2$ upward (the middle of the cylinder). Finally, from his test results, Hermann discovered that after the onset of turbulence, $Nu \propto Gr^{1/3}$ because of the increased mixing due to the turbulent exchange of momentum and energy.

A third subject which Hermann studied was the correlation of the results of several previous investigators, principally at lower values of the Grashof number. He presented log-log graphs of Nu versus Gr for the data of Ayrton and Kilgour, Langmuir, Bijlevelt, Kennelly,Wright and Bijlevelt, Petavel, Wamsler and Koch. All of these experiments were performed in air and for the most part on wires of small diameters ($10^{-4} < Gr < 10$). Only the data of Wamsler and of Koch represented heat transfer from cylinders of any appreciable size ($10^4 < Gr < 10^7$). The point of interest in this representation of data was that in the higher range of Grashof numbers, the results could be represented by a single straight line while for Grashof numbers below 10, the curves of the different experimenters diverged and levelled out at $Gr < 10^{-4}$ to constant but different values of Nu.

The reason for this divergence was thought to be the invalidity of the boundary layer approximations at very

small values of the Grashof number, where the thickness of the boundary layer with respect to the diameter of the cylinder and also the curvature of the surface became significant. Hermann reasoned that in this region, fluid velocities were small and conditions were very close to those of static heat conduction, which was in agreement with Langmuir's film theory. By introducing a new variable, $T_e = \theta_p/T_\infty$, he found that a single curve of Nu versus Gr could be obtained for any specific value of T_e. Also, the Nusselt number decreased as T_e increased, since this was equivalent to lowering T_∞ for a constant value of T_p, the surface temperature, which introduced more cold fluid into the boundary layer, resulting in a lower average value of the thermal conductivity.

During the 1940's, Elenbaas [13] incorporated Langmuir's film theory with previous work done by Hermann, to more thoroughly describe the free convection process from wires at low values of the Rayleigh number (Ra = Gr·Pr). He agreed with Hermann's conclusion that the rate of heat transfer at low Rayleigh numbers must be affected by T_e, as well as by Gr and Pr. Combining this assumption with the film theory, Elenbaas derived:

$$\overline{Nu}_p \cdot \exp(-2/\overline{Nu}_f) = C \cdot (Gr \cdot Pr)_p^{1/3} / g^* (Gr \cdot Pr)_p \quad \text{.....(1-22)}$$

where the subscripts p and f referred to properties evaluated at the surface and film temperatures respectively. For $Ra < 10^4$, $C = 0.16$ and $g^*(Gr.Pr)_p$ = constant = 1. Therefore, for $Ra < 10^4$:

$$\overline{Nu}_p \cdot \exp(-2/\overline{Nu}_f) = 0.16(Gr \cdot Pr)_p^{1/3} \quad \text{.....(1-23)}$$

For larger values of the Rayleigh number, the function $g^*(Gr.Pr)_p$ increased and $\exp(-2/\overline{Nu}_f) \to 1$. From experiment, it was concluded that $g^*(Gr \cdot Pr)_p \propto (Gr \cdot Pr)_p^{1/12}$. Therefore, for $Ra \gg 10^4$:

$$\overline{Nu}_p = C(Gr \cdot Pr)_p^{1/4} \quad \text{.....(1-24)}$$

which was identical to the form of Hermann's heat transfer relation.

Elenbaas and previous investigators had assumed that the temperature of the fluid at the surface was at the same temperature as the surface. This is valid for gases, as long as the mean free path of the gas is small, so that molecular collisions are frequent. At very low pressures, however, the mean free path increases and this assumption is no longer valid. A temperature discontinuity develops at the gas-solid interface. Madden and Piret [23], in 1951, solved this

problem and found that:

$$\Phi = \ln(b/D)$$
$$= (2/\overline{Nu}) - [(8/Pr)\cdot(\lambda/D)]/[\sigma(\kappa+1)]$$
$$+ \ln[1+(2\lambda/D)] \quad \ldots\ldots\ldots\ldots\ldots\ldots (1\text{-}25)$$

where λ was the mean free path of the gas, κ was the ratio of specific heats for a gas, σ was the accommodation coefficient for a gas and Φ was Madden and Piret's heat transfer function. At high pressures, the second and third terms on the right hand side of equation (1-25) became very small and it reduced to:

$$\overline{Nu} = 2/\ln(b/D) \quad \ldots\ldots\ldots\ldots\ldots\ldots\ldots (1\text{-}26)$$

which was identical to Langmuir's results. They then experimentally measured Φ and established that:

$$\Phi = \ln[6.82/(Gr\cdot Pr)^{1/3}] \quad \ldots\ldots\ldots\ldots\ldots (1\text{-}27)$$

In 1953, Ostrach [28] duplicated the work of Pohlhausen and solved the transformed differential equations for a flat plate, for many Prandtl numbers. This allowed Hermann's work to be extended into the liquid range of Prandtl numbers.

The next year, McAdams [24] correlated earlier experimental work on horizontal cylinders and determined that the equation which best fit the data was:

$$\overline{Nu} = 0.53(Gr \cdot Pr)^{1/4} \quad \text{.....(1-28)}$$

If Hermann's equation for air (Pr = 0.733) were generalized for any fluid, the resulting equation would be:

$$\overline{Nu} = 0.40\ (Gr \cdot Pr)^{1/4} \quad \text{.....(1-29)}$$

which was not in very good agreement with McAdams'formula. However, with the aid of Ostrach's solution, it can be shown that t'(0), used in Hermann's equation, did not vary exactly as the quarter power of the Prandtl number. Therefore equation (1-28) gave a better correlation than (1-29) in general, although Eckert and Soehnghen [10] verified that Hermann's solution was excellent for air.

Another transformation was used by Merk and Prins [26] in 1954, in conjunction with an integral technique, to solve the partial differential equations in terms of the azimuth function $H(\xi)$ (Appendix II). They found that for a cylinder:

$$u(x,y) = (\nu/D) \cdot Gr^{1/2} \cdot \eta \cdot (1-\eta)^2 \cdot F(\xi) \quad \text{.....(1-30)}$$

$$\theta(x,y) = \theta_p \cdot (1-\eta)^2 \quad \text{.....(1-31)}$$

$$h(x) = 2(k/D) \cdot Gr^{1/4} \cdot G(\xi) \quad \text{.....(1-32)}$$

$$Nu(x) = h(x) \cdot D/k$$
$$= 2Gr^{1/4} \cdot G(\xi) \quad \text{.....(1-33)}$$

$$\overline{Nu} = [2Gr^{1/4}] \cdot [H(\pi)/\pi] \cdot [G(\xi)/H'(\xi)] \quad \text{....(1-34)}$$

where $G(\xi)$ and $F(\xi)$ and η were functions of $H(\xi)$ and $H'(\xi)$ and where $G(\xi)/H'(\xi)$ and $H(\pi)$ were constant for any Prandtl number. It should be noted that $H(\xi)$ also depended on the Prandtl number. Carrying out the calculations:

$$Pr = 5 \; ; \; \overline{Nu} = 0.511(Gr \cdot Pr)^{1/4} \quad \text{.....(1-35a)}$$
$$Pr = 8 \; ; \; \overline{Nu} = 0.518(Gr \cdot Pr)^{1/4} \quad \text{.....(1-35b)}$$
$$Pr = 10; \; \overline{Nu} = 0.520(Gr \cdot Pr)^{1/4} \quad \text{.....(1-35c)}$$
$$\text{and } Pr = \infty \; ; \; \overline{Nu} = 0.528(Gr \cdot Pr)^{1/4} \quad \text{.....(1-35d)}$$

Equation (1-33) was in excellent agreement with equation (1-15), derived by Hermann, except at large values of ξ. In this region, Hermann predicted that the heat transfer would vanish while Merk and Prins predicted that it would tend

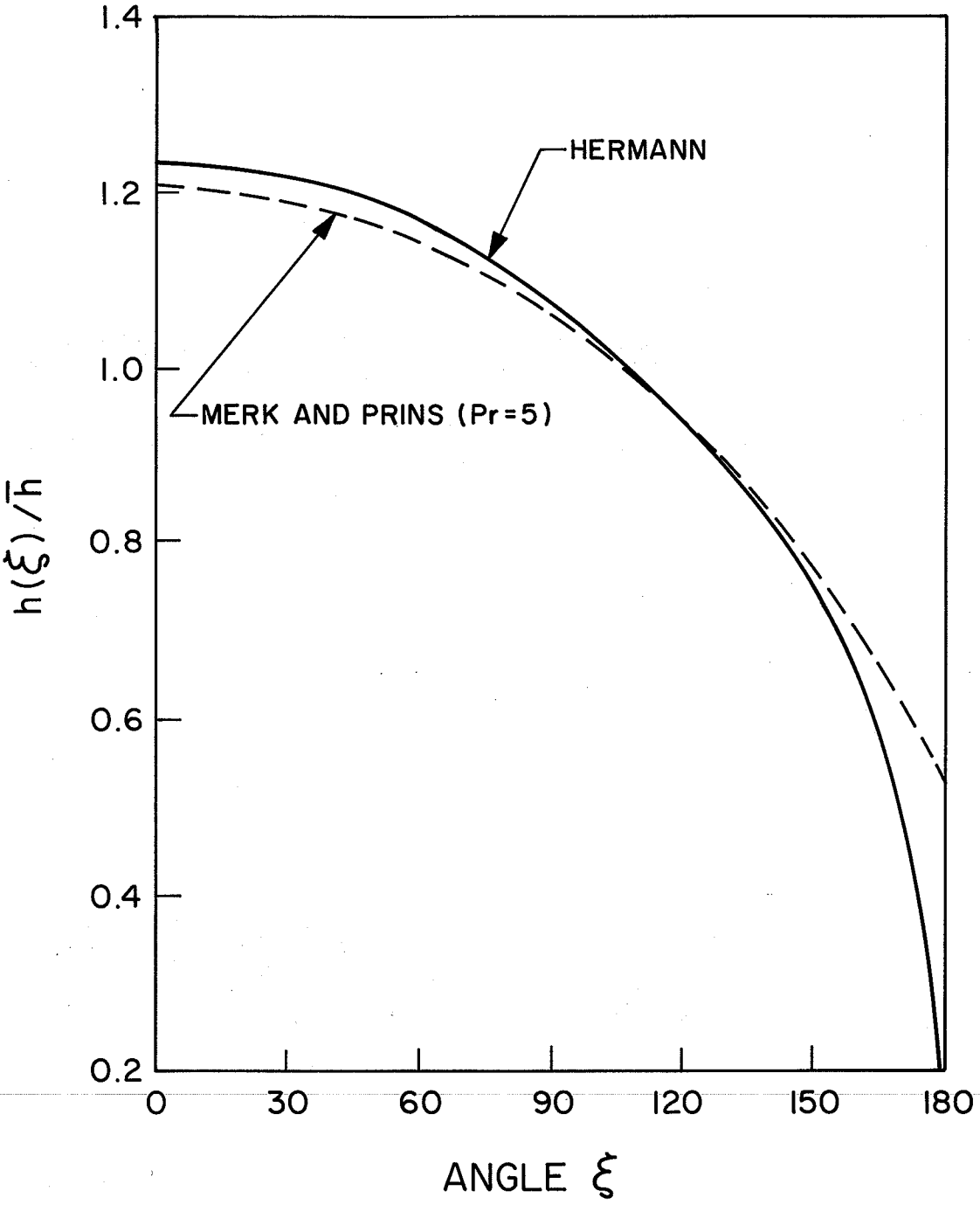

Fig. 2 . Comparison of Analytic Local Distributions of Heat Flux.

toward some finite value (Figure 2). The latter prediction was in good agreement with experimental observations. It was also evident that equation (1-35) yielded closer results, when compared to experimental data or to McAdams' empirical formula, than Hermann's equation (1-29). The only drawback of Merk and Prins' approach was that the form of the temperature and velocity profiles were assumed and were arbitrarily set equal to zero at $\eta = 1$. This meant that the temperature and velocity profiles did not approach zero asymptotically and furthermore, they reached zero at the same value of η, both of which are untrue. The latter statement would be correct only if Pr = 1 (See Figure 3a and 3b). Jodlbauer's experiments confirmed that Hermann's temperature and velocity profiles were much more accurate than those of Merk and Prins.

In order to correlate free and forced convection heat transfer results for flow regimes where both mechanisms were in existence, van der Hegge Zijnen [42] formulated his own empirical formula:

$$\overline{Nu} = 0.35 + 0.25(Gr \cdot Pr)^{1/8} + 0.45(Gr \cdot Pr)^{1/4} \quad \text{.....(1-36)}$$

which he found predicted the Nusselt number at low values of Gr.Pr much better than the formulas of Merk and Prins or of Hermann.

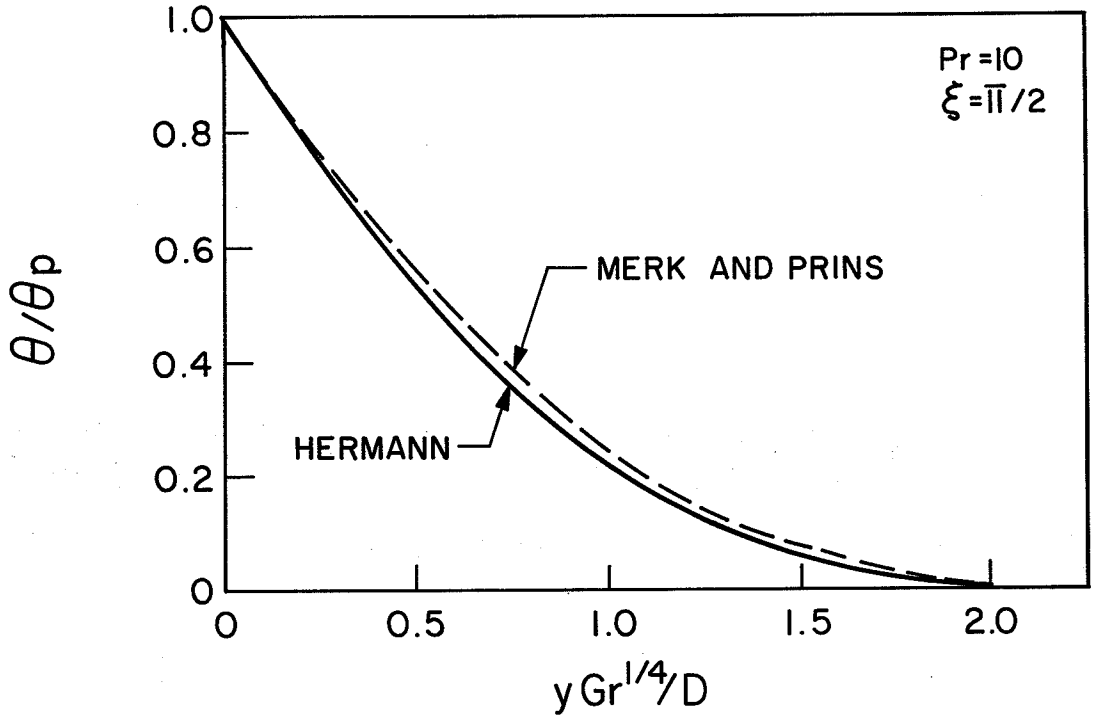

Fig. 3a. Comparison of Analytic Boundary Layer Temperature Profiles.

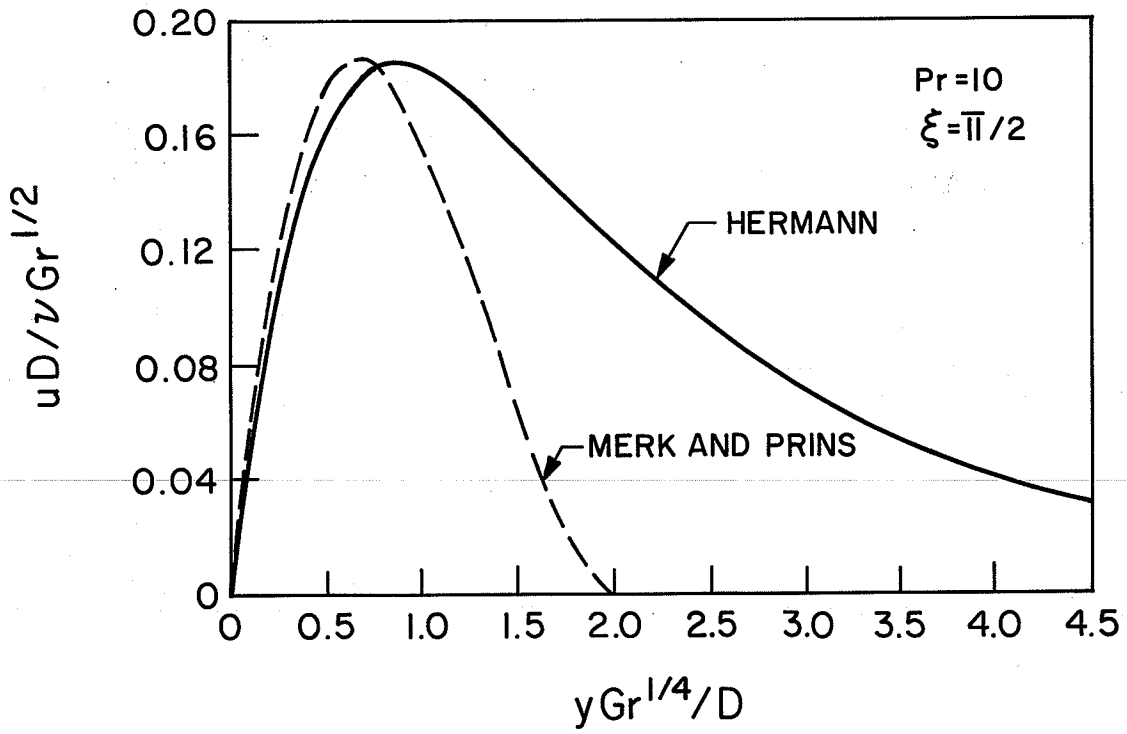

Fig. 3b. Comparison of Analytic Boundary Layer Velocity Profiles.

One of the major problems in using any of these derived or empirical formulas is that the fluid properties were considered constant, whereas in reality, this is far from being the case. For instance, the kinematic viscosity of water decreases by a factor of two between $0^{o}C$ and $25^{o}C$. Sparrow and Gregg [40], however, solved the boundary layer equations for a flat plate using variable fluid properties (ρ, k, μ and c_p). They compared the heat transfer results with those obtained by using a reference temperature, in conjunction with the constant property solution. For liquids and gases, satisfactory agreement was obtained by using the constant property solution and evaluating all fluid properties at the film temperature, which they defined as:

$$T_f = 0.5(T_p + T_\infty) \quad \ldots\ldots\ldots\ldots\ldots\ldots (1\text{-}37)$$

The applicability of the reference temperature method has been extended to other configurations (i.e. the horizontal cylinder) with excellent results. Henceforth, it will be assumed that all properties are evaluated at T_f, unless otherwise specified.

Eckert and Drake [9] derived their own solution by integrating the boundary layer equations and by assuming the form of the temperature and velocity profiles. Their results

were in the form:

$$\overline{Nu} = .540[Pr/(.952+Pr)]^{1/4} \cdot (Gr \cdot Pr)^{1/4} \quad \ldots (1\text{-}38)$$

Here the Nusselt number was not simply a function of $(Gr \cdot Pr)^{1/4}$ but depended on another function of the Prandtl number as well. For various Prandtl numbers:

$$Pr = 5 \; ; \; \overline{Nu} = .517(Gr \cdot Pr)^{1/4} \quad \ldots\ldots (1\text{-}39a)$$

$$Pr = 8 \; ; \; \overline{Nu} = .525(Gr \cdot Pr)^{1/4} \quad \ldots\ldots (1\text{-}39b)$$

$$Pr = 10; \; \overline{Nu} = .528(Gr \cdot Pr)^{1/4} \quad \ldots\ldots (1\text{-}39c)$$

$$\text{and } Pr = \infty \; ; \; \overline{Nu} = .540(Gr \cdot Pr)^{1/4} \quad \ldots\ldots (1\text{-}39d)$$

It is interesting to note what would happen if Hermann's heat transfer equation (1-16) was generalized for all Prandtl numbers by assuming that the function t'(0) varied with Pr in an analogous manner to equation (1-38) (See Appendix III). The result of such a generalization is:

$$Pr = 5 \; ; \; \overline{Nu} = .474(Gr \cdot Pr)^{1/4} \quad \ldots\ldots (1\text{-}40a)$$

$$Pr = 8 \; ; \; \overline{Nu} = .481(Gr \cdot Pr)^{1/4} \quad \ldots\ldots (1\text{-}40b)$$

$$Pr = 10; \; \overline{Nu} = .484(Gr \cdot Pr)^{1/4} \quad \ldots\ldots (1\text{-}40c)$$

$$\text{and } Pr = \infty \; ; \; \overline{Nu} = .495(Gr \cdot Pr)^{1/4} \quad \ldots\ldots (1\text{-}40d)$$

While (1-40) does not compare as well as (1-39) with McAdams'

correlation (1-28), it is a marked improvement over the simplified generalization (1-29) of Hermann's results.

During the last fifteen years, several investigators have worked on various aspects of heat transfer from horizontal cylinders. Sesonske [39] measured the temperature and velocity fields around a cooled horizontal cylinder. His results matched those of Jodlbauer, which proved that Hermann's azimuth functions correctly represented the temperature and velocity behaviour about a horizontal tube.

Chiang and Kaye [2] solved the boundary layer equations for arbitrary surface temperature or heat flux distributions by introducing the surface temperatures or heat fluxes as power series and then transforming the partial differential equations into a number of ordinary differential equations, which were then numerically solved. Their results, for a constant surface temperature, verified Hermann's earlier theoretical work.

Poots [31] derived a general similarity solution for an isothermal three dimensional surface, near the stagnation point. The differential equations were simplified and solved for the two limiting cases, the horizontal cylinder and the sphere. Poots' solutions were similar to ones derived by Merk and Prins near the stagnation point. However, the breakdown of boundary layer theory in this region rendered

these results somewhat suspect.

Koh [20] utilized Hermann's theory to find the temperature distribution around a horizontal cylinder when the heat flux varied in the following manner:

$$\dot{q}/\dot{q}_o = 1 + m_1\xi^2 + m_2\xi^4 \quad \text{.....(1-41)}$$

where $\dot{q}_o$ represented the heat flux at $\xi = 0$. He found that for constant heat flux, the local and average Nusselt numbers were approximately 8% and 3% higher respectively, than those for the isothermal case.

Koh and Price [21] used a perturbation technique, similar to that employed by Chiang and Kaye, to solve the differential equations for the case where the surface temperature of the horizontal cylinder varied as:

$$\theta_p/\theta_{po} = 1 + n_1\xi^2 + n_2\xi^4 \quad \text{.....(1-42)}$$

where θ_{po} represented the temperature difference at $\xi = 0$. Their results were in agreement with those of Hermann and with those of Chiang and Kaye, for $n_1 = n_2 = 0$ (isothermal cylinder). They also ascertained that Eckert and Drake's form of the variation of Nusselt number with Prandtl number may be used to extend their solutions to other values of Pr. One

interesting result of their work was the divergence of heat transfer solutions as the surface temperature deviated from the isothermal case. For instance, it was determined that if $n_1 = n_2 = 0.2$, then the Nusselt number at $\xi = 1$ was 39% greater than the Nusselt number under isothermal conditions. From this, it could be concluded that even a small degree of non-isothermality will cause a large change in the local heat transfer.

Dyer [8] studied the problem of constant heat flux using an integral technique similar to that of Eckert and Drake and a modified Grashof number, Gr'. The use of Gr' allowed the average heat transfer results to be generalized. That is to say, Gr' was constant for the cylinder while the conventional Grashof number, in this case, varied with the angular position, ξ. Dyer found that:

$$\overline{Nu} = 0.61(Gr' \cdot Pr)^{.192} \quad \text{.....(1-43)}$$

However, the validity of this solution was dubious since the assumed form of the boundary layer velocity profile had been shown by Sesonske and others to be incorrect.

Another solution for an isothermal cylinder was developed by Saville and Churchill [34] in 1967. They transformed the partial differential equations using Goertler-type

transformations and series expansions, rather than the Blasius-type employed by Chiang and Kaye and then numerically solved the resulting set of ordinary differential equations. Their temperature and velocity profiles were in good agreement with Jodlbauer's results and furthermore, their series expansions converged much faster than the Blasius-type expansions.

Peterka and Richardson [29] analyzed the free convection problem for moderate values of the Grashof number. They reasoned that in this range, the rectilinear coordinates used by Hermann, Chiang and Kaye and others, were not valid since the boundary layer curvature could no longer be neglected. Instead, they formulated the problem in two dimensional cylindrical coordinates and solved the boundary layer equations in a manner quite similar to that of Chiang and Kaye. The important result of their work was their discovery that while the temperature profiles through the boundary layer were generally similar for a large range of Grashof numbers, there were marked differences in the slope of the temperature profile at the surface. Translated, this meant that the surface heat flux for $Gr = 10^3$ was roughly 30% greater than that predicted by other experimenters, most notably Hermann and Chiang and Kaye. Also noted was the fact that these differences were still significant (>4%) at Grashof numbers in the order of 10^6.

A further confirmation of Hermann's original work was produced by Aihara and Saito [1]. They measured the temperature and velocity fields around a horizontal cylinder as the limiting case of a horizontal torus with an infinite radius of rotation. Their velocity measurements were obtained using an optical technique and were considered to be very precise. The agreement with Hermann's non-dimensional "similar" profiles was remarkably good.

A recent study was carried out in 1974 by Gentry and Wollersheim [15] on free convection to non-Newtonian power law fluids. These are fluids whose shear stress relationship may be represented as:

$$\tau = (\kappa/g_c) \cdot (\partial u/\partial y)^n \quad \ldots\ldots\ldots\ldots\ldots\ldots (1\text{-}44)$$

For conventional fluids, n = 1 and κ, the consistency index, becomes the dynamic viscosity, μ. They developed an integral solution for the heat transfer around the cylinder as a function of a modified Grashof and Prandtl number, Gr' and Pr' respectively. Two points of interest arose from this study. The first was that the local Nusselt number was not maximum at the bottom of the cylinder but began at a finite value and increased to a maximum at some point away from the bottom before decreasing to zero at the top. This effect was

more pronounced as the value of n decreased. For n = 1, this effect died out completely and the Nusselt number was exactly the same as that predicted by Hermann. The second result was that the average Nusselt number was well represented by McAdams' correlation, namely:

$$\overline{Nu} \simeq 0.53(Gr' \cdot Pr')^{1/4} \quad \ldots\ldots\ldots\ldots\ldots\ldots (1\text{-}45)$$

Fand and Keswani [14], in 1973, reported on their study of the mass flow rates of convective plumes above horizontal cylinders in water. A particularly interesting aspect of their work was the effect of the free surface on the mass flow and heat transfer rates around the cylinder. A typical surface temperature versus time profile for a horizontal cylinder is shown in Figure 4a. During the entire time interval during which heat is transferred from the cylinder, there is a plume of fluid rising from the cylinder. When this layer reaches the surface it bifurcates and forms a horizontal heated layer. The initial increase in surface temperature is due to the short time in which convection has not had time to become established and during which conduction is the only mode of heat transfer. The surface temperature then becomes steady until the time when the heated layer of water on the surface has built up and descended to the level of the

cylinder. From this time forward, no steady state can be maintained. Fand and Keswani performed tests which indicated to them that if Y/D (See Figure 4b) was less then 10, then no steady state segment could be established at all, because the cylinder could "sense" the free surface and would be immediately affected by it. They did indicate that this minimum ratio was probably dependent on the driving force, θ_p, as well, but they did not investigate this aspect of the problem. Indeed, it seems more likely that the controlling parameter would be $(Y/D)/\theta_p$ instead of simply Y/D. They also derived an empirical formula for the time taken for the hot layer of fluid to descend to the level of the cylinder:

$$t^* = 131.58\, W(Gr\cdot Pr)^{-.53}\nu^{-1}D\cdot$$
$$[(Y/D)^{.3} - (1/2)^{.3}] \qquad \text{.....(1-46)}$$

where the constants were determined experimentally.

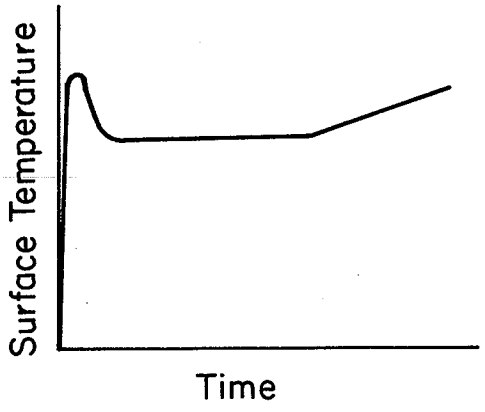

Fig. 4a. Surface Temperature Versus Time

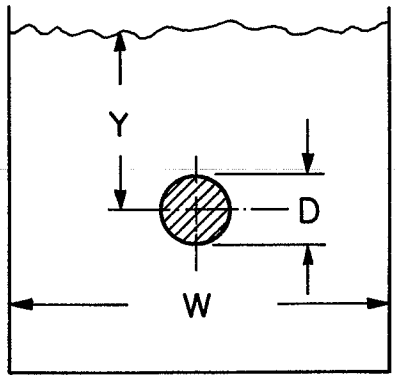

Fig. 4b. Definition of Tank Variables

1.3.2 Free Convection in Water Near $4^{o}C$

The effect of the density anomaly of water on its heat transfer characteristics was initially discovered by Codegone [3] in 1939. He observed that the heating and cooling rates of a flask of water were minimum when the water was at $4^{o}C$.

The unusual heat transfer characteristics of water near $4^{o}C$ were also reported by Ede [11] in 1951. He was able to correlate heat transfer rates to the difference between the plate and fluid temperatures for several liquids with the exception of water when the water temperature was below $4^{o}C$ and the plate temperature was above $4^{o}C$. In this specific instance, the unusual density variation near $4^{o}C$ influenced the results and rendered them incomparable to conventional theoretical results.

Tkachev [41], in 1953 while studying the melting of ice, discovered that for horizontal cylinders, a minimum Nusselt number occurred at a water temperature of $5.5^{o}C$. This he attributed to the presence of two opposing convective currents around the cylinder.

Dumoré, Merk and Prins [7], also in 1953, observed that when ice spheres were melted by free convection, the minimum Nusselt number occurred at a water temperature of $4.5^{o}C$. This result could be well duplicated theoretically by

replacing the conventional thermal expansion coefficient in the empirical equation:

$$Nu = 0.6(Gr \cdot Pr)^{1/4} \quad \ldots\ldots\ldots\ldots\ldots\ldots (1\text{-}47)$$

with a new coefficient which was a linear function of the bulk fluid temperature.

The next year, Merk [25] used the Squire-Eckert integral technique and a third order polynomial for density as a function of temperature, to solve the differential equations for melting ice spheres for an infinite Prandtl number. The results were then extrapolated to a Prandtl number of 10 where a minimum Nusselt number was predicted for a bulk water temperature of $5.3^{o}C$.

A year following this, Ede [36], compared Merk's theory to his own earlier experimental work on heat transfer from a heated vertical flat plate. The agreement was quite good in the regions of pure upflow and pure downflow but in the bidirectional region, the theoretical results were as much as 50% low.

In 1956, Schechter and Isbin [36], studying heat transfer from a heated flat plate, were the first to apply a similarity solution to the problem. The transformation was similar to that used by Ostrach [28], with the exception that

they introduced Merk's expression for density into the boundary layer equations. The transformed ordinary differential equations were solved numerically for a range of plate temperatures from $1^{o}C$ to $14^{o}C$ ($T_{\infty} = 0^{o}C$). Their results showed that the Nusselt number decreased up to $T_p = 14^{o}C$, at which point the velocity gradient at the plate surface was zero. This they called the transition point to bidirectional flow. No similarity solution was possible above this point because the velocity field was no longer similar.

Schechter [35] experimentally measured temperature and velocity profiles for conditions similar to the above and observed regions of pure upflow, pure downflow and a bidirectional region with an upflowing current near the plate and a downflowing current further from the plate.

Schechter and Isbin [36] also found a solution by using an integral technique, the results of which were:

$$Nu_x = 0.489(Gr_x \cdot Pr_f \cdot \alpha)^{1/4} \quad \text{.....(1-48)}$$

$$\overline{Nu} = 0.652(Gr \cdot Pr_f \cdot \alpha)^{1/4} \quad \text{.....(1-49)}$$

where α was a dimensionless buoyancy function which is derived in Appendix V.

Schechter's analysis could not be applied at a bulk water temperature of $4^{o}C$ because the thermal expansion

coefficient, β_∞, became zero at this point. Goren [16] in 1966, avoided this problem by introducing a parabolic expression for the density change of water as a function of its temperature deviation from 4^oC. He then applied a similarity transformation technique and numerically solved the differential equations. This density variation for water and hence his solution were only valid near 4^oC.

A year later, Oborin [27] first studied free convection from a heated sphere and cylinder, the sphere being 7^oC warmer and the cylinder 2.1^oC warmer than the bulk fluid. Minimum Nusselt numbers were obtained at a water temperature of 2.4^oC for the sphere and 3.3^oC for the cylinder. By assuming that this minimum occurred when the density at the mean boundary layer temperature was equal to the density of the bulk fluid, he derived an expression for the bulk water temperature at which the minimum Nusselt number occurred:

$$T_\infty(\text{min}) = 4 - \theta_p/4 \quad \text{.....(1-50)}$$

In a study of melting ice spheres, conducted in 1968, Schenk and Schenkels [37] observed all three modes of flow, upflow when the water was above 6^oC, downflow below 4^oC and a bidirectional flow regime, similar to that observed by Schechter [35], when the water temperature was between

these two temperatures. They found a minimum Nusselt number occurring at 5.3°C, which was the same temperature as that predicted by Merk [25]. However, Merk's predicted Nusselt numbers in the bidirectional region were drastically lower then those measured by Schenk and Schenkels, due to the fact that the velocity profile that Merk used for his integral technique did not fit the bidirectional flow regime.

Vanier and Tien [46,47], during the late 1960's investigated melting ice spheres and determined that the minimum Nusselt number occurred at a bulk water temperature of 5.35°C. They also obtained an empirical equation to fit their experimental data:

$$Nu = 2 + C(Gr \cdot Pr)^{1/4} \quad \text{.....(1-51)}$$

Three different values of C were obtained, corresponding to different ranges of water temperatures. They also [44,45] performed a theoretical study of free convection by numerically integrating the ordinary differential equations obtained by Schechter and Isbin [36] and by Goren [16]. A variable Prandtl number was introduced to study the effect of variable fluid properties. The agreement of these results with those obtained by using a constant Prandtl number evaluated at the film temperature was quite good. Their analysis, based on

similarity assumptions, could not be extended into the bi-directional flow region. A similar study was conducted on melting vertical plates of ice and the results were compared:

$$\overline{Nu}(\text{plate})/\overline{Nu}(\text{sphere}) = 1.106(L/D)^{3/4} \quad \ldots(1\text{-}52)$$

The most extensive investigation to date of the bi-directional flow phenomenon in water near $4^{o}C$, was performed by Yuill [48], who attempted both experimentally and analytically to describe the local variation of heat flux on a vertical flat plate. For the unidirectional flow regions (regions I, III and IV in Figure 1), he solved the boundary layer equations using a similarity transformation which included the effect of varying viscosity and a numerical integration technique. The results were presented in the normal form (the Nusselt number as a function of the Grashof and Prandtl numbers). In region I:

$$Nu_x = C_I(Gr_x^* \cdot Pr)^{1/4} \quad \ldots(1\text{-}53)$$

$$Gr_x^* = 3\alpha g \beta_\infty \theta_p x^3/\nu^2 \quad \ldots(1\text{-}54)$$

$$C_I = 0.568 - 0.098[1 - \exp(AZ + BZ^2 + GZ^3 + DZ^4)] \quad \ldots(1\text{-}55)$$

where $Z = \alpha - 0.02825$

$$A = -23.043$$

$$B = 130.688$$

$$G = -469$$

and $$D = 406$$

and in regions III and IV:

$$Nu_x = C_{III-IV}(Gr_x^* \cdot Pr)^{1/4} \quad \text{.....(1-56)}$$

$$C_{III-IV} = 0.426 + 0.039[1 - \exp(A\phi + B\phi^2 + G\phi^3 + D\phi^4)] \quad \text{.....(1-57)}$$

where $A = -1.28369\ {}^{o}C^{-1}$

$B = 0.321533\ {}^{o}C^{-2}$

$G = -0.0581512\ {}^{o}C^{-3}$

and $D = -0.00377369\ {}^{o}C^{-4}$

The variable Z was used to correct for the fact that α was not zero along the I-II boundary. This was due to the fact that the temperature profile used in the derivation of α was not quite correct. ϕ was the perpendicular distance from the II-III boundary. The coefficients C_I and C_{III-IV} are also presented in Figures 5 and 6.

In region II, no similarity transformation was possible since two opposing flows were present. Yuill

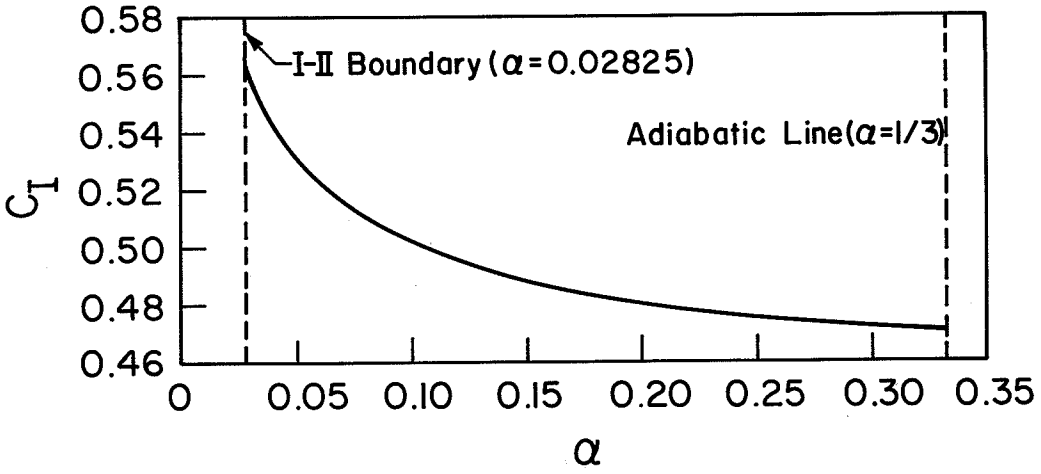

Fig. 5. Yuill's Coefficient, C_I Versus α in Region I.

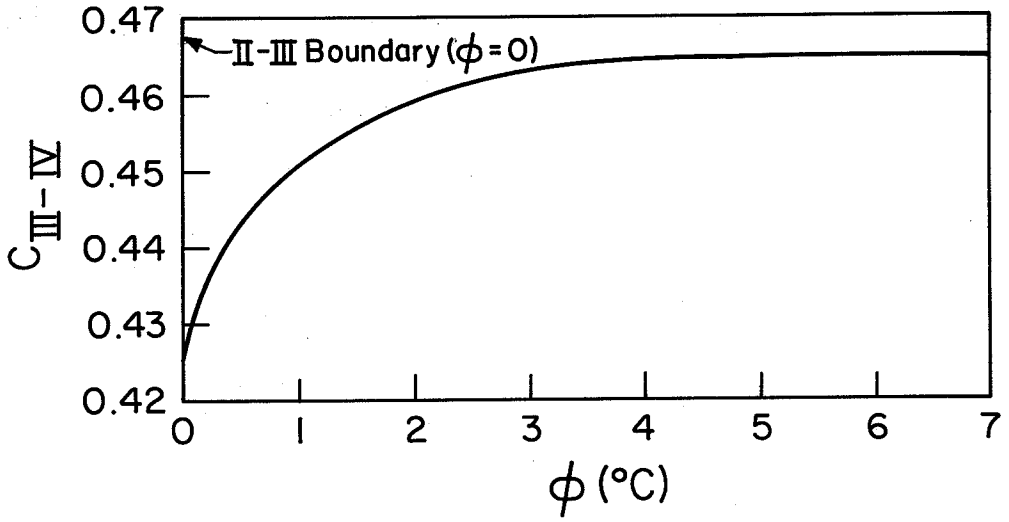

Fig. 6. Yuill's Coefficient, C_{III-IV} Versus ϕ in Region III and IV.

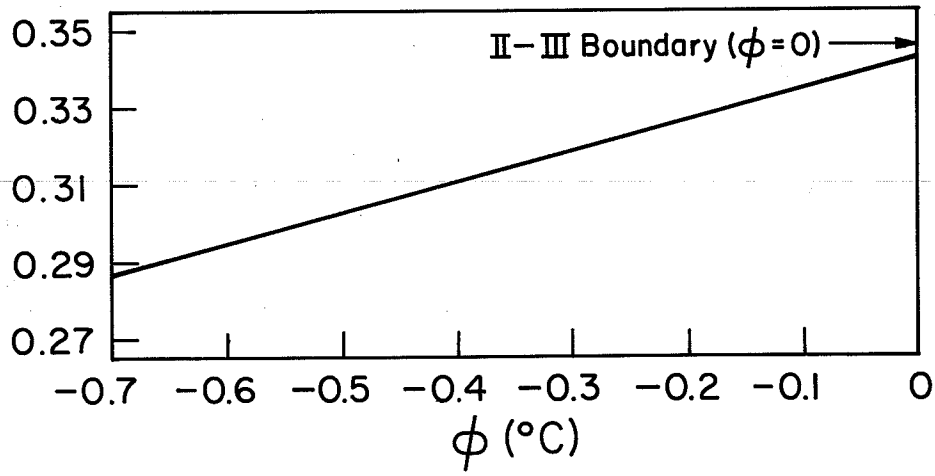

Fig. 7. Yuill's Coefficient, C_{II-N} Versus ϕ in Region II-N.

postulated that in this bidirectional region, two boundary layers were present also; an inner layer growing upward and an outer layer growing down the plate. From an interpretation of his results, he also hypothesized the existence of separated and non-separated sub-regions within region II; the distinction between the two being that the inner boundary layer for non-separated flow continued upward past the top of the heated plate while for separated flow, this inner boundary layer separated from the plate to flow back down as the outer boundary layer. The line $\phi = -0.6$ was chosen as the boundary between the two, to fit the experimental results, although the amount of data was not sufficient to fix this boundary absolutely.

The heat transfer results in the non-separated region were found to be similar to those in the unidirectional upflow region, probably because the inner boundary layer was much more dominant than the outer boundary layer. The results were correlated by the equation:

$$Nu_x = C_{II\text{-}N}(Gr^*_{ix} \cdot Pr_i)^{1/4} \quad \text{.....(1-58)}$$

$$Gr^*_{ix} = 3\alpha_i g\beta_\infty \theta_p x^3/\nu^2 \quad \text{.....(1-59)}$$

$$C_{II\text{-}N} = 0.3425 + 0.080\ \phi \quad \text{.....(1-60)}$$

$C_{II\text{-}N}$ is graphically presented in Figure 7. α_i was the

dimensionless mean inner boundary layer density deficit defined in Appendix V.

In the separated region, both boundary layers had an influence on the heat transfer coefficients. Yuill defined the local thermal resistance as:

$$R_x = 1/h_{ix} + 1/h_{ox}$$
$$= C_i(x/k_i)\cdot(Gr^*_{ix}\cdot Pr_i)^{-n}$$
$$+ C_o[(L-x)/k_o]\cdot(Gr^*_{ox}\cdot Pr_o)^{-m} \quad \text{.....(1-61)}$$

$$C_i = 6.988\gamma + A\phi\gamma + B\phi\gamma^2 \quad \text{.....(1-62)}$$

$$C_o = 2.3313 - 8.6188\gamma + G\phi\gamma + D\phi\gamma^2 \quad \text{.....(1-63)}$$

$$n = 0.25 + E\phi \quad \text{.....(1-64)}$$

$$m = 0.25 + F\gamma \quad \text{.....(1-65)}$$

where $A = -23.329\ {}^{o}C^{-1}$

$B = 34.907\ {}^{o}C^{-1}$

$G = 6.5212\ {}^{o}C^{-1}$

$D = -19.089\ {}^{o}C^{-1}$

$E = -0.021943\ {}^{o}C^{-1}$

and $F = -0.051359$

L was the length of the heated plate and γ was the angle of rotation about the point $T_p = T_\infty = 4^{o}C$, with the I-II boundary arbitrarily chosen as datum. The terms Gr^*_{ix} and Pr_i were

evaluated at the film temperature of the inner boundary layer while Gr^*_{ox} and Pr_o were evaluated at the film temperature of the outer boundary layer. These film temperatures, along with the division point between the two opposing flows, Σ, are also defined in Appendix V.

CHAPTER 2

EXPERIMENTAL STUDY

2.1 Objectives of the Experiment

The first objective of this experiment was to obtain local heat flux distributions, representing the variable fluid property situation and to compare them with the distributions obtained analytically by previous investigators, in order to see the relative effect of fluid property changes through the boundary layer on the heat flux at the cylinder surface. To introduce these fluid property variations into the theoretical analysis of this problem was beyond the scope of the present work. It was also desired to check out the quality of the heat transfer apparatus by performing the comparison, so that the temperature region around $4^{o}C$ could be investigated and the results could be used with a reasonable degree of confidence. In the majority of analytic work on free convection from cylinders, the fluid properties have been assumed constant, with the exception of the density change in the buoyancy term of the momentum equation. In particular, neither Hermann [18] nor Merk and Prins [26] considered the variation with temperature of the viscosity, conductivity or Prandtl number in their theoretical analyses of the problem. Yuill introduced expressions for these variables, along with

the density, into his similarity transformation of the boundary layer equations for a vertical flat plate (See Appendix IV). No such analysis has been done for the horizontal cylinder problem. Since these properties do exhibit changes with temperature, the introduction of variable fluid properties might noticeably alter the analytic local heat flux distributions obtained by Hermann, Merk and Prins and others.

The second major objective of this study was to correlate the average heat transfer data for the four different flow regimes in the region around $4^{o}C$. Although extensive work has been done on the general problem of free convection from horizontal cylinders, none has been performed in the region around a bulk water temperature of $4^{o}C$, where the density maximum radically alters the flow patterns and again, none has taken into account the change in fluid properties through the boundary layer. Yuill [48] had identified four different sets of heat transfer results in this region, corresponding to cases of pure downflow, bidirectional separated and non-separated flow and pure upflow along a vertical flat plate and had derived correlations for each. It was considered likely that his correlations could be modified somewhat, so that they could be applicable to the heat transfer from a horizontal cylinder. By comparing the obtained correlations with the accepted standard correlations for horizontal

cylinders, a measure of the effect of the density maximum on the heat transfer characteristics of horizontal cylinders could be obtained. Should this effect be of sufficient magnitude, it was desired to know exactly how far removed from the point of maximum density the bulk water temperature would have to be before this effect died out.

2.2 Experimental Apparatus

2.2.1 The Horizontal Cylinder

The cylinder consisted of two parts, the support structure and the heat transfer surface. The support structure was fabricated from 10.16 cm. (4 in.) O.D. plexiglass tubing cut to a length of 58.42 cm. (23 in.). Upon the middle 20.32 cm. (8 in.) of this tubing were mounted the heated surfaces, which were prepared and installed as follows. Circumferential lines were scribed on the tubing so as to divide this 20.32 cm. section into three parts; a 10.16 cm. section in the middle with a 5.08 cm. section on either side. These sections would correspond to the main test section and to guard sections on either side, designed to eliminate end losses from the test section. Following this, longitudinal lines were scribed so as to divide the periphery of the tubing into twelve equal sections. Since the circumference of the tubing was 31.92 cm., each of these sections was approximately 2.66

cm. wide. The end effect was to produce thirty-six individual rectangular blocks on the outside of the tubing, which would be used to locate the thirty-six heaters which made up the apparatus. Through various portions of these sections, holes were drilled to allow thermocouple, voltage tap and heater leads to be drawn through the plexiglass into the inside of the tubing.

The heaters employed were a Minco brand, Kapton insulated, thin etched thermofoil resistance heaters whose heat generation rate was constant over their surfaces. The twelve main heaters were 2.54 cm. by 10.16 cm. (1 in. by 4 in.) with a resistance of 1.92 ohms and the guard heaters were each 2.54 cm. by 5.08 cm. (1 in. by 2 in.) with resistances of 0.96 ohms. The leads and voltage taps were soldered to the back (or inside) of the heaters and fed through the holes into the interior of the tubing. Each heater was located by means of the scribed lines and cemented into place on the plexiglass surface with contact cement. Both the heater leads and the voltage taps were constructed with 22 AWG insulated copper wire.

Next, small holes were drilled through the insulated parts of the heaters, at the appropriate places, and through the tubing as well, to allow the thermocouples to be fed through from the inside of the tubing. The thermocouples were

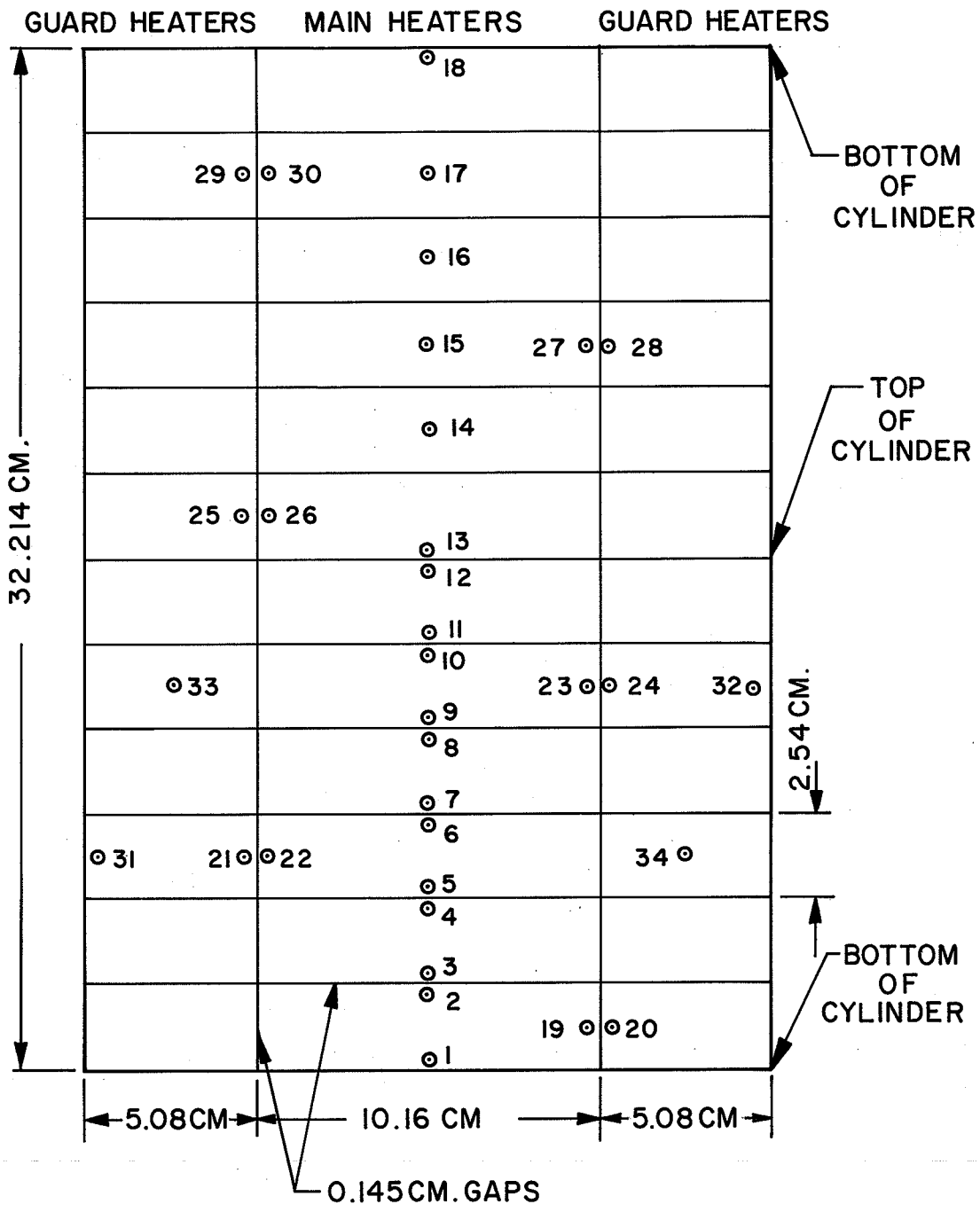

Fig. 8. THERMOCOUPLE POSITION AND CYLINDER DIMENSIONS.

constructed of 30 AWG copper-constantan thermocouple wire. Thirty-four thermocouples were employed in the apparatus. Their positions are indicated in Figure 8, along with the dimensions of the cylinder. They were fixed into position on the outside of the heaters by bending them over as they emerged through the heaters and pressing them into shallow slots on the heater surfaces.

A 0.056 cm. (0.022 in.) thick, curved rectangular copper plate was installed over each individual heater. These were manufactured by first rolling a sheet of copper into an approximately 10.16 cm. (4 in.) tube, then scribing this tube in an identical manner to the plexiglass tubing and finally, cutting the tube into thirty-six sections with a very fine slitting saw. These copper sections were individually alligned over the heaters and cemented into place with contact cement. A cross-section of the apparatus is shown in Figure 9. Three circular hose clamps were used during the installation to provide pressure between the copper plates and the heaters. This insured a good bond between the two and also insured good contact between the thermocouples and the inside of the copper plates.

The finished product consisted of twenty-four thermally isolated individual sections, one corresponding to each main heater and one corresponding to each pair of guard heaters

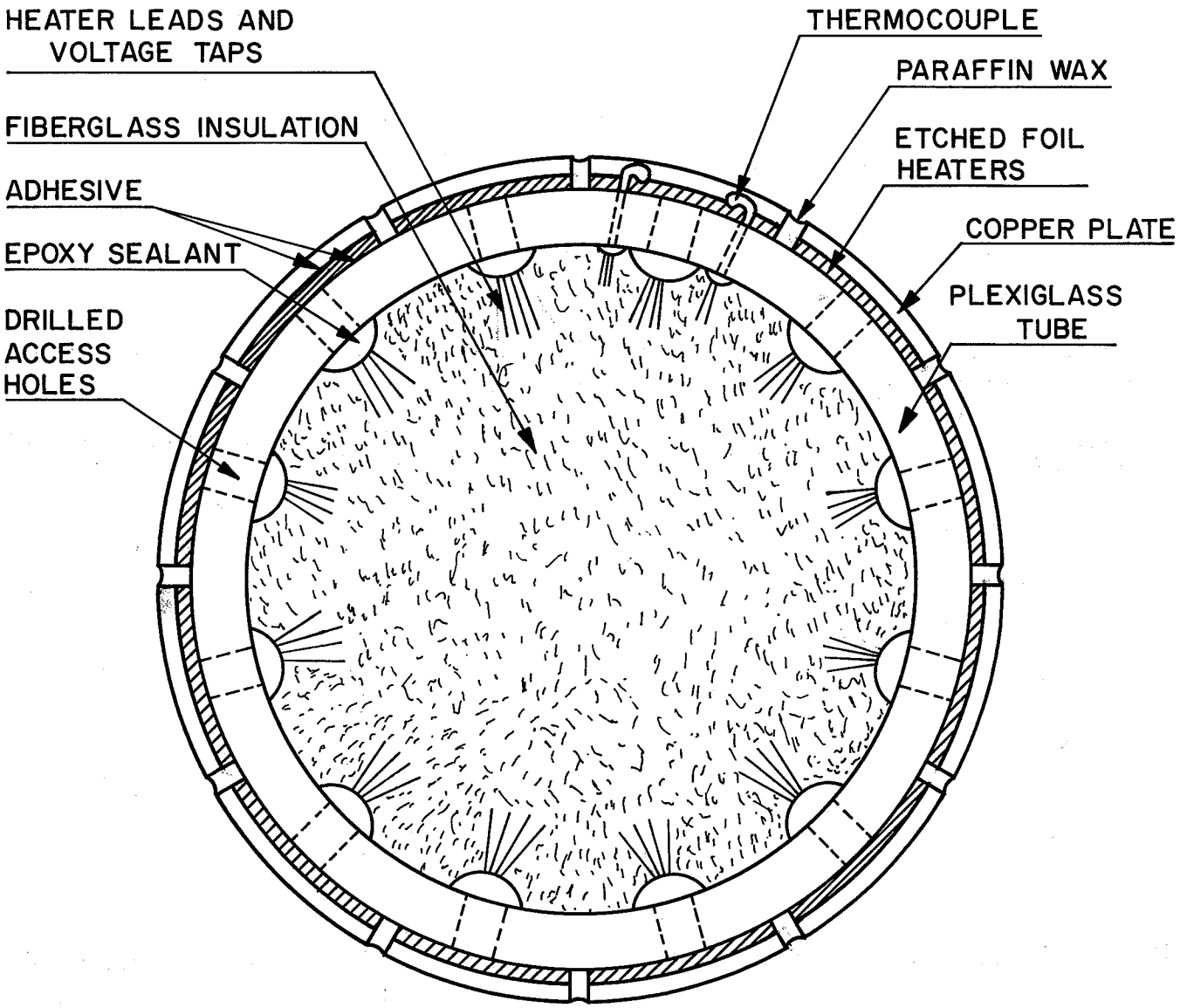

Fig. 9. CROSS-SECTION OF CYLINDER

(each pair of guard heaters on either side of a main heater were connected in series).

A circumferential profile was run with a dial guage at three different points on the main, or test section as a check on the roundness of the finished apparatus. The initial results indicated that there was a small tendency for the copper plates to flatten out once they had been cut from the larger tube. Small amounts of filing and polishing had to be performed on the edges of the plates to secure a finish of satisfactory roundness (See Appendix VI).

The final step was to fill in all of the internal cracks between the heaters with melted paraffin wax to insure that there was no thermal contact between the heaters and also to provide a continuous outer surface to insure a smooth free convective flow. The two outer circumferential edges between the guard heaters and the plexiglass tubing were sealed with a silicone sealant. The entire heated surface was then polished and a check of the average outside diameter was performed with vernier calipers (See Appendix VI).

Working from the inside of the plexiglass tubing, the holes for the thermocouple, voltage tap and heater leads were sealed with an epoxy cement to ensure that the inside of of the cylinder would be watertight. The wires were fed through to one end of the tubing and the remaining interior

space packed with fiberglass insulation. Three holes were made in the plexiglass tubing, close to one end and plexiglass fittings were cemented over them to provide an exit for the leads from the apparatus. All leads were led up through flexible 1.91 cm. (0.75 in.) I.D. plastic tubing to the outside of the tank. The hose was clamped to the plexiglass fittings and covered with silicone sealant. Plexiglass end plates were manufactured to fit onto the ends of the cylinder. All plexiglass-to-plexiglass connections were achieved using methylene chloride, a chemical which melts plexiglass surfaces and fuses them together. The assembled test section is illustrated in Figure 10.

2.2.2 The Tank and Support Structure

All of the analytic work on horizontal cylinders which was discussed in chapter 1 was based on two assumptions; an infinitely long cylinder and an infinite heat transfer medium, which in this case was water. Experimentally, neither criterion can be readily satisfied. The use of guard heaters practically eliminates end effects for cylinders of finite length, but the problem remains of how to simulate an infinite medium. If a tank is used to confine the water, it must be of sufficient size so that the confining surfaces (the tank walls and the free surface on top) do not appreciably affect the flow. The tank used in this experiment was 0.51 $m.^3$

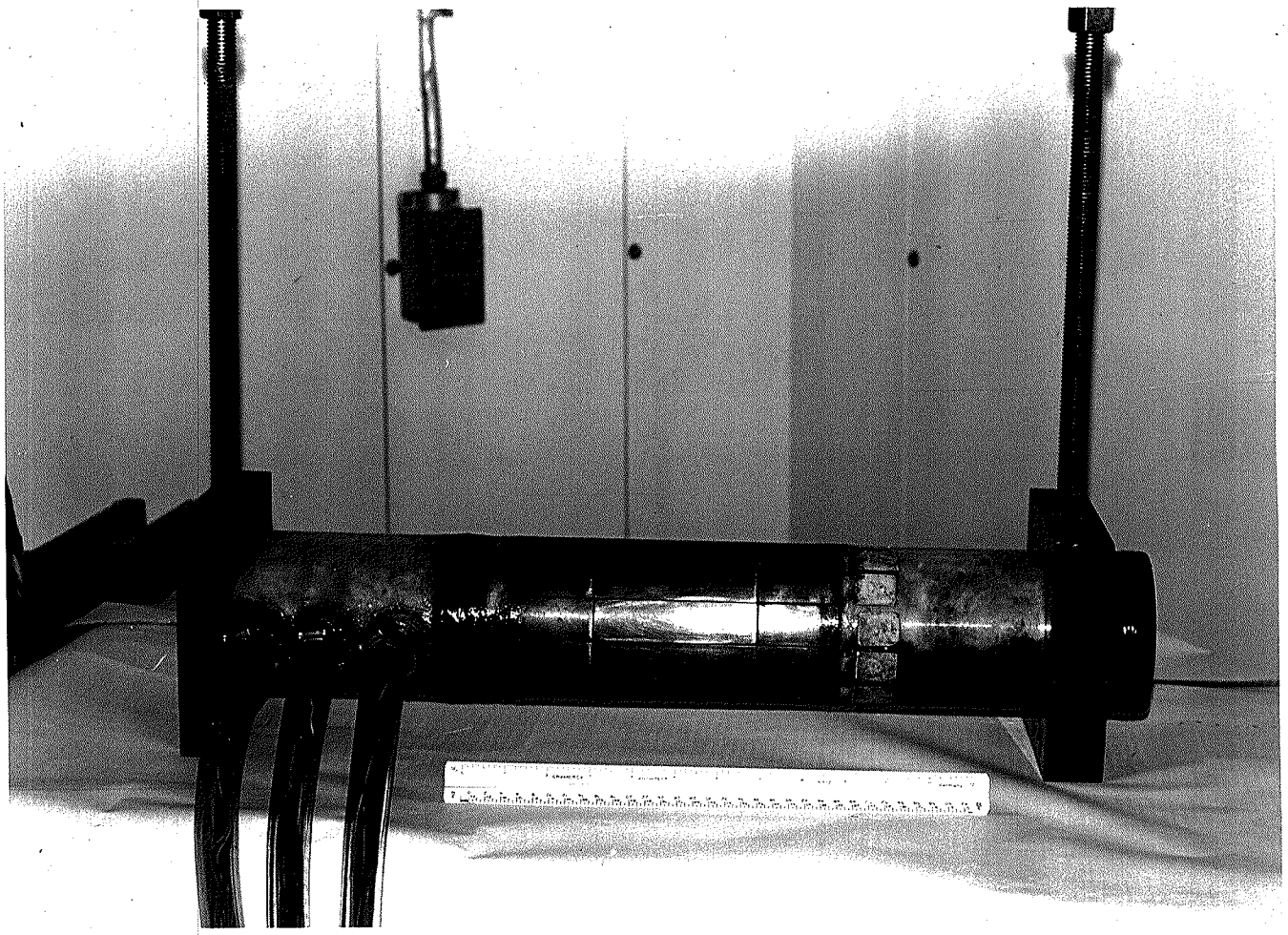

Figure 10

The Horizontal Cylinder Test Section

($18\ ft.^3$), measuring 60.96 cm. by 91.44 cm. by 91.44 cm. deep (2 ft. by 3 ft. by 3 ft. deep) and was constructed of 20 AWG AISI 304 stainless steel. A 5.08 cm. by 10.16 cm. (2 in. by 4 in.) wooden support stand was built for the tank to sit on in order to damp out vibrations from the fan motor and compressor in the refrigerated room and a wooden frame of similar dimensions constructed around the tank to increase the rigidity of the vertical sides of the tank and to provide a mounting surface for instruments and connections (See Figure 11).

Support for the cylinder was furnished by two 15.24 cm. (6 in.) square by 2.54 cm. (1 in.) thick blocks of PVC in which 10.16 cm. (4 in.) holes were machined. These fitted over each end of the plexiglass cylinder, leaving the cylinder loose enough to be turned by hand but tight enough to prevent rotation under test conditions. Threaded rods 1.59 cm. (0.625 in.) in diameter were screwed into these blocks. These rods were bolted to a steel support. This type of fixture allowed the cylinder to be adjusted infinitesimally, either rotationally around its longitudinal axis, or vertically in the tank (See Figure 12).

2.2.3 The Cold Room

The entire test setup was situated in a Coldstream refrigerated room whose temperature range was between $-18^{o}C$ and $24^{o}C$. Temperature control could be achieved to within

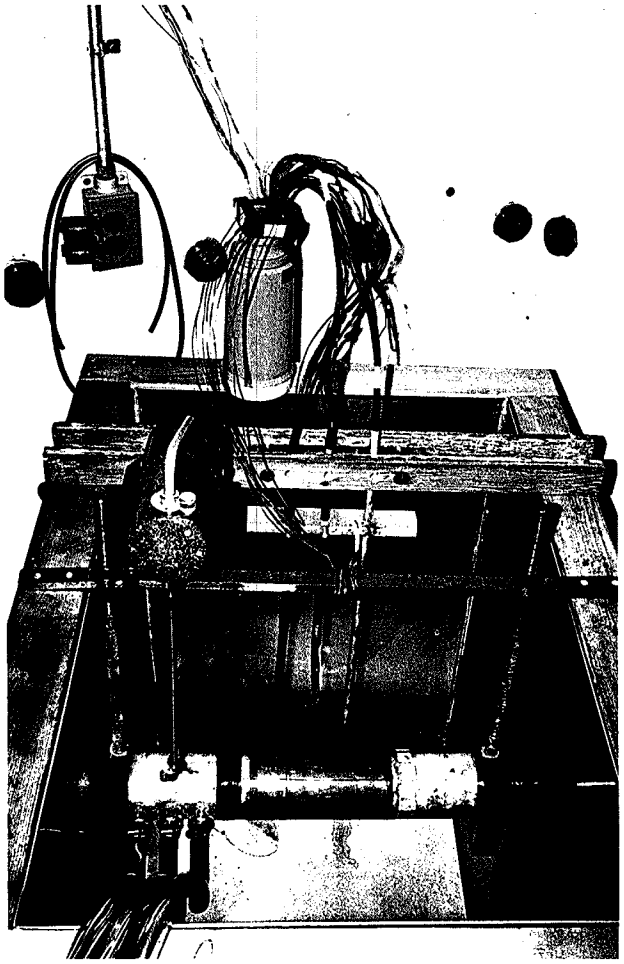

Figure 12

Interior of Test Tank and Cylinder Support

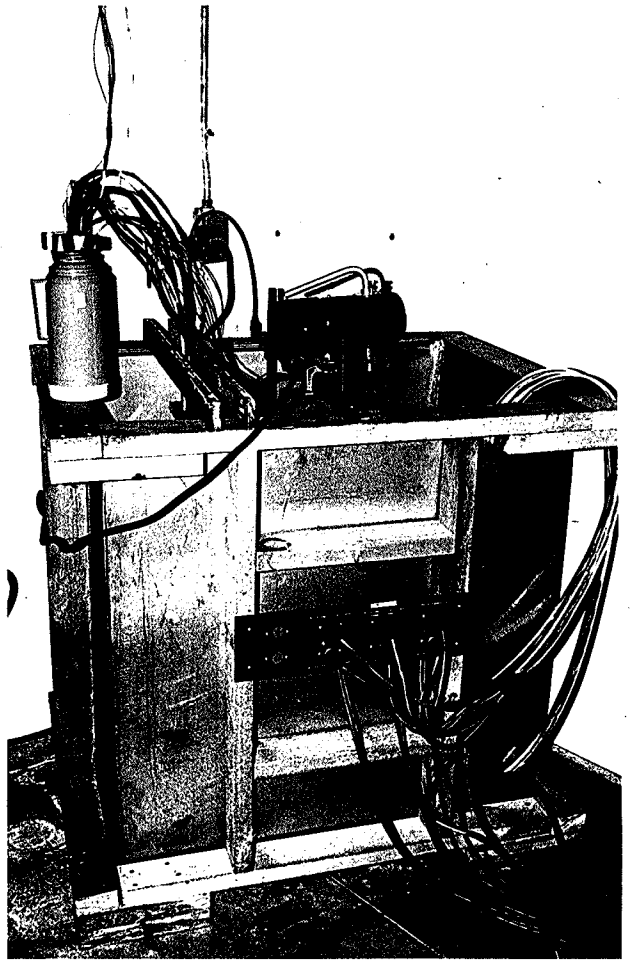

Figure 11

Exterior of Test Tank and Mounting Panel

± 0.5°C. The room was a walk-in type with inside dimensions of 183 cm. by 274 cm. by 244 cm. high (6 ft. by 9 ft. by 8 ft. high). Access ports were installed on the three exposed sides of the room to allow entry of electrical circuitry and hosing (See Figure 14).

2.2.4 The Heater Circuitry

A schematic of all heater circuitry is shown in Figure 13. A 1 KW high current, low voltage Hewlett Packard model 6260 D,C. power supply was used for the experimental study. Direct current was chosen for ease of power measurement and also for stability, since thermocouples were employed to measure surface temperatures. The power supply was connected to twenty-four parallel circuits, one circuit corresponding to each main heater and one corresponding to each pair of guard heaters on either side of a particular main heater.

Control of the power proportioned to each circuit was accomplished with the use of a rheostat and a potentiometer in parallel. The rheostats were Ohmite type L, rated at 150 W. Those in the main heater circuits were 5Ω while the rheostats in the guard heater circuits were 7.5Ω. Most of the current in each circuit flowed through these rheostats, so that they could be adjusted to provide rough control of the power through each circuit. Fine control was furnished with the use of Amphenol series 2201B, 10-turn, 50Ω micropots, each rated

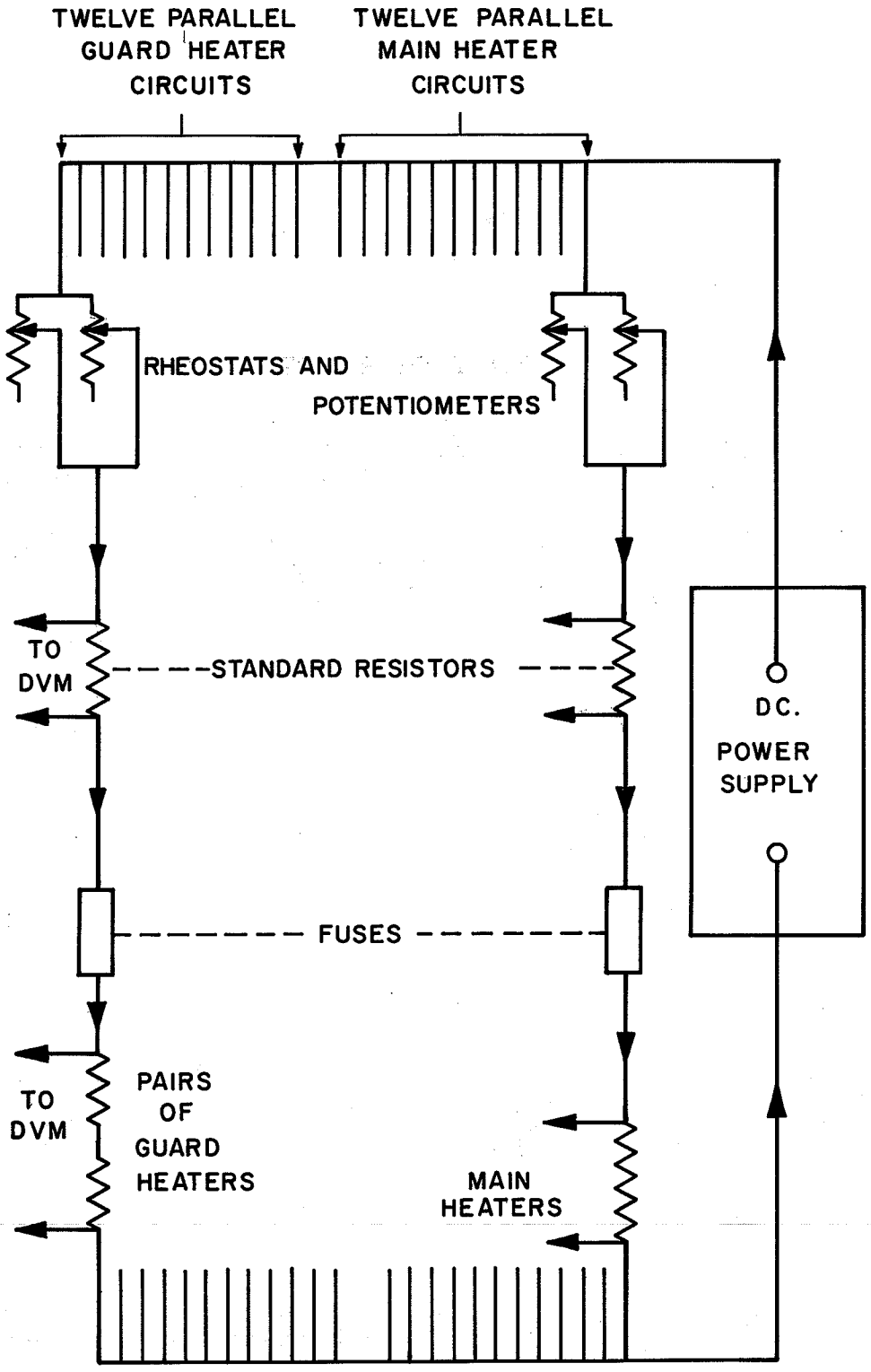

Fig. 13. SCHEMATIC OF HEATER CIRCUITRY.

at 5 W.

In order to measure the current through each circuit, an accurate calibrated resistor was incorporated into each circuit. The type used were Dale type RH50, 0.5Ω wire-wound resistors rated at 50 W with a tolerance within 1% (.005Ω). Voltage taps were connected on either side of each resistor. These resistors were mounted inside an aluminum box which was filled with mineral oil to maintain them at a constant temperature.

For overload protection, 2 A fuses were installed in each circuit. Since the maximum voltage of the power supply was 10 V, the fuses would blow at a maximum power of 20 W. The fuses also provided a means of controlling the number of heaters in operation during any test. All of these components were mounted in a control panel outside of the refrigerated room (See Figure 15). Leads from the fuses and also from the standard resistor voltage taps were soldered into female plugs at the back of the panel.

Inside the cold room, the incoming power leads to the test rig and the heater voltage taps were soldered into male plugs after exiting from the cylinder. The return power leads were connected to a bus-type clamp upon exit from the cylinder while the thermocouples were run directly to the control panel with no intermediate connections. Plug-in extension

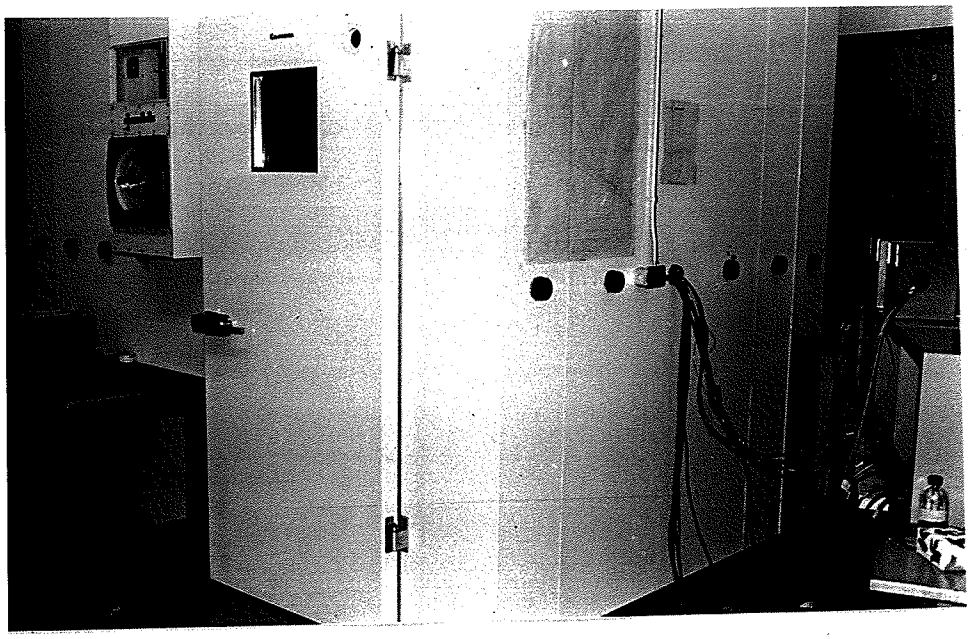

Figure 14

Exterior of Refrigerated Room

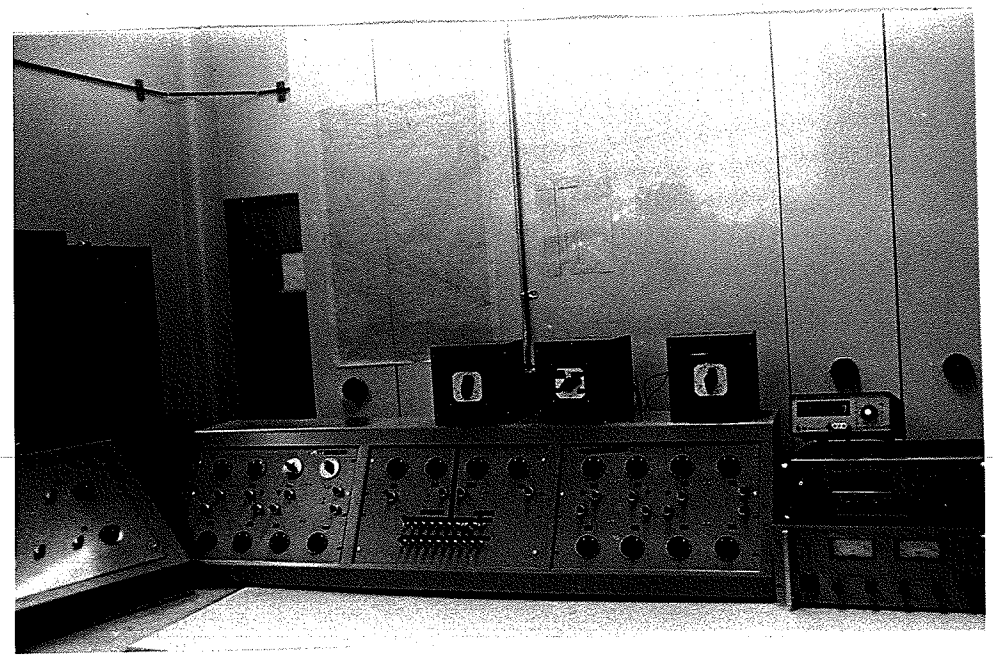

Figure 15

Control Panel and Instrumentation

cords were constructed to connect the incoming power leads and heater voltage taps to the control panel. A common return was furnished to the power supply with #2 stranded power cable. The common lead from the power supply was fed to a bus-bar in the control panel from which point power was distributed to the various components of the circuits.

2.2.5 The Measurement Systems

As previously mentioned, thirty-four 30 AWG copper-constantan thermocouples were used to measure surface temperatures around the cylinder. In order to obtain an accurate estimate of the bulk water temperature, three 9-point 20 AWG copper-constantan thermopiles were constructed. Their measuring junctions were cemented into starburst patterns and were mounted in L-shaped glass tubes which could be adjusted vertically in the tank. The tubes were held rigidly in a fixture which was in turn fastened to the support stand at the top of the tank. A fourth thermopile was constructed to monitor the air temperature in the refrigerated room. The thermocouples were wired in the switching apparatus so that a single reference junction was required. This reference junction, along with those of each of the thermopiles, were kept in a thermos bottle filled with finely crushed ice, which was kept inside the refrigerated room. By periodically supplying more ice to this cold junction, an accurate ice-point was maintained.

All thermocouple leads were connected to terminal strips in the control panel which were compensated for use with copper-constantan thermocouple wire. A styrofoam box was constructed around these terminals to eliminate stray voltages generated by temperature gradients across the connections. The copper leads from the cold junctions to the thermopiles were also connected to terminal strips in the control panel. The use of these terminal strips, together with the male and female plugs for the other components of the system, meant that the cylinder was completely removeable from the control panel. This meant that other apparatuses could be hooked up to the same control system.

After the terminal strips, the thermocouple and thermopile leads were connected to a series of Thermo-Electric double-pole, double-throw compensated thermocouple switches. These switches were soldered to the leads with thermal-free solder and then enclosed in a styrofoam box, again to eliminate temperature gradients.

The variables to be measured were thirty-eight surface temperatures, twenty-four heater voltage drops and twenty-four standard resistor voltage drops. To accomplish this, three different switches were required. The first was a Honeywell model 911AZ four-pole switch which was used to select which function was to be measured (i.e. temperatures,

heater voltage drops or standard resistor voltage drops). The other two switches were similar but with twenty-four poles each to measure heater or standard resistor voltage drops in each of the twenty-four circuits. Their leads were soldered into male plugs and connected to the appropriate receptacles on the control panel.

Connected to the first switch was the measuring device. A Hewlett Packard model 3440A digital voltmeter was used initially but its resolution was not small enough to accurately measure the thermocouple voltages. The instrument used for the bulk of the experimental work was a Keithley model 160 digital multimeter which could measure D.C. voltages as small as 1 μV. Surface and bulk water temperatures were calculated from the thermocouple and thermopile voltages. The current in each circuit was obtained from the voltage drops across each standard resistor and the known resistance. The power supplied to each heater was determined from the voltage drop across each heater (or pair of heaters) and the current in that circuit.

2.3 Experimental Procedure

In this experiment, the infinite heat transfer medium was simulated using a tank of water with a volume of 5.097 x 10^5 cm^3 (0.51 m^3). Fand and Keswani [14] hypothesized that the cylinder should be a minimum of ten diameters below the

free surface (Y/D = 10) to allow for a build-up of a heated layer of fluid on the free surface. For a cylinder the size of the one used in the present work, this would have meant placing the cylinder at least 105.4 cm. below the surface. Since the present study included a region of downflow, it was also reasonable to assume that the cylinder should be placed in the middle of the tank, in order to allow for a build-up of a heated layer at the bottom of the tank as well. These two facts would have necessitated a tank depth of over two meters.

A more likely controlling parameter was one which included the driving force, θ_p, since θ_p determines the heat transfer rate and hence the amount of hot fluid. It was proposed to use $(Y/D)/\theta_p$ as this parameter. The minimum value of this ratio used by Fand and Keswani was 0.41. The maximum theoretical temperature excess, at least in the bidirectional region, was 26.8°C, which would have meant positioning the cylinder 115.8 cm. below the surface. However, if the driving force was restricted to approximately 10°C, then the cylinder would theoretically only need to have been placed 43 cm. below the surface. In fact, the actual water depth used was 86 cm. with the cylinder centered in the tank. According to the above criterion, this restricted the driving force, θ_p, to 10°C. Some tests were performed successfully above this temperature difference (i.e. a steady state cylinder temperature was obtainable), indicating that the minimum allowable ratio

of $(Y/D)/\theta_p$ was not absolutely correct.

In order to obtain isothermal surface conditions, it was necessary to individually adjust and readjust the currents in twenty-four heater circuits. Time was required between adjustments to allow the heaters to reach steady state conditions and following this, to record the voltage drops across the twenty-four heaters as well as the thirty-four thermocouple and four thermopile voltages. For the test with the maximum heat rate (test #1), assuming no heat was lost to the cold room, the overall temperature rise for a completely mixed tank (i.e. homogeneous temperature) would have been 0.14 ^{o}C/hr. Since the tank was not mixed, the temperature rise locally in some parts of the tank would have been much higher. According to equation (1-46), derived by Fand and Keswani, the heated layer in this particular test would have descended to the level of the cylinder in approximately thirteen minutes. The major problem then, during the experimental work, was trying to complete a test before the arrival of the descending (or rising) layer of heated water, as detected by the thermopiles.

Initially the cold room was set at roughly the desired temperature and the tank brought to equilibrium with the room using an electric mixer. Finer adjustments of the bulk water temperature were accomplished by adding ice to the tank or by turning on the heaters for short periods of time

with the mixer operating. When the tank was fully mixed and at the desired temperature, the mixer was turned off and the water allowed to come to rest. Neutrally buoyant spheres in the water indicated when all motion had ceased.

Each region was investigated separately during the course of the experiment, beginning with region III (upflow). Initially, all rheostats and potentiometers were set at their maximum resistances and the power supply turned on. Each circuit was then roughly adjusted with the rheostats to obtain an angular power distribution over the cylinder which was similar to the distribution derived by Hermann [18]. After the thermocouples had reached steady state, they were monitored in order to see what adjustments had to be made to the power settings. The process of adjusting these variable resistances and scanning the thermocouples continued until the cylinder was isothermal. At this point, the thirty-four thermocouple and four thermopile voltages were scanned and recorded. Following this, the standard resistor and heater voltage drops were scanned, recorded and checked and finally the thermocouples and thermopiles were checked and recorded again. All of the temperatures which were calculated were based on the average of the two sets of thermocouple and thermopile readings. The entire process took anywhere from fifteen minutes to forty-five minutes, depending on the region and on the magnitude of the driving force, θ_p.

The most difficult tests were the first ones in each region. In these tests, the power settings often had to be radically altered from the tests in the previous region and as a result, a lot of time was required to come to the steady state. In one region in particular, region II-S, the initial test could not be completed before sufficient heat had been generated in the tank to affect the thermopiles. However, once a pattern of power settings had been established in each region, the remaining tests in that region required only minor adjustments to attain isothermal conditions.

The only real problem encountered during the testing process was in region IV, the last one investigated. At the higher bulk water temperatures in this region, air came out of solution and adhered to the surface of the cylinder in the form of small air bubbles. These bubbles had the capacity to severely affect the heat transfer characteristics, if the testing prodedure was of long enough duration to allow them to form. Care had to be taken after each test in this region to inspect the cylinder so as to decide whether or not the results of that test were meaningful. Just prior to each test in this region, the entire cylinder was wiped free of air bubbles. The testing procedure required considerable practice to perfect the technique for obtaining isothermal conditions, However, the design of the apparatus permitted very accurate local measurements to be taken.

CHAPTER 3

ANALYSIS OF RESULTS

3.1 Distribution of Results

In this experiment, data was collected at fifty-six points in the four different flow regions defined by Yuill [48]. The boundaries between the regions are given in Appendix VII. However, Yuill's arbitrary location of the border between separated and non-separated flow, $\phi = -0.6$, did not fit the data of the present experiment very well. An examination of the properties of the boundary layer in region II revealed that Σ, the point in the boundary layer whose density was the same as that of the bulk fluid, seemed to be the controlling parameter. With the value $\Sigma = 0.31$ arbitrarily chosen as the point of comparison, the data could be divided into two groups, one with values of Σ above 0.31 and the other below 0.31 (See Appendix VII).

With these fixed boundaries, the experiments were distributed in the following manner. Three tests were conducted in the downflowing region I, twenty-one in the separated bidirectional region II-S, fourteen in the non-separated bidirectional region II-N and eighteen in the upflowing regions III and IV (seven in region III and eleven in region IV). The distribution of results is graphically presented in Figure 16.

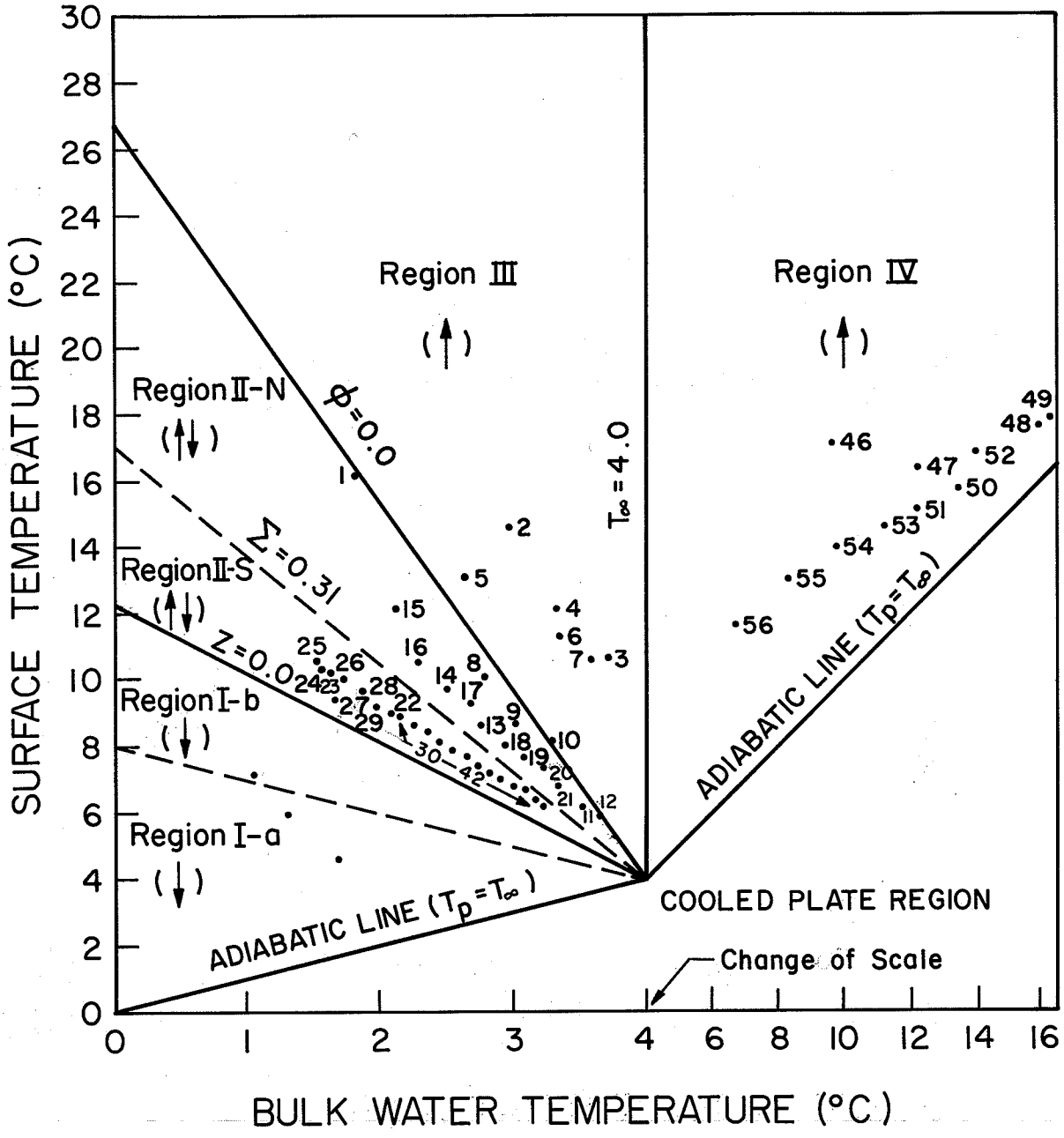

Fig. 16. Distribution of Results.

3.2 Calculation of Heat Transfer Variables

All heat transfer calculations were performed on an IBM 370/75 digital computer. Thermocouple and thermopile voltages were converted to temperatures as the initial step. Deviations from the isothermal condition are shown in Table 11 in Appendix VIII. The maximum percentage deviation on each plate ranged from -6.80% to 5.27% while the root mean square percentage deviation on each plate varied from 0.69% to 4.93%.

The current in each circuit was calculated from the known resistance of each standard resistor and the voltage drop through that particular standard resistor. The power to each main heater (or pair of guard heaters) was found from the previously calculated current and the voltage drop across the heater. Power losses by conduction along the tubing, insulation, leads, etcetera, were not of sufficient magnitude to be important to the experimental results. A discussion of these and other related experimental errors is presented in Appendix VIII.

Since the heat transfer results were symmetrical about a vertical plane through the center of the cylinder, calculations were only performed for the six main heaters on one side of this plane. The other readings were taken only as a check on the symmetry of the apparatus. All of the calculations were performed using the variable fluid property relations described in Appendix IV, in conjunction with a reference temperature, taken to be the film temperature of the boundary layer.

3.3 Presentation of Results

As previously mentioned, the purpose of the present experimental investigation was twofold; first to correlate the local heat transfer data and second to correlate the average heat transfer data. This necessitated two different methods of presentation of the results.

3.3.1 Local Heat Transfer Results

One method of presentation would have been to graph the variation of the local heat transfer coefficient, $h(\xi)$ with the angular position, ξ. As can be seen in Figure 17, the drawback was that although the profiles in the same region might have similar shapes, they would still not necessarily coincide with one another because they were also functions of the driving force, θ_p. Also, Hermann's analytical solution for the heat transfer coefficient was a function of his surface temperature function, $t'(0)$, which in itself was a function of the Prandtl number (i.e. a function of the fluid itself). By presenting the results as the ratio of the local value of the heat transfer coefficient over the average value, $h(\xi)/\overline{h}$, versus the angle, ξ, both of these problems could be eliminated.

3.3.2 Average Heat Transfer Results

Most conventional correlations are of the form:

$$\overline{Nu} = C(Gr \cdot Pr)^{1/4} \quad \text{.....(3-1)}$$

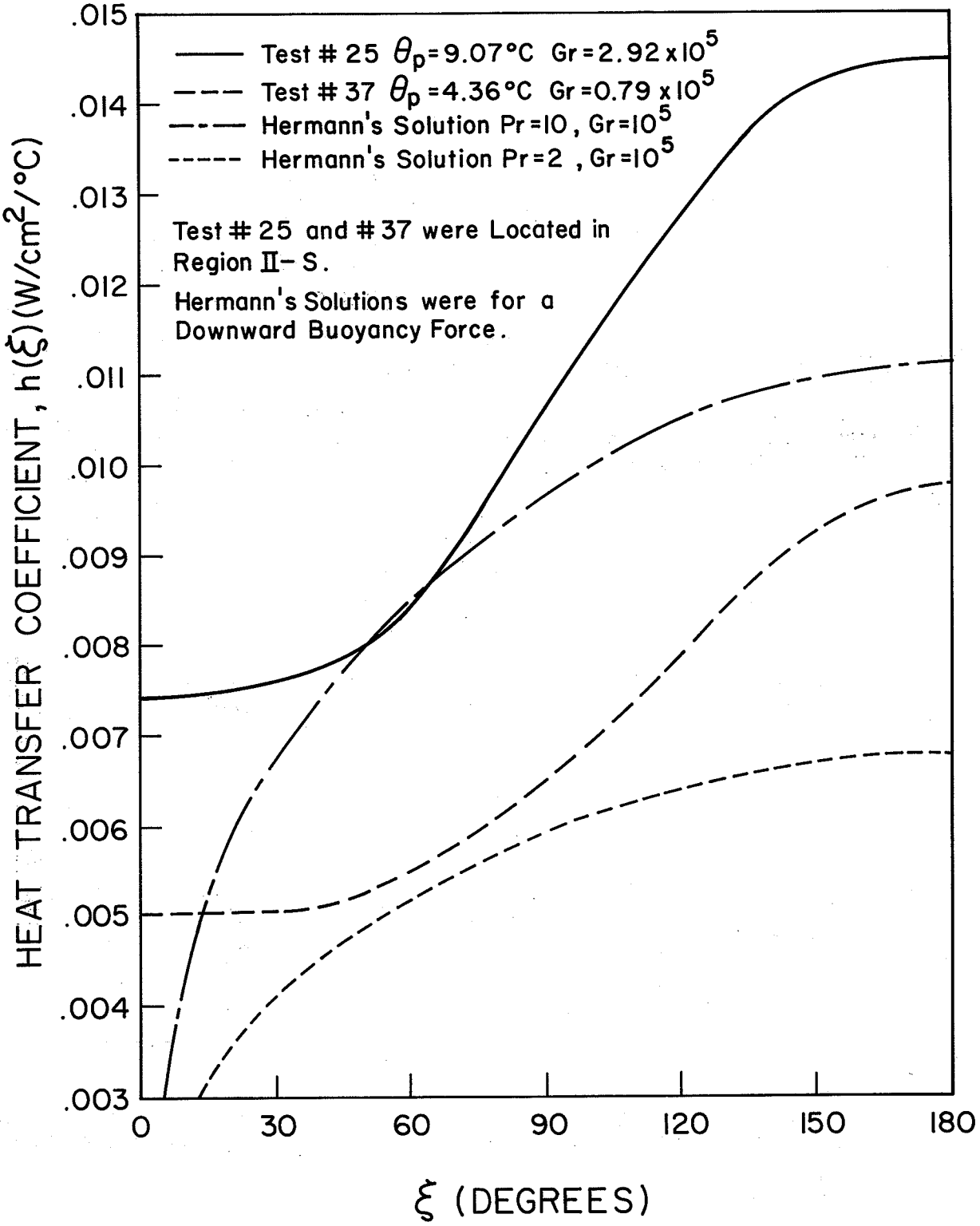

Fig. 17. Heat Transfer Coefficient, h (ξ) Versus Angle, ξ

Yuill [48] presented his results in an analogous manner and correlated the coefficient C against various parameters in the region around a bulk water temperature of $4^{o}C$. Therefore, in order to compare the results for a horizontal cylinder with those of Yuill for a vertical flat plate, the average heat transfer results of the present experiment were presented in a similar manner. The average heat transfer coefficients and Nusselt numbers in the present investigation were calculated by taking the average of the six local values around the circumference of half of the cylinder. They therefore represent the averaging of a stepwise changing relationship, instead of a continuous one. This in itself introduced an error into the anlaysis but since it would not have been practical to incorporate more heaters into the apparatus, this error could not be minimized any further.

3.4 Correlation of Local Data With Hermann's Solution

The values of the ratios, $h(\xi)/\overline{h}$, plotted versus angle, ξ, for each region in Figure 18, were obtained by averaging the values of all of the tests in each particular region. Local values of this heat transfer ratio are tabulated in Table 1. The average values of $h(\xi)/\overline{h}$, as well as the root mean square deviations for each region are presented in Table 2. Values of ξ were taken as the midpoint of each heated section.

TABLE 1

Experimental Results - $h(\xi)/\overline{h}$ For Each Test

Test No.	Region	Angle (degrees) 15	45	75	105	135	165
1	II-N	1.193	1.049	0.964	0.866	0.741	1.187
2	III	1.233	1.133	1.037	0.949	0.751	0.898
3	III	1.201	1.181	1.119	1.056	0.800	0.643
4	III	1.201	1.172	1.124	1.054	0.800	0.649
5	III	1.180	1.059	0.993	0.923	0.755	1.090
6	III	1.192	1.166	1.100	1.055	0.810	0.677
7	III	1.216	1.201	1.081	1.081	0.817	0.603
8	II-N	1.107	1.016	0.992	0.927	0.763	1.196
9	II-N	1.089	1.048	0.989	0.875	0.799	1.201
10	III	1.176	1.052	0.958	0.943	0.820	1.051
11	II-N	1.191	1.114	0.993	0.976	0.848	0.879
12	II-N	1.133	1.074	0.996	0.978	0.853	0.967
13	II-N	1.025	0.958	0.904	0.876	0.877	1.360
14	II-N	1.047	0.959	0.893	0.903	0.862	1.337
15	II-N	1.111	0.998	0.966	0.941	0.805	1.179
16	II-N	1.034	0.954	0.931	0.859	0.854	1.369
17	II-N	1.141	0.966	0.931	0.855	0.813	1.293
18	II-N	1.138	0.946	0.931	0.881	0.813	1.291
19	II-N	1.091	0.983	0.959	0.922	0.818	1.226
20	II-N	1.107	1.050	0.998	0.939	0.854	1.052
21	II-N	1.157	1.015	0.973	0.921	0.872	1.062
22	II-S	0.727	0.738	0.838	1.105	1.290	1.303
23	II-S	0.728	0.736	0.839	1.098	1.280	1.320
24	II-S	0.643	0.725	0.953	1.159	1.235	1.285
25	II-S	0.693	0.727	0.884	1.080	1.276	1.341
26	II-S	0.698	0.709	0.861	1.135	1.273	1.324
27	II-S	0.379	0.831	1.090	1.196	1.228	1.275
28	II-S	0.730	0.748	0.831	1.037	1.311	1.343
29	II-S	0.675	0.678	0.919	1.127	1.304	1.296
30	II-S	0.713	0.678	0.925	1.111	1.279	1.293
31	II-S	0.701	0.690	0.960	1.131	1.243	1.275
32	II-S	0.707	0.701	0.961	1.116	1.241	1.274
33	II-S	0.730	0.695	0.919	1.064	1.268	1.323
34	II-S	0.718	0.690	0.899	1.106	1.255	1.333
35	II-S	0.725	0.663	0.902	1.066	1.269	1.377
36	II-S	0.710	0.719	0.969	1.107	1.179	1.317
37	II-S	0.728	0.736	0.861	1.025	1.257	1.394
38	II-S	0.662	0.693	0.862	1.025	1.312	1.446
39	II-S	0.701	0.782	0.900	0.996	1.205	1.414

TABLE 1 (continued)

Experimental Results - $h(\xi)/\overline{h}$ For Each Test

Test No.	Region	Angle (degrees) 15	45	75	105	135	165
40	II-S	0.779	0.766	0.871	0.974	1.199	1.412
41	II-S	0.755	0.824	0.863	0.987	1.186	1.386
42	II-S	0.767	0.781	0.827	0.985	1.218	1.422
43	I	0.683	0.890	0.956	1.042	1.186	1.243
44	I	0.558	0.864	1.025	1.120	1.206	1.227
45	I	0.611	0.901	1.026	1.128	1.163	1.172
46	IV	1.100	1.091	1.064	1.059	0.808	0.878
47	IV	1.201	1.115	1.072	1.086	0.797	0.729
48	IV	1.239	1.165	1.065	1.072	0.818	0.642
49	IV	1.239	1.163	1.066	1.072	0.818	0.642
50	IV	1.263	1.189	1.077	1.065	0.797	0.608
51	IV	1.273	1.249	1.101	1.006	0.789	0.583
52	IV	1.260	1.254	1.118	0.994	0.789	0.585
53	IV	1.231	1.206	1.131	1.020	0.821	0.591
54	IV	1.247	1.209	1.129	1.003	0.816	0.597
55	IV	1.231	1.202	1.119	1.021	0.814	0.613
56	IV	1.255	1.258	1.116	0.974	0.795	0.601

TABLE 2

Experimental Results - $h(\xi)/\overline{h}$ For Each Region

Region		Angle (degrees) 15	45	75	105	135	165
I	$h(\xi)/\overline{h}$	0.618	0.885	1.002	1.097	1.185	1.214
I	σ	0.063	0.019	0.040	0.048	0.022	0.037
II-S	$h(\xi)/\overline{h}$	0.699	0.729	0.902	1.078	1.253	1.341
II-S	σ	0.080	0.046	0.062	0.062	0.040	0.054
II-N	$h(\xi)/\overline{h}$	1.112	1.009	0.959	0.908	0.827	1.186
II-N	σ	0.053	0.052	0.035	0.041	0.041	0.149
III-IV	$h(\xi)/\overline{h}$	1.216	1.161	1.071	1.014	0.800	0.737
III-IV	σ	0.040	0.065	0.055	0.060	0.026	0.190

where σ is the standard deviation of the data in each region.

In Figure 18a, the results are plotted for regions I and II-S. Also plotted is Hermann's analytical solution for a region with a downward buoyancy force, which is a mirror image of his solution for the upward buoyancy force case. As could be expected, in region I (downflow), the experimental results were almost identical to the analytic solution. Although only three tests were performed in this region, the local results were considered quite reliable by the author, since the average heat transfer results in this region also correlated well. The deviation of the two curves at small values of ξ was also expected because Hermann's curve approaches zero while in the actual case, the boundary layer theory breaks down in this region of ξ and the heat transfer from the cylinder to the sinking plume of warm fluid decreases to some finite value. The results in region II-S, the region of separated bidirectional flow, were generally similar in shape to those in region I. It was evident from the slope of the graph that the outer, downward flowing boundary layer predominated in this area. The levelling out of the results at small values of ξ was attributed to either unsteady effects or increased mixing in the sinking plume of fluid which were not explainable using conventional boundary layer theory.

In Figure 18b, the results are presented for regions II-N, III and IV, along with Hermann's theoretical solution.

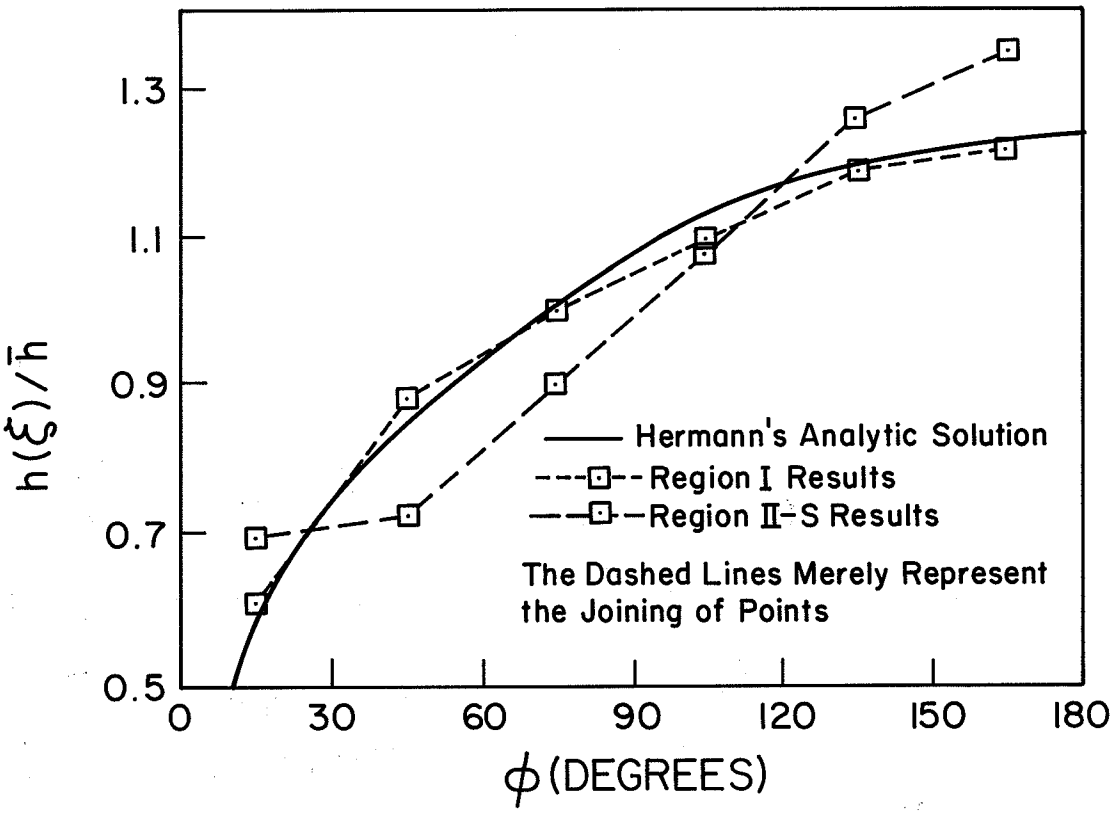

Fig. 18a Dimensionless Heat Transfer Ratio, $h(\xi)/\bar{h}$ Versus Angle, ξ in Regions I and II − S.

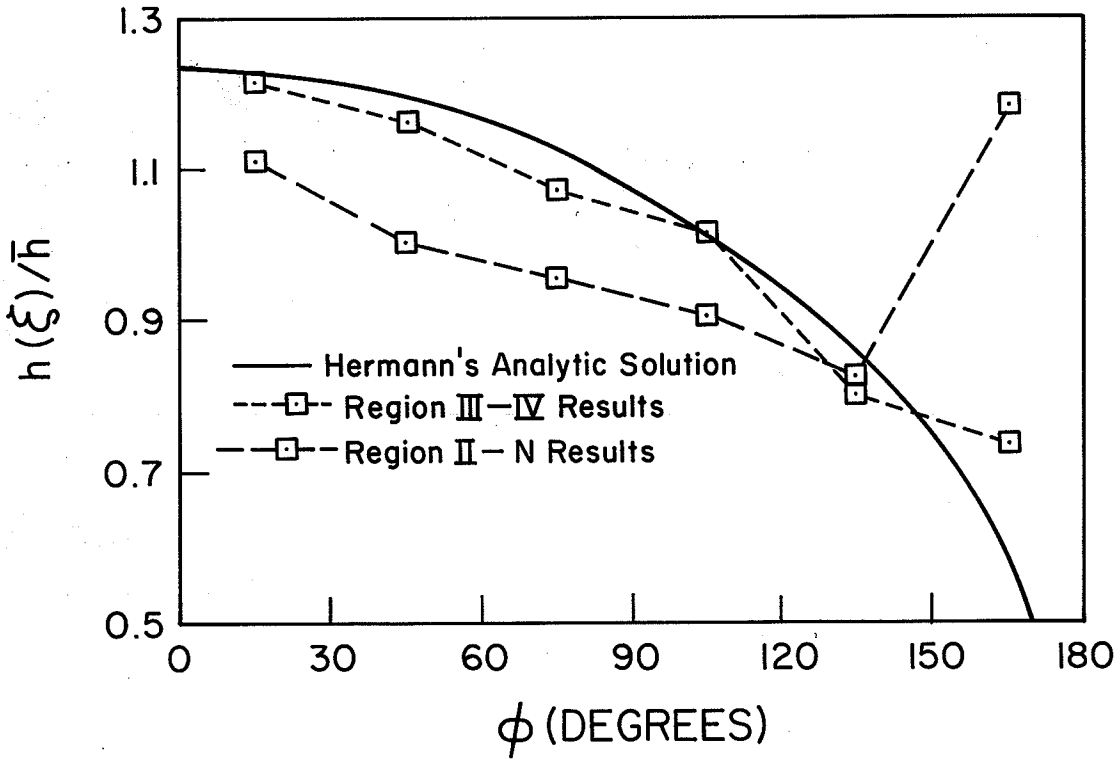

Fig. 18b Dimensionless Heat Transfer Ratio, $h(\xi)/\bar{h}$ Versus Angle, ξ in Regions II − N, III and IV.

Again his solution is not valid in the area above 150^{o} because the boundary layer approximations are no longer valid in this area (i.e. there is no longer a boundary layer but a plume of rising fluid). The results for regions III and IV (upflow) compare quite favorably with the analytic solution up to $\xi = 150^{o}$. In the actual case, at values of ξ above 150^{o}, the heat transfer ratio does not go to zero as predicted, but tends to some finite value. Upon examination of individual test results in Table 1, it was evident that some unsteadiness at large values of ξ was present for a few cases in this area, particularly in region III. The results for region II-N, the region of non-separated bidirectional flow, demonstrated the same general trend in slope of the curve up to a point around $\xi = 150^{o}$. Again the actual test results indicated a very high value of this ratio for the last heater, most likely due once more to an increased exchange of energy in the plume, accentuated by the presence of two boundary layers flowing in opposite directions.

3.5 Correlation of Averaged Data With Yuill's Hypotheses

3.5.1 Unidirectional Downflow: Region I

In this region, Yuill used a similarity transformation to solve the boundary layer equations and derived a semi-empirical formula for the coefficient C_I in the formula

for the local Nusselt number:

$$Nu_x = C_I (Gr_x \cdot Pr)^{1/4} \quad \ldots\ldots\ldots\ldots\ldots\ldots (3\text{-}2)$$

$$\text{or } h_x = C_I (k/x) \cdot (Gr_x \cdot Pr)^{1/4} \quad \ldots\ldots\ldots\ldots\ldots\ldots (3\text{-}3)$$

where C_I was a function of α, the dimensionless boundary layer buoyancy function (equation 1-55). By integrating the expression for the heat transfer coefficient over the plate surface, it can easily be shown that:

$$\overline{Nu} = (4/3) \cdot Nu_x \Big|_{x=L} \quad \ldots\ldots\ldots\ldots\ldots\ldots (3\text{-}4)$$

In order to relate these results to a horizontal cylinder, equation (1-18), derived by Hermann, was employed:

$$\text{If } D = L, \ \overline{Nu}_D = 0.777 \ \overline{Nu}_L \quad \ldots\ldots\ldots\ldots\ldots\ldots (3\text{-}5)$$

Combining both of the above, it was determined that Yuill's local values of the coefficient C_I for a vertical flat plate could be modified for the average heat transfer results from a horizontal cylinder by multiplying them by 1.036:

$$C_I = 0.5884 - 0.1015[1 - \exp(AZ + BZ^2 + GZ^3 + DZ^4)] \quad \ldots\ldots\ldots\ldots\ldots\ldots (3\text{-}6)$$

where $Z = \alpha - 0.02825$

$A = -23.043$

$B = 130.688$

$G = -469$

and $D = 406$

The results of the three tests performed in this region and comparisons with the theoretical model are presented in Table 3. The average and root mean square percentage deviations of the experimental data were 1.93% and 2.57% respectively. Although the results were in close agreement with Yuill's correlation, an insufficient number of tests were conducted for the correlation to be considered verified. Figure 19 graphically presents the relationship of C_I as a function of α for the horizontal cylinder, as well as showing the location of the experimental points.

TABLE 3

Comparison of Experimental and Analytical Heat Transfer Results in Region I

Test No.	α	Z	C_I (theoretical)	C_I (experimental)	Error(%)
43	.20430	.17605	.4985	.5113	2.57
44	.12305	.09480	.5125	.5164	0.76
45	.15872	.13047	.5054	.5178	2.45

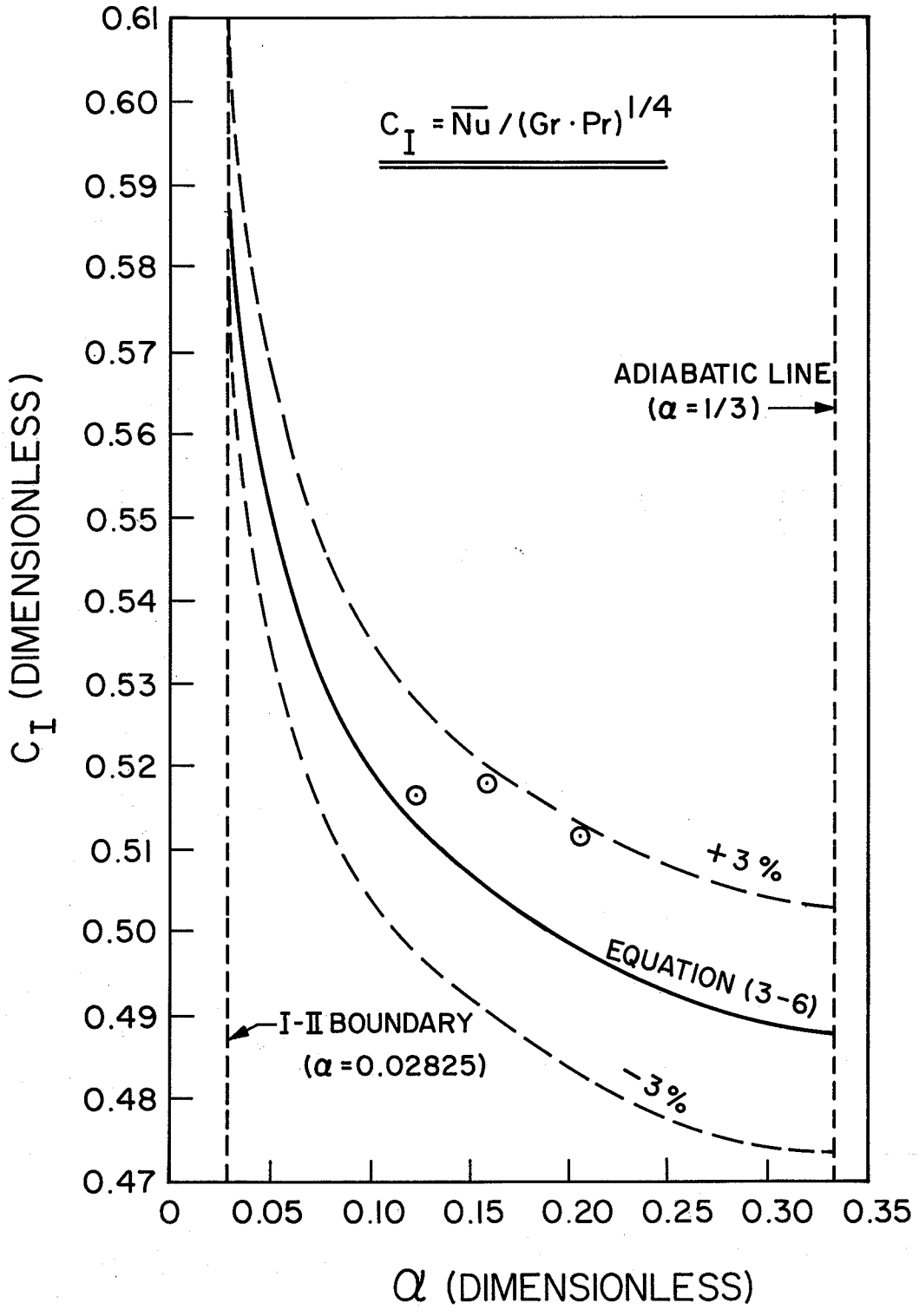

Fig. 19. Coefficient C_I Versus α in Rigion I.

3.5.2 Unidirectional Upflow: Regions III and IV

These regions were again ones in which a similarity transformation of the boundary layer equations was possible. Yuill solved the boundary layer equations and once more derived a formula to match the values of C_{III-IV} with the theoretical results. He found that, in this instance, α could not be used successfully as the correlating variable but that ϕ, the perpendicular distance from the II-III boundary, could be successfully employed.

As in region I, Yuill's local values of C_{III-IV} for a vertical flat plate were modified in order to compare them with the experimental average values for the horizontal cylinder:

$$C_{III-IV} = 0.4413 + 0.0404[1 - \exp(A\phi + B\phi^2 + G\phi^3 + D\phi^4)] \quad \ldots\ldots\ldots\ldots (3\text{-}7)$$

where $A = -1.28369\ {}^{o}C^{-1}$

$B = 0.321533\ {}^{o}C^{-2}$

$G = -0.0581512\ {}^{o}C^{-3}$

and $D = -0.00377369\ {}^{\Theta}C^{-4}$

Eighteen tests were performed in these two regions. The results of these tests along with a comparison to the theoretical

solutions are presented in Table 4. Figure 20 shows the variation of C_{III-IV} with ϕ, as well as the experimental results. The average percentage deviation from Yuill's correlation in these regions was 1.02% while the root mean square deviation was 8.79%.

The results, however, had more significance when they were broken down into two separate regions. It was clear that with the exception of test #3, all of the experimental results in region III were lower than predicted while in region IV, with the exceptions of tests #46 and #47, all of the experimental results were higher than those predicted by Yuill's correlation. There were three possible explanations for these discrepancies. The first was that Yuill's correlation was not accurate. The second was that Hermann's relationship between the average Nusselt numbers for flat plates and horizontal cylinders was incorrect and the third was that there was some systematic error in the results.

At large values of ϕ, Yuill's correlation for the flat plate correctly converged to Ostrach's solution for a fluid with a Prandtl number of ten, which was 5% higher than McAdams' correlation of experimental data for vertical flat plates. Yuill's correlation in this region was based on an analytic solution and should therefore be quite accurate. Hermann's analytic solution for a fluid with a Prandtl number

TABLE 4

Comparison Of Experimental And Analytical
Heat Transfer Results In Regions III And IV

Test No.	Region	ϕ	C_{III-IV} (theoretical)	C_{III-IV} (experimental)	Error(%)
2	III	0.8168	.4648	.4203	-9.57
3	III	0.9004	.4660	.5041	8.18
4	III	0.7506	.4637	.4453	-3.97
5	III	0.2403	.4515	.4482	-0.73
6	III	0.6144	.4613	.4243	-8.02
7	III	0.7272	.4633	.4258	-8.09
10	III	0.0231	.4425	.3883	-12.25
46	IV	7.7574	.4817	.4310	-10.53
47	IV	10.2068	.4817	.4410	-8.45
48	IV	13.9544	.4817	.5348	11.02
49	IV	14.4028	.4817	.5364	11.36
50	IV	11.3035	.4817	.5274	9.49
51	IV	9.9989	.4817	.5351	11.09
52	IV	12.0272	.4817	.5374	11.56
53	IV	8.8885	.4817	.5030	4.42
54	IV	7.3418	.4817	.5086	5.58
55	IV	5.8180	.4817	.4946	2.68
56	IV	4.0187	.4814	.5031	4.51

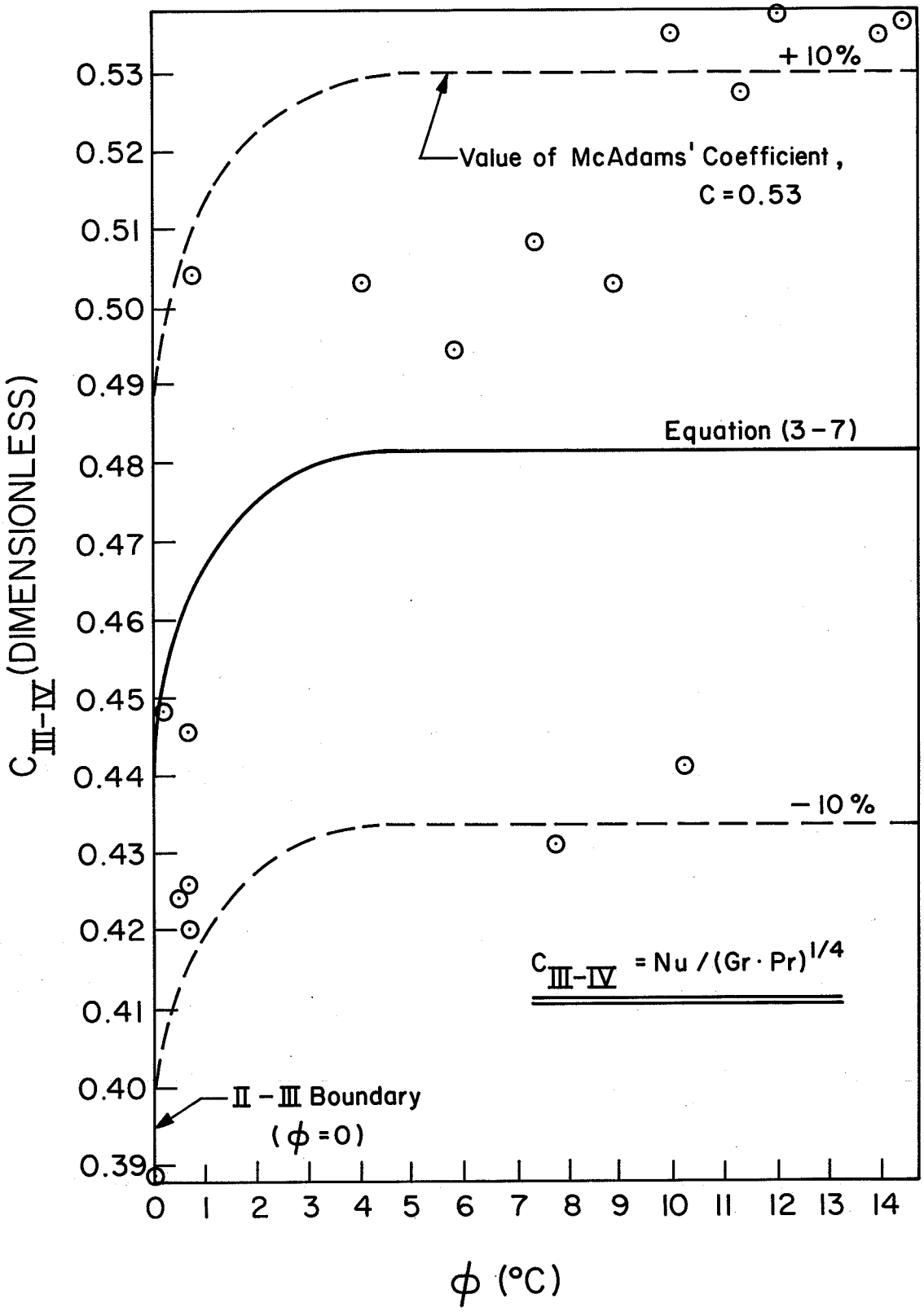

Fig. 20. Coefficient C_{III-IV} Versus ϕ in Regions III and IV

of ten, as given by equation (1-40), did not agree with McAdams' correlation of experimental data for horizontal cylinders but in fact was 10% lower than this experimental correlation. An inspection of the test results for the smaller values of ϕ revealed that the temperatures in the tests with the highest deviations from the correlation had not reached steady state but were still increasing. This would cause the Nusselt number and hence the coefficient C_{III-IV} to be artificially low. These tests were among the first experiments performed. The experimental values of C_{III-IV} at large values of ϕ seemed to converge towards McAdams' value of 0.53. The final conclusion that was drawn was that the values of C_{III-IV} in the lower regions of ϕ should have been higher, owing to experimental error and that the entire correlation should have been shifted upward 5-10% due to an apparent inaccuracy in Hermann's correlation of flat plate and horizontal cylinder results.

3.5.3 Bidirectional Non-Separated Flow: Region II-N

In this region, no analytic solution was possible. In order to correlate his experimental data, Yuill developed his own empirical equation between C_{II-N} and ϕ, the perpendicular distance from the II-III boundary. C_{II-N} was related to the inner boundary layer which was thought to be dominant in this region. His experimental data had a root mean square

deviation of 6.35% from this equation. When this line was modified for the average results from a horizontal cylinder, it was found that the present experimental data had an average error of 1.55% and a root mean square deviation of 5.79% from Yuill's modified correlation, which was given by:

$$C_{II-N} = 0.3548 + 0.0829\phi \quad \text{.....(3-8)}$$

The fact that the present data fitted the correlation better than Yuill's own data seemed to indicate that the correlation well represented the variation of data in this region.

However, upon closer examination of Yuill's equation it was noted that the matching of C_{II-N} and C_{III-IV} at the II-III boundary was not correct. That is to say, Yuill's constant was determined by assuming that at $\phi = 0$:

$$\begin{aligned} C_{II-N}/C_{III-IV} &= (\alpha/\alpha_i)^{1/4} \\ &= 0.8040 \quad \text{.....(3-9)} \end{aligned}$$

This is not strictly true. A more accurate statement would be:

$$\begin{aligned} C_{II-N}/C_{III-IV} &= (\overline{Nu}/\overline{Nu}_i)\cdot(GrPr/Gr_iPr_i)^{1/4} \\ &= (k/k_i)\cdot(\nu_i^2\alpha Pr/\nu^2\alpha_i Pr_i)^{1/4} \\ &= 0.7747 \quad \text{.....(3-10)} \end{aligned}$$

Using this new value of the ratio at $\phi = 0$, a least squares fit was attempted for the present experimental results. The new correlating equation became:

$$C_{II-N} = 0.3419 + 0.0220\phi \quad \text{.....(3-11)}$$

Figure 21 shows how the experimental results compared to both Yuill's modified line and to the corrected correlating equation (3-11). The results of the fourteen tests performed in region II-N and a comparison with the new correlating equation are presented in Table 5. The average and root mean square percentage deviations were 0.49% and 5.09%, respectively. Although the new equation did not significantly improve the correlation of the experimental results, it did provide a much better fit at the II-III boundary.

3.5.4 Bidirectional Separated Flow: Region II-S

This region was similar to region II-N in that no easily obtainable analytic solution was possible. Once again, Yuill correlated his data empirically against two controlling parameters, ϕ, the perpendicular distance from the II-III boundary and γ, the angle of rotation about the point $T_p = T_\infty = 4^oC$, measured clockwise from the I-II boundary. The model involved calculating the coefficients for both the inner and outer boundary layers and then combining them in such a way

TABLE 5

Comparison Of Experimental And Empirical
Heat Transfer Results In Region II-N

Test No.	ϕ	C_{II-N} (empirical)	C_{II-N} (experimental)	Error(%)
1	-.0450	.3409	.3497	2.58
8	-.1374	.3389	.3219	-5.02
9	-.1520	.3386	.3074	-9.21
11	-.0057	.3418	.3817	11.67
12	-.1106	.3395	.3438	1.27
13	-.4379	.3323	.3187	-4.09
14	-.4850	.3312	.3396	2.54
15	-.4145	.3328	.3439	3.34
16	-.5412	.3300	.3314	0.42
17	-.3932	.3332	.3425	2.79
18	-.3555	.3341	.3367	0.78
19	-.2626	.3361	.3190	-5.09
20	-.1708	.3381	.3435	1.60
21	-.1496	.3386	.3495	3.22

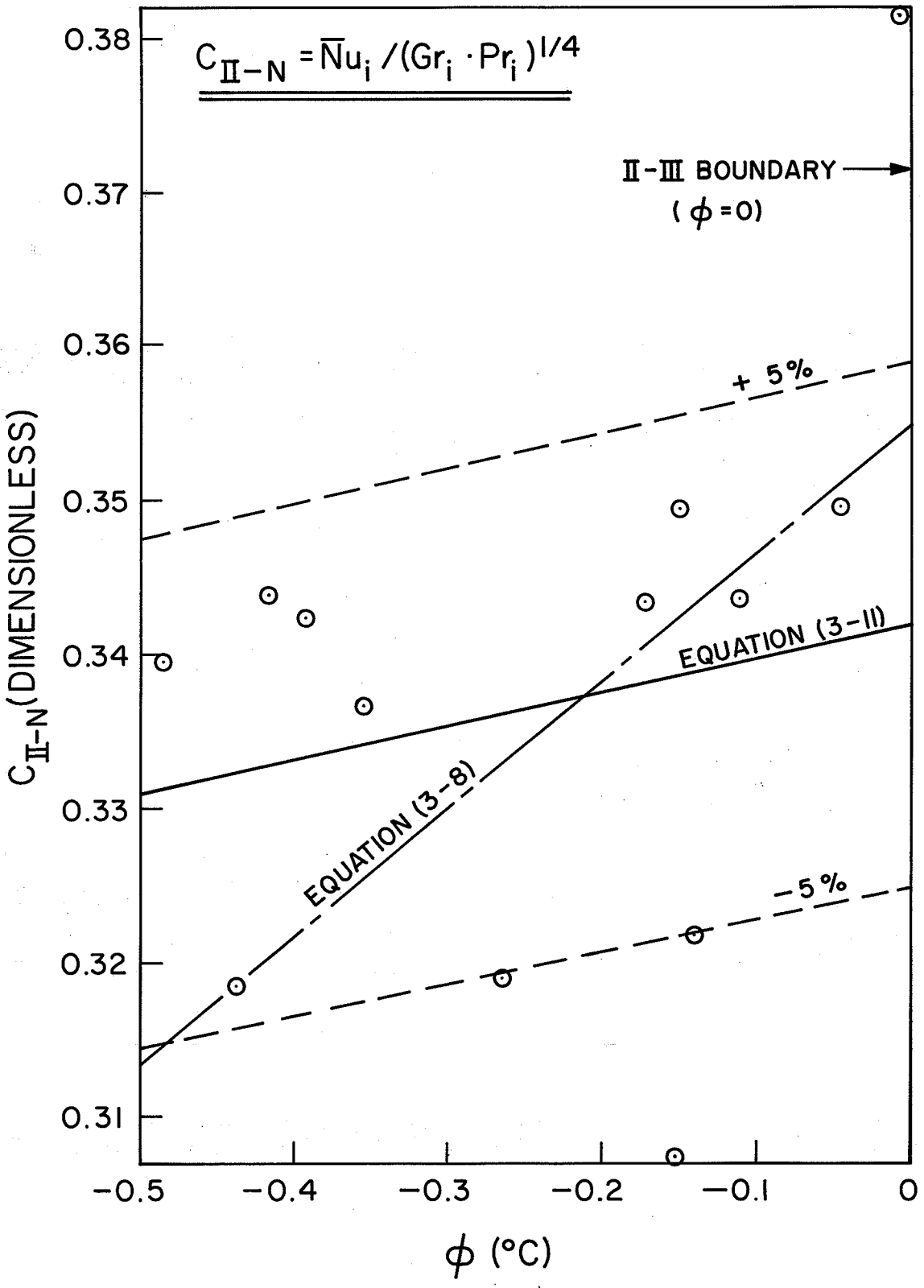

Fig. 21 Coefficient C_{II-N} Versus ϕ in Region II – N

as to predict the local heat flux from the plate.

In the present study, this method of correlation was rejected as being too complicated and as not giving a clear enough physical picture of the dependence of heat flux on the various parameters. In addition, Hasinoff [17] showed that Yuill's correlation in this region required a good deal of refinement. He analyzed his experimental deviations from this correlation and found them to be functions of ϕ and γ, the two correlating variables. As could be seen from the local results (Figure 18a), the local surface heat flux in this region had the same general shape as the curve in the unidirectional downflowing region I. It was therefore assumed that in this region, at least for a horizontal cylinder, the outer downward flowing boundary layer predominated. If this proved to be a correct assumption, then the heat transfer results in this region could be correlated in a similar manner to region II-N, except that the coefficient C_{II-S} would be based on properties of the outer boundary layer.

A least squares fit of the data from the twenty-one tests in this region was attempted. In order for the coefficient C_{II-S} to match the value of C_I at the I-II boundary, where $Z = 0$, the proper constant had to be evaluated for the correlating equation. This was done by calculating the ratio:

TABLE 6

Comparison Of Experimental And Empirical Heat Transfer Results In Region II-S

Test No.	α	Z	C_{II-S} (empirical)	C_{II-S} (experimental)	Error(%)
22	-.02432	-.05257	.4867	.5043	3.62
23	-.02189	-.05014	.4876	.4950	1.52
24	-.02089	-.04914	.4880	.4897	0.35
25	-.02692	-.05517	.4857	.4957	2.06
26	-.02070	-.04895	.4881	.4738	-2.93
27	.00865	-.01960	.4990	.5374	7.70
28	-.02850	-.05675	.4852	.4913	1.26
29	-.01400	-.04225	.4906	.4840	-1.35
30	-.02539	-.05364	.4863	.4668	-4.01
31	-.02263	-.05088	.4873	.4689	-3.78
32	-.02738	-.05563	.4856	.4644	-4.37
33	-.02438	-.05263	.4867	.4809	-1.19
34	-.02286	-.05111	.4873	.4824	-1.01
35	-.03454	-.06279	.4829	.4650	-3.71
36	-.03261	-.06086	.4836	.4727	-2.25
37	-.04080	-.06905	.4806	.4689	-2.43
38	-.03795	-.06620	.4816	.4446	-7.68
39	-.04629	-.07454	.4785	.4957	3.59
40	-.05193	-.08018	.4764	.4960	4.11
41	-.05381	-.08206	.4757	.5102	7.25
42	-.04605	-.07430	.4786	.4925	2.90

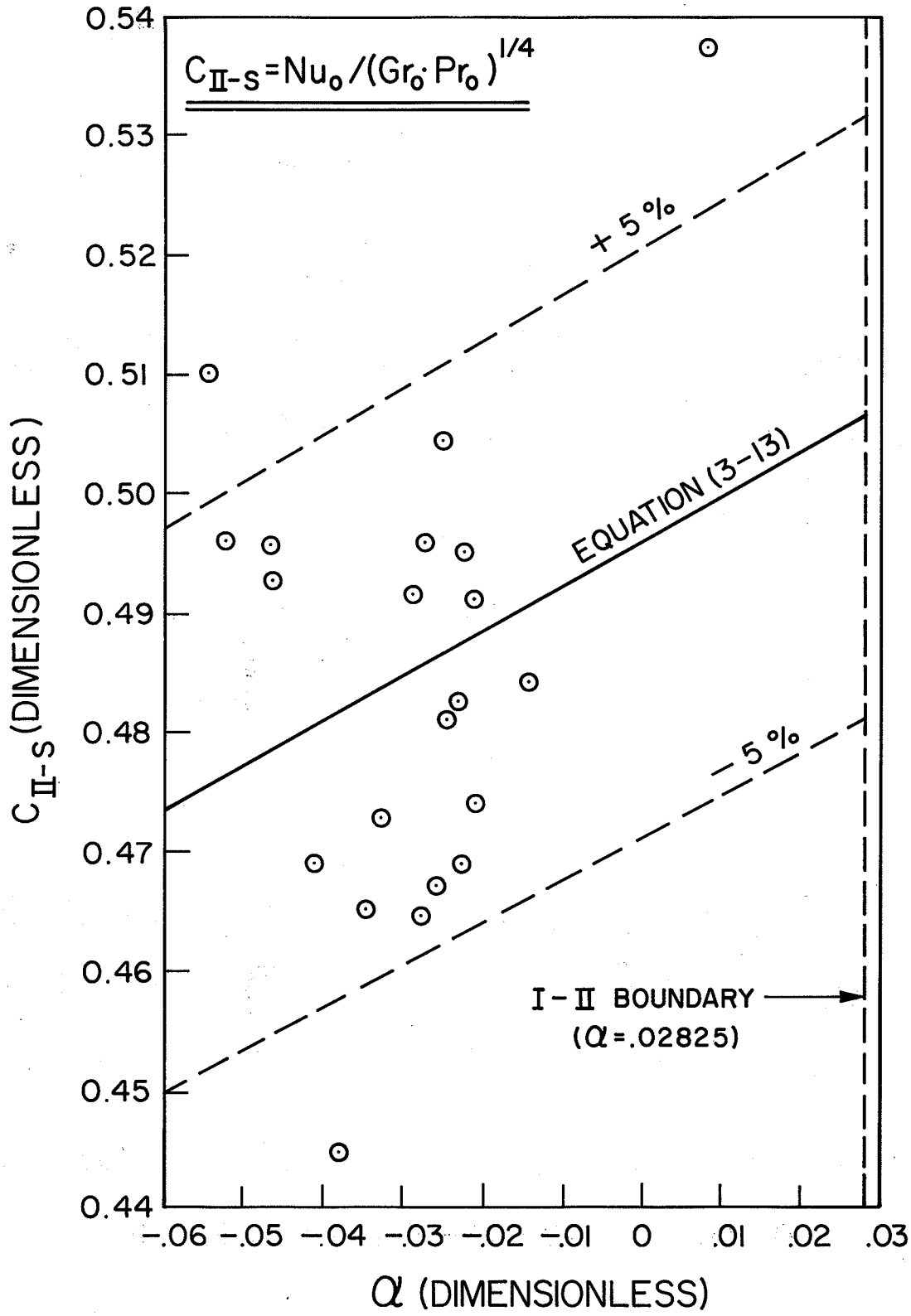

Fig. 22 . Coefficient C_{II-S} Versus α in Region II — S .

$$C_I/C_{II\text{-}S} = (k_o/k)\cdot(\nu^2\alpha_o Pr_o/\nu_o^2\alpha Pr)^{1/4}$$
$$= 1.1622 \quad \ldots\ldots\ldots\ldots\ldots\ldots (3\text{-}12)$$

Knowing the value of C_I at the boundary, from the analysis of the data in region I, the value of $C_{II\text{-}S}$ at the boundary was obtained. The least squares fit of the results then yielded:

$$C_{II\text{-}S} = 0.5063 + 0.3752\ Z \quad \ldots\ldots\ldots\ldots\ldots (3\text{-}13)$$

where again $Z = \alpha - 0.02825$. The plot of this equation and the experimental results are presented in Figure 22. The empirical and experimental results are also tabulated in Table 6. The average error of the data from the predicted values was -0.02% while the root mean square deviation was 3.98%. Although the correlation was quite good, there was little variation in α in the experimental points. In order to obtain a more reliable correlation, more experimental points would be required, both further from and closer to the I-II boundary (i.e. over a wider range of α).

3.6 Comparison of Results With Classical Theory

Although the previous correlations for regions II-N and II-S were valid, they were quite cumbersome since they depended on evaluating properties of the inner and outer boundary

layers, respectively. To gain an understanding of the effect of the density anomaly on the magnitude of the heat transfer results, the mean overall coefficient, C, for the entire boundary layer was computed for all tests and was plotted in Figure 23, versus α, the dimensionless boundary layer buoyancy function which characterized the density anomaly. In regions I and III-IV, the coefficients C_I and C_{III-IV} were identical to the overall coefficient C. In classical theory, the coefficient, C, is taken to be 0.53 while $\alpha = 1/3$.

The variation of α may be described as follows. Along the adiabatic line, $\alpha = 1/3$. Clockwise rotation about the point $T_p = T_\infty = 4^oC$ away from the adiabatic line, decreases the value of α. At approximately the I-II boundary, α becomes zero. In regions II and III, α is negative, decreasing steadily in magnitude towards negative infinity as the bulk temperature nears 4^oC. Above 4^oC, α decreases rapidly from positive infinity to a value of 1/3 at the adiabatic line and also at all points far enough away from $T_\infty = 4^oC$. The discontinuity of α at the point $T_\infty = 4^oC$ made analysis near this point difficult.

Shown in Table 7 are the experimental values of the appropriate heat transfer variables for the test points, as well as theoretical values for four points at a large distance from $T_\infty = 4^oC$. All of the theoretical values were based on a

TABLE 7

Experimental Values Of Nusselt Numbers
Heat Transfer Coefficients And Heat Fluxes

Test No.	Region	α	C	$\overline{Nu}$	$\overline{h}$ ($W/cm^2/^oC$)	θ_p (^oC)	$\dot{q}$ (W/cm^2)
1	II-N	-0.28708	.4453	31.42	.017702	14.37	.2544
2	III	-0.73273	.4203	29.27	.016478	11.59	.1910
3	III	-2.22019	.5041	28.58	.016008	6.94	.1111
4	III	-0.91257	.4453	27.47	.015416	8.89	.1370
5	III	-0.40381	.4482	27.93	.015677	10.44	.1637
6	III	-0.82809	.4243	24.51	.013735	7.93	.1089
7	III	-1.25529	.4258	23.76	.013303	7.05	.0938
8	II-N	-0.25227	.4140	20.19	.011280	7.29	.0822
9	II-N	-0.23250	.3986	16.93	.009443	5.69	.0537
10	III	-0.33832	.3883	16.02	.008927	4.86	.0434
11	II-N	-0.31339	.4769	13.26	.007365	2.27	.0167
12	II-N	-0.19735	.4537	12.79	.007105	2.66	.0189
13	II-N	-0.12382	.4505	17.47	.009735	5.84	.0569
14	II-N	-0.13679	.4738	20.86	.011643	7.23	.0842
15	II-N	-0.18768	.4602	25.36	.014201	10.08	.1431
16	II-N	-0.13796	.4622	21.79	.012170	8.23	.1010
17	II-N	-0.15201	.4702	20.08	.011200	6.57	.0736
18	II-N	-0.13282	.4704	17.13	.009539	5.03	.0480
19	II-N	-0.15926	.4341	15.51	.008634	4.56	.0394
20	II-N	-0.19695	.4541	16.01	.008910	4.15	.0370
21	II-N	-0.19323	.4628	14.88	.008275	3.48	.0288
22	II-S	-0.02432	.4767	17.31	.009640	6.92	.0667
23	II-S	-0.02189	.4728	18.58	.010360	8.24	.0854
24	II-S	-0.02089	.4696	19.05	.010626	8.84	.0939
25	II-S	-0.02692	.4580	19.30	.010769	9.07	.0977
26	II-S	-0.02070	.4554	18.17	.010132	8.58	.0869
27	II-S	0.00865	.6758	20.77	.011569	7.73	.0894
28	II-S	-0.02850	.4519	17.79	.009916	7.86	.0779
29	II-S	-0.01400	.4890	17.27	.009619	7.20	.0693
30	II-S	-0.02539	.4388	15.79	.008794	6.75	.0594
31	II-S	-0.02263	.4488	15.41	.008581	6.30	.0541
32	II-S	-0.02738	.4327	14.80	.008237	6.02	.0496
33	II-S	-0.02438	.4564	15.02	.008359	5.71	.0477
34	II-S	-0.02286	.4628	14.58	.008112	5.31	.0431

TABLE 7 (continued)

Experimental Values Of Nusselt Numbers
Heat Transfer Coefficients And Heat Fluxes

Test No.	Region	α	C	$\overline{Nu}$	$\overline{h}$ ($W/cm^2/^oC$)	θ_p (^oC)	$\dot{q}$ (W/cm^2)
35	II-S	-0.03454	.4183	13.42	.007467	5.05	.0377
36	II-S	-0.03261	.4300	13.18	.007327	4.67	.0342
37	II-S	-0.04080	.4099	12.44	.006919	4.36	.0302
38	II-S	-0.03795	.3946	11.44	.006359	4.05	.0258
39	II-S	-0.04629	.4234	12.15	.006753	3.78	.0255
40	II-S	-0.05193	.4136	11.70	.006500	3.57	.0232
41	II-S	-0.05381	.4226	11.46	.006368	3.26	.0208
42	II-S	-0.04605	.4224	10.67	.005926	2.94	.0174
43	I	0.20430	.5113	21.78	.012035	2.95	.0355
44	I	0.12305	.5164	24.94	.013824	6.16	.0852
45	I	0.15872	.5178	24.27	.013431	4.69	.0630
46	IV	0.45159	.4310	36.67	.020942	7.50	.1571
47	IV	0.37874	.4410	33.81	.019364	4.52	.0798
48	IV	0.34660	.5348	35.80	.020649	1.78	.0368
49	IV	0.34598	.5364	36.12	.020861	1.76	.0367
50	IV	0.35537	.5274	35.60	.020406	2.31	.0471
51	IV	0.36594	.5351	37.26	.021298	2.94	.0626
52	IV	0.35843	.5374	38.85	.022324	2.80	.0625
53	IV	0.37670	.5030	35.27	.020113	3.39	.0682
54	IV	0.39962	.5086	36.21	.020580	4.21	.0866
55	IV	0.43246	.4946	34.30	.019427	4.68	.0909
56	IV	0.50363	.5031	32.65	.018404	4.96	.0913
T1	IV	0.33333	.5300	65.89	.039303	14.00	.5502
T2	IV	0.33333	.5300	59.95	.035539	10.00	.3554
T3	IV	0.33333	.5300	52.22	.030765	6.00	.1846
T4	IV	0.33333	.5300	39.28	.022998	2.00	.0460

T1, T2, T3 and T4 are theoretical points, calculated for

$\alpha = 1/3$, $C = 0.53$ and $T_\infty = 20^oC$.

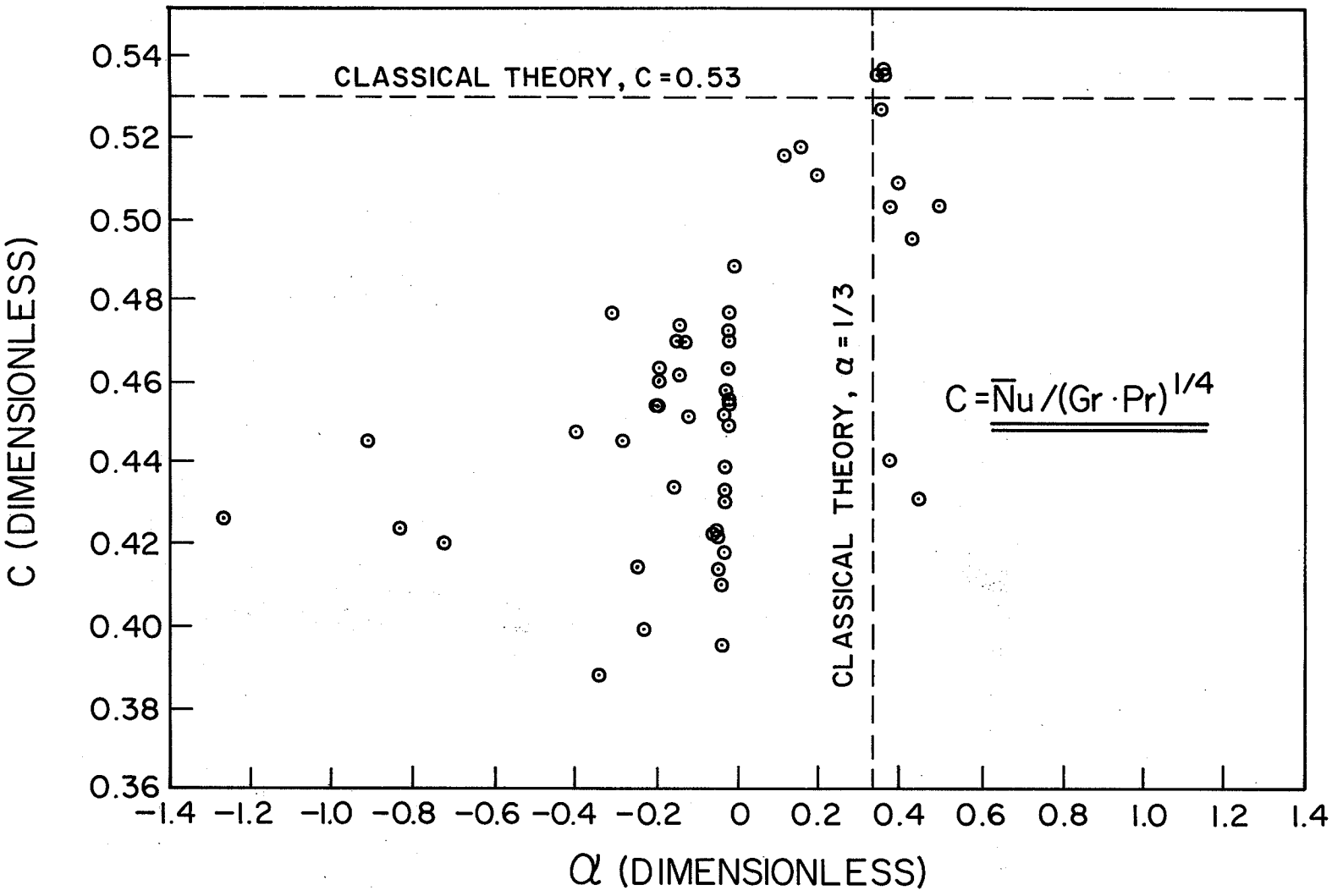

Fig. 23. Overal Coefficient, C Versus Boundary Layer Buoyancy Function, α

bulk water temperature of 20°C. Inspection of this table more clearly demonstrated the relative effect of the density anomaly on the heat transfer results. Comparing the results of test #1, for instance, with the first theoretical point, which had a similar value of θ_p, it was observed that while the values of the overall coefficients differed by only 0.0847 (16.0%), the amount of heat transfer per unit area in the theoretical case was over twice that of test #1. This was due to the fact that the heat transfer rate (i.e. the Nusselt number), depended on the Grashof number as well as the coefficient C and the Grashof number in turn was a function of α. Test #32 showed an even more dramatic decrease, as opposed to the third theoretical point. In this test, the rate of heat transfer was only 27% of what it was for the theoretical case, which was far removed from $T_\infty = 4°C$ and which had an almost equal driving force, θ_p. Finally, the table demonstrated that in region IV, the test results were converging towards the theoretical results for the constant property solution, as would be expected.

CHAPTER 4

SUMMARY AND CONCLUSIONS

In correlating the local values of the heat transfer coefficient, it was found that the results in region I and in regions III and IV agreed remarkably well with Hermann's analytic local distributions (Figure 18). The results in region II were divided into two sub-regions; region II-N, a region of non-separated bidirectional flow in which the inner upward flowing boundary layer seemed to predominate and region II-S, a region of separated bidirectional flow in which the outer downward flowing boundary layer seemed to be of greater importance. The distribution of heat fluxes in these two sub-regions correlated fairly well with the respective analytic solutions for upflow and downflow, although the presence of two opposing flows seemed to increase the rate of heat transfer from the area of the cylinder where the plume of warm fluid left the cylinder to rise or sink in the tank.

With the present experimental setup, it was impossible to determine whether or not separation was actually occurring in region II. As previously mentioned, if one looked purely at the local distribution of heat fluxes, the two sub-regions would appear to correspond more to upflow and downflow than to separated and non-separated bidirectional flow.

In this respect, a flow visualization study would be of great benefit in determining the nature of the flow phenomena in these two regions, as well as in qualitatively showing the reason for the increased heat transfer in the plume, which was also apparent in region II.

Hermann's analytic solution for the average heat transfer from an isothermal horizontal cylinder, which was used to modify Yuill's correlations in regions III and IV, appeared to make the curve of C_{III-IV} level out at a value much smaller than the value that was used by McAdams to correlate the experimental data of several investigators (Figure 20). The experimental results in region IV also tended to agree with McAdams' value of the coefficient (i.e. the deviation of the data from the correlating equation was rather large). It should be noted, however, that Hermann's solution was based on similarity assumptions which were not strictly applicable for the case of the horizontal cylinder. In region I (Figure 19), the correlating equation again predicted lower results than those which were experimentally determined, although since only three tests were performed in this region, no firm conclusions should be drawn.

In region II-N, Yuill's correlation was altered somewhat to give a better fit of C_{II-N} and C_{III-IV} at the II-III boundary. The experimental data seemed to correlate

fairly well with this modified correlation (Figure 21), although again, more tests would have been necessary to confirm its validity. The results in the separated bidirectional region II-S, although they correlated quite well with equation (3-13), were also very closely grouped in terms of the value of α, the correlating variable (Figure 22). A more representative least squares fit would have been possible had the experimental points been picked with a wider range of values of α.

In conclusion, it was shown that Hermann's analytical solution predicted the local variation of heat flux around an isothermal horizontal cylinder very well but this same solution yielded numerical results for the average rate of heat transfer which appeared to be somewhat low in magnitude. Yuill's flat plate correlations for the region around a bulk water temperature of $4^{o}C$ were adequately modified for the horizontal cylinder in the same temperature region and enabled a fairly accurate estimate of the average Nusselt number to be made. More importantly, however, the effect of the variable fluid property relations and the density anomaly on the heat flux from an isothermal horizontal cylinder was quite dramatically demonstrated. Heat transfer rates in the vicinity of a bulk water temperature of $4^{o}C$ may be expected to be as much as three times less than what they would be in

water at a higher temperature or than the rates which would be predicted in this temperature range using classical theory. This result might be of great practical importance in northern latitudes with respect to heat transfer from submerged pipelines or from other underwater bodies of different geometry.

REFERENCES

1. AIHARA, T. and SAITO, E., Measurement of the Free Convection Velocity Field Around the Periphery of a Horizontal Torus, A.S.M.E. Trans., J. of Heat Transfer, 94, 95-98 (1972).

2. CHIANG, T. and KAYE, J., On Laminar Free Convection From a Horizontal Cylinder, Proc. of the Fourth U.S. National Congress of Appl. Mech. (A.S.M.E.), University of California, Berkley, 1213-1219 (1962).

3. CODEGONE, C., Su un punto d'inversione dei moti convetti, Accad. Sci. Torino Atti, 75, 167-171 (1939).

4. DAVIS, A.H., Convection of Heat and Similitude, Philosophical Magazine, 40, 692-703 (1920).

5. DAVIS, A.H., Natural Convective Cooling in Fluids, Philosophical Magazine, 44, 920-940 (1923).

6. DORSEY, N.E., Properties of Pure Water in all its Phases, Hafner, 183-273, (1968).

7. DUMORÉ, J.M., MERK, H.J. and PRINS, J.A., Heat Transfer From Water to Ice by Thermal Convection, Nature, 172, 460-461 (1953).

8. DYER, J.R., Laminar Natural Convection From a Horizontal Cylinder With a Uniform Convective Heat Flux, Mechanical and Chemical Transactions of the Institution of Engineers, Australia, MC1, 125-128 (1965).

9. ECKERT, E.R.G. and DRAKE, R.M., Heat and Mass Transfer, McGraw-Hill, 311-322 (1959).

10. ECKERT, E.R.G. and SOEHGHEN, E., Studies on Heat Transfer in Laminar Free Convection With the Zehnder-Mach Interferometer, U.S.A.F. Technical Report 5747, Wright-Patterson AFB, (1948).

11. EDE, A.J., Heat Transfer by Natural Convection In Refrigerated Liquids, Proc. of the Eighth International Congress of Refrigeration, London, 260-269 (1951).

12. EDE, A.J., The Influence of Melting and Anomalous Expansion on Natural Convection in Water, Applied Scientific Research, A5, 458 (1955).

13. ELENBAAS, W., The Dissipation of Heat by Free Convection From Vertical and Horizontal Cylinders, J. of Applied Physics, 19, 1148-1154 (1948).

14. FAND, R.M. and KESWANI, K.K., Mass Rate of Flow in the Natural Convection Plume Above a Heated Horizontal Cylinder Immersed in a Liquid, A.S.M.E. Trans., J. of Heat Transfer, 95, 192-198 (1973).

15. GENTRY, C.C. and WOLLERSHEIM, D.E., Local Free Convection to Non-Newtonian Fluids From a Horizontal Isothermal Cylinder, A.S.M.E. Trans., J. of Heat Transfer, 96, 3-8 (1974).

16. GOREN, S.L., On Free Convection in Water at 4°C, Chemical Engineering Science, 21, 515-518 (1966).

17. HASINOFF, M.P., Free Convection From a Vertical Plate to Water Near 4°C, M.Sc. Thesis, University of Manitoba (1976).

18. HERMANN, R., Wärmeiibergang bei freier Ströhmung am wagrechten Zylinder in zweiatomigen Gasen, VDI Forschungsheft, 379, 1-24 (1936), translated in NACA TM 1366 (1954).

19. JODLBAUER, K., Das Temperatur-und Geschwindigkeitsfeld um ein geheiztes Rohr bei freier Konvektion, Forschung auf dem Gebiete des Ingenieurwesens, 4, n4, 157-172 (1933).

20. KOH, J.C.Y., Laminar Free Convection From a Horizontal Cylinder With Prescribed Surface Heat Flux, Int. J. of Heat and Mass Transfer, 7, 811-813 (1964).

21. KOH, J.C.Y. and PRICE, J.F., Laminar Convection From a Non-isothermal Cylinder, A.S.M.E. Trans., J. of Heat Transfer, 87, 237-242 (1965).

22. LANGMUIR, I., Convection and Conduction of Heat in Gases, The Physical Review, 34, 401-423 (1912).

23. MADDEN, A.J. and PIRET, E.L., Heat Transfer From Wires to Gases at Sub-atmospheric Pressures Under Natural Convection Conditions, Proc. of the General Discussion on Heat Transfer - London Conference (A.S.M.E.-I.M.E.), 328-333 (1951).

24. McADAMS, W.H., Heat Transmission, McGraw-Hill, 175-180 (1954).

25. MERK, H.J., The Influence of Melting and Anomalous Expansion on the Thermal Convection in Laminar Boundary Layers, Applied Scientific Research, A4, 435-452 (1954).

26. MERK, H.J. and PRINS, J.A., Thermal Convection in Laminar Boundary Layers I, II and III, Applied Scientific Research, A4, 11-24, 195-206, 207-221 (1954).

27. OBORIN, L.A., Special Features of Free Convection in Water at Temperatures Below 277°K, Inzhenerno - Fizicheskii Zhurnal, 13, n6, 837-841 (1967).

28. OSTRACH, S., An Analysis of Laminar Free Convection Flow and Heat Transfer About a Flat Plate Parallel to the Direction of the Generating Body Force, NACA TR 1111 (1953).

29. PETERKA, J.A. and RICHARDSON, P.D., Natural Convection From a Horizontal Cylinder at Moderate Grashof Numbers, Int. J. of Heat and Mass Transfer, 12, 749-752 (1969).

30. POHLHAUSEN, E., Das Temperatur-und Geschwindigkeitsfeld vor einer Wärme abgebenden senkrechter Platte bei natürlicher Konvektion, Tech. Mech. u Thermodynamik 1, n11, 391-406 (1930).

31. POOTS, G., Laminar Free Convection Near the Lower Stagnation Point on an Isothermal Curved Surface, Int. J. of Heat and Mass Transfer, 7, 863-874 (1964).

32. RICE, C.W., Free and Forced Convection of Heat in Gases and Liquids, A.I.E.E. Trans., 42, 653-706 (1923).

33. RICE, C.W., Free Convection of Heat in Gases and Liquids - II, A.I.E.E. Trans., 43, 131-144 (1924).

34. SAVILLE, D.A. and CHURCHILL, S.W., Laminar Free Convection in Boundary Layers Near Horizontal Cylinders and Vertical Axisymmetric Bodies, J. of Fluid Mechanics, 29, 391-399 (1967).

35. SCHECHTER, R.S., Natural Convection Heat Transfer in Regions of Maximum Density, Ph.D. Thesis, University of Minnesota (1956).

36. SCHECHTER, R.S. and ISBIN, H.S., Natural Convection Heat Transfer in Regions of Maximum Fluid Density, J. of the American Institute of Chemical Engineers, 4, 81-89 (1958).

37. SCHENK, J. and SCHENKELS, F.A.M., Thermal Free Convection From an Ice Sphere in Water, Applied Scientific Research, 19, 465-476 (1968).

38. SCHMIDT, E. and BECKMANN, W., Das Temperatur-und Geschwindigkeitsfeld vor einer Wärme abgebenden senkrechter Platte bei natürlicher Konvektion, Tech. Mech. u Thermodynamik, 1, n10, 341-349 (1930).

39. SESONSKE, A., Velocity and Temperature Distributions About a Horizontal Cylinder in Free Convection Heat Transfer, J. of the American Institute of Chemical Engineers, 7, n2, 352-353 (1961).

40. SPARROW, E.M. and GREGG, J.L., The Variable Fluid Problem in Free Convection, A.S.M.E. Trans., 80, 879-886 (1958).

41. TKACHEV, A.G., Heat Exchange in the Freezing and Melting of Ice, AEC-TR-3405, 169-178 (1953).

42. van der HEGGE ZIJNEN, B.G., Modified Correlation Formulae for the Heat Transfer by Natural and by Forced Convection From Horizontal Cylinders, Applied Scientific Research, A6, 129-140 (1956).

43. VANIER, C.R., Free Convection Melting of Ice, M.Sc. Thesis, Syracuse University (1968).

44. VANIER, C.R. and TIEN, C., Further Work on Free Convection in Water at 4°C, Chemical Engineering Science, 22, 1747-1751 (1967).

45. VANIER, C.R. and TIEN, C., Effect of Maximum Density and Melting on Natural Convection Heat Transfer From a Vertical Plate, Chemical Engineering Progress Symposium Series, 64, 240-254 (1968).

46. VANIER, C.R. and TIEN, C., Letter to the Editor, Applied Scientific Research, 21, 387-388 (1969).

47. VANIER, C.R. and TIEN, C., Free Convection Melting of Ice Spheres, J. of the American Institute of Chemical Engineers, 16, 76-82 (1970).

48. YUILL, G.K., Free Convective Heat Transfer From a Vertical Isothermal Plate to Water Near 4°C, Ph.D. Thesis, University of Minnesota (1972).

APPENDIX I

HERMANN'S TRANSFORMATION AND DERIVATION OF AZIMUTH FUNCTIONS $f(\xi)$ AND $g(\xi)$

Hermann began with the standard differential equations:

$$\text{Momentum: } u(\partial u/\partial x) + v(\partial u/\partial y) = \nu(\partial^2 u/\partial y^2) + g\beta\theta\cdot\sin(x/r) \quad \ldots\ldots(I\text{-}1)$$

$$\text{Continuity: } (\partial u/\partial x) + (\partial v/\partial y) = 0 \quad \ldots\ldots(I\text{-}2)$$

$$\text{Energy: } u(\partial\theta/\partial x) + v(\partial\theta/\partial y) = \alpha(\partial^2\theta/\partial y^2) \quad \ldots\ldots(I\text{-}3)$$

Introducing:

$$u = \partial\psi/\partial y \quad \ldots\ldots(I\text{-}4)$$

$$v = -\partial\psi/\partial x \quad \ldots\ldots(I\text{-}5)$$

$$\xi = x/r \quad \ldots\ldots(I\text{-}6)$$

$$\eta = (y/r)\cdot Gr_r^{1/4} \quad \ldots\ldots(I\text{-}7)$$

$$\zeta = (\psi/\nu)\cdot Gr_r^{-1/4} \quad \ldots\ldots(I\text{-}8)$$

$$\tau = \theta/\theta_p \quad \ldots\ldots(I\text{-}9)$$

$$Gr_r = g\beta\theta_p r^3/\nu^2 \quad \ldots\ldots(I\text{-}10)$$

$$\theta = T - T_\infty \quad \ldots\ldots(I\text{-}11)$$

$$\theta_p = T_p - T_\infty \quad \ldots\ldots(I\text{-}12)$$

The differential equations became:

$$\zeta_\eta \cdot \zeta_{\xi\eta} - \zeta_\xi \cdot \zeta_{\eta\eta} - \zeta_{\eta\eta\eta} = \tau \cdot \sin(\xi) \quad \text{.....(I-13)}$$

$$\zeta_\eta \cdot \tau_\xi - \zeta_\xi \cdot \tau_\eta = (1/Pr) \cdot \tau_{\eta\eta} \quad \text{.....(I-14)}$$

where the subscripts indicated differentiation.

Now introducing:

$$q = \eta \cdot g(\xi) \quad \text{.....(I-15)}$$

$$\zeta(\xi,\eta) = p(q) \cdot f(\xi) \quad \text{.....(I-16)}$$

$$\tau(\xi,\eta) = t(q) \quad \text{.....(I-17)}$$

The equations were transformed to:

$$p'^2(f^2gg' + ff'g^2) - pp''(ff'g^2) = p'''(fg^3) + t \cdot \sin(\xi) \quad \text{.....(I-18)}$$

$$(1/Pr)gt'' + f'pt' = 0 \quad \text{.....(I-19)}$$

The independent variables were now ξ and q. The primes on p and t denoted differentiation with respect to q, while the primes on f and g denoted differentiation with respect to ξ. To eliminate ξ from the differential equations, Hermann let:

$$f' = a \cdot g \quad \text{.....(I-20)}$$

$$f^2gg' = b \cdot \sin(\xi) \quad \text{.....(I-21)}$$

$$ff'g^2 = c\cdot\sin(\xi) \quad \text{.....(I-22)}$$

$$fg^3 = d\cdot\sin(\xi) \quad \text{.....(I-23)}$$

where $$g(0) = g_o \quad \text{.....(I-24)}$$

$$f'(0) = a\cdot g_o \quad \text{.....(I-25)}$$

$$f(0) = 0 \quad \text{.....(I-26)}$$

The differential equations then became:

$$(b + c)p'^2 - (c)pp'' = (d)p''' + t \quad \text{.....(I-27)}$$

$$t'' + (a\cdot Pr)pt' = 0 \quad \text{.....(I-28)}$$

Introducing $$F(\xi) = f(\xi)/ag_o \quad \text{.....(I-29)}$$

$$G(\xi) = g(\xi)/g_o \quad \text{.....(I-30)}$$

Equations (I-20), (I-21), (I-22) and (I-23) became:

$$F' = G \quad \text{.....(I-31)}$$

$$F^2GG' = (b/a^2g_o^4)\cdot\sin(\xi) \quad \text{.....(I-32)}$$

$$FF'G^2 = (c/a^2g_o^4)\cdot\sin(\xi) \quad \text{.....(I-33)}$$

$$FG^3 = (d/ag_o^4)\cdot\sin(\xi) \quad \text{.....(I-34)}$$

subject to $$F(0) = 0 \quad \text{.....(I-35)}$$

$$F'(0) = 1 \quad \text{.....(I-36)}$$

$$G(0) = 1 \quad \text{.....(I-37)}$$

By substituting (I-31) into (I-34) and letting d = c/a:

$$F' = G \quad \text{.....(I-38)}$$

$$F^2GG' = (b/a^2g_o{}^4)\cdot\sin(\xi) \quad \text{.....(I-39)}$$

$$FF'G^2 = (c/a^2g_o{}^4)\cdot\sin(\xi) \quad \text{.....(I-40)}$$

which was equivalent to three equations in two unknowns. If the transformations (I-15), (I-16) and (I-17) were valid, then (I-39) and (I-40) would have identical solutions.

$$\text{letting } \varepsilon = b/a^2g_o{}^4 \quad \text{.....(I-41)}$$

$$\gamma = c/a^2g_o{}^4 \quad \text{.....(I-42)}$$

$$\omega = \xi - \pi/2 \quad \text{.....(I-43)}$$

$$\text{then } FF'^3 = \gamma\cdot\cos(\omega) \quad \text{.....(I-44)}$$

$$F^2F'F'' = \varepsilon\cdot\cos(\omega) \quad \text{.....(I-45)}$$

Hermann found that (I-44) and (I-45) did not have identical solutions, but were only approximately equal. Only the solution to (I-44) fit the boundary conditions at $\xi = 0$ (or $\omega = -\pi/2$). Therefore, this solution was used to find G.

$$F(\omega) = 1.504(1+.581\omega-.05626\omega^2-.01412\omega^3 - .00165\omega^4-.00066\omega^5) \quad \text{.....(I-46)}$$

$$G(\omega) = \left[\{1-(\omega^2/2)+(\omega^4/24)-(\omega^6/720) + (\omega^8/40{,}320)\} / F(\omega)\right]^{1/3} \quad \text{.....(I-47)}$$

$$\gamma = 1 \quad \text{.....(I-48)}$$

$$\varepsilon = -1/3 \quad \text{.....(I-49)}$$

Therefore $b = -(1/3)a^2 g_o^4$ .....(I-50)

$$c = a^2 g_o^4 \quad \text{.....(I-51)}$$

$$d = a g_o^4 \quad \text{.....(I-52)}$$

where a and g_o were arbitrary constants. Hermann let:

$$a = 3 \quad \text{.....(I-53)}$$

$$g_o = 3^{-1/4} \quad \text{.....(I-54)}$$

and obtained $b = -1$ .....(I-55)

$$c = 3 \quad \text{.....(I-56)}$$

$$d = 1 \quad \text{.....(I-57)}$$

Finally, the differential equations were transformed to:

$$p''' + 3pp'' - 2p'^2 + t = 0 \quad \text{.....(I-58)}$$

$$t'' + 3Pr \cdot pt' = 0 \quad \text{.....(I-59)}$$

These equations were identical to the ones originally

solved by Pohlhausen for air and by Ostrach for a variety of Prandtl numbers. Ostrach has tabulated p'', p', p, t' and t for various values of η and for several values of the Prandtl number. Substituting (I-53) and (I-54) into (I-29) and (I-30), the azimuth functions were:

$$f(\xi) = 2.280 \cdot F(\xi) \quad \text{.....(I-60)}$$

$$g(\xi) = 0.760 \cdot G(\xi) \quad \text{.....(I-61)}$$

Figure 24 shows the variation of $g(\xi)$ and $f(\xi) \cdot g(\xi)$ with ξ.

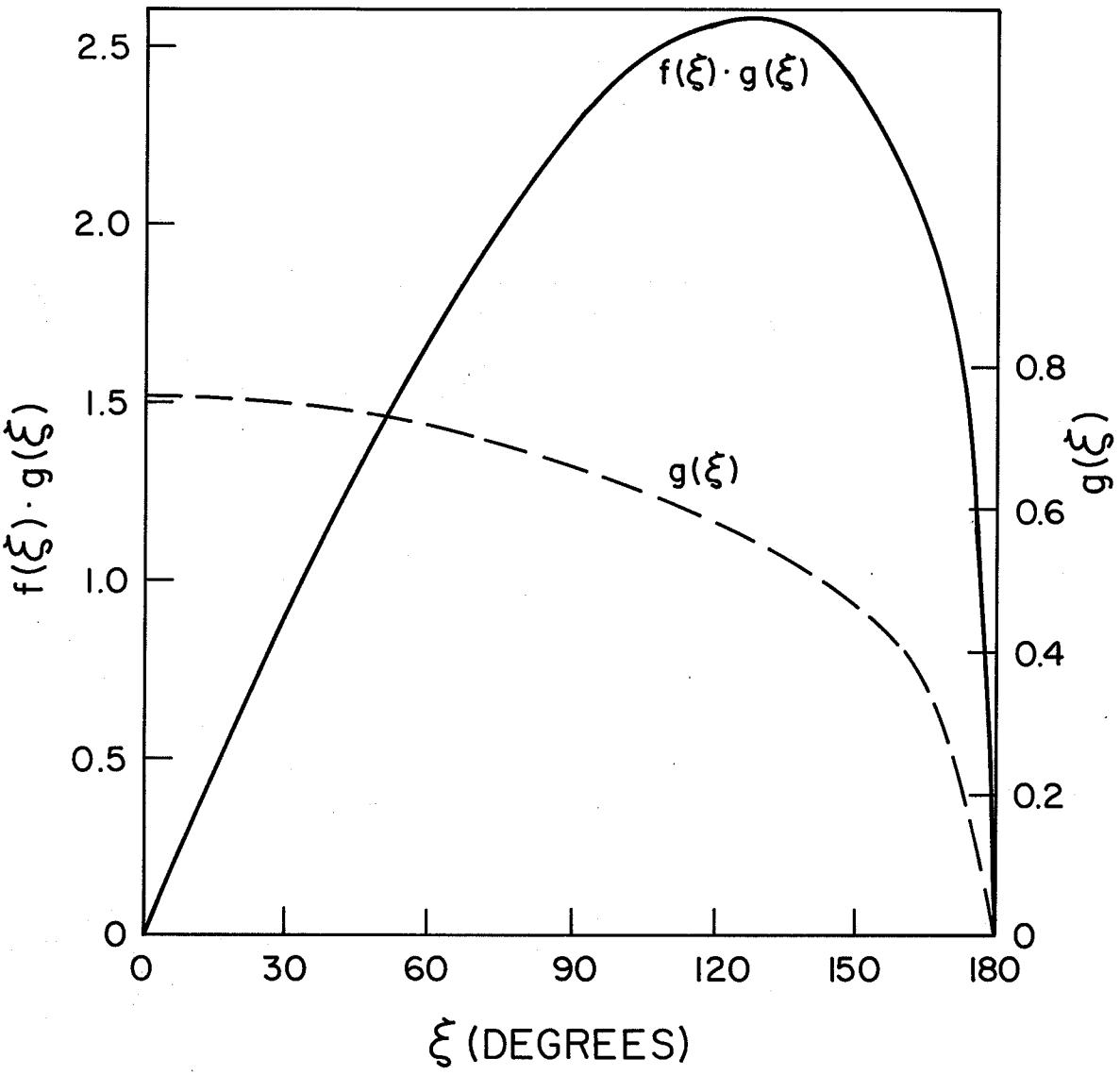

Fig. 24. Hermann's Azimuth Functions, $g(\xi)$ and $f(\xi) \cdot g(\xi)$ Versus Angle ξ.

APPENDIX II

MERK AND PRINS' TRANSFORMATION AND DERIVATION OF AZIMUTH FUNCTION $H(\xi)$

Merk and Prins began with differential equations identical to those employed by Hermann:

$$\text{Momentum: } u(\partial u/\partial x) + v(\partial u/\partial y) = \nu(\partial^2 u/\partial y^2) + g\beta\theta\cdot\sin(x/r) \quad \ldots(II\text{-}1)$$

$$\text{Continuity: } (\partial u/\partial x) + (\partial v/\partial y) = 0 \quad \ldots\ldots\ldots\ldots\ldots\ldots(II\text{-}2)$$

$$\text{Energy: } u(\partial\theta/\partial x) + v(\partial\theta/\partial y) = \alpha(\partial^2\theta/\partial y^2) \quad \ldots\ldots\ldots(II\text{-}3)$$

An integral technique was used, the limits of integration being the extremities of the boundary layer ($0 < y < \delta$), with the result that (II-1) and (II-3) were transformed to:

$$d[\textstyle\int_o^\delta u\cdot dy]/dx = g\beta\theta\cdot\sin(x/r)\cdot\int_o^\delta\theta\cdot dy - \nu(\partial u/\partial y)_{y=0} \quad \ldots\ldots\ldots\ldots(II\text{-}4)$$

$$d[\textstyle\int_o^\delta u\theta\cdot dy]/dx = -\alpha(\partial\theta/\partial y)_{y=0} \quad \ldots\ldots\ldots\ldots(II\text{-}5)$$

Non-dimensional variables were then introduced:

$$\xi = x/r \quad \ldots\ldots\ldots\ldots\ldots\ldots\ldots\ldots\ldots\ldots(II\text{-}6)$$

$$\eta = y/\delta = (y/D)\cdot Gr^{1/4}\cdot G(\xi) \quad \text{.....(II-7)}$$

$$\tau = \theta/\theta_p \quad \text{.....(II-8)}$$

$$u = (\nu/D)\cdot Gr^{1/2}\cdot \zeta(\xi,\eta) \quad \text{.....(II-9)}$$

$$u_1 = (\nu/D)\cdot Gr^{1/2}\cdot F(\xi) \quad \text{.....(II-10)}$$

Substituting (II-6) to (II-10) into (II-4) and (II-5):

$$2\cdot d\left[\int_o^1 (\zeta^2/G)d\eta\right]/d\xi = \sin(\xi)\cdot\int_o^1 (\tau/G)d\eta - G\cdot(\partial\zeta/\partial\eta)_{\eta=0} \quad \text{...(II-11)}$$

$$2\cdot d\left[\int_o^1 (\zeta\tau/G)d\eta\right]/d\xi = -(1/Pr)\cdot G\cdot(\partial\tau/\partial\eta)_{\eta=0} \quad \text{.....(II-12)}$$

Subject to the boundary conditions:

At $\eta = 0$: $\zeta = 0$ .....(II-13)

$\tau = 1$ .....(II-14)

At $\eta = 1$: $\zeta = 0$ .....(II-15)

$\partial\zeta/\partial\eta = 0$ .....(II-16)

$\tau = 0$ .....(II-17)

$\partial\tau/\partial\eta = 0$ .....(II-18)

To satisfy (II-11) and (II-12), subject to the boundary conditions, Merk and Prins defined:

$$\tau = (1-\eta)^2 \quad \text{.....(II-19)}$$

$$\zeta = F(\xi)\cdot\eta(1-\eta)^2 \quad \text{.....(II-20)}$$

Substituting (II-19) and (II-20) into (II-11) and (II-12) and carrying out the integration:

$$(2/105)\cdot d(F^2/G)/d\xi = (1/3)\cdot\sin(\xi)/G - FG \quad \text{.....(II-21)}$$

$$(2/30)\cdot d(F/G)/d\xi = (2/Pr)\cdot G \quad \text{.....(II-22)}$$

Instead of introducing the functions $F(\xi)$ and $G(\xi)$ separately, in such a way as to fulfill the similarity conditions, they introduced the ratio of the two:

$$F/G = [9{,}000/\{Pr^2(Pr+8/7)\}]^{1/4}\cdot H(\xi) \quad \text{...(II-23)}$$

which, when substituted into (II-22), resulted in:

$$G(\xi) = [Pr/30]\cdot[9{,}000/\{Pr^2(Pr+8/7)\}]^{1/4}\cdot H'(\xi) \quad \text{.....(II-24)}$$

where the primes denoted differentiation with respect to ξ. When (II-24) was substituted back into (II-23), an expression for $F(\xi)$ was obtained:

$$F(\xi) = [Pr/30]\cdot[9{,}000/\{Pr^2(Pr+8/7)\}]^{1/2} \cdot H(\xi)\cdot H'(\xi) \quad \text{.....(II-25)}$$

The final step was substituting (II-24) and (II-25) into equation (II-21) which resulted in their obtaining one differential equation in one unknown:

$$H^2H'H'' + MHH'^3 = M\cdot\sin(\xi) \quad \text{.....(II-26)}$$

$$\text{where } M = 2 + (7/4)Pr \quad \text{.....(II-27)}$$

Equation (II-26) was solved by assuming that both $H(\xi)$ and $\sin(\xi)$ were power series:

$$H(\xi) = h_1(\xi + h_3\xi^3 + h_5\xi^5 + \ldots.) \quad \text{.....(II-28)}$$

$$\sin(\xi) = s_1(\xi + s_3\xi^3 + s_5\xi^5 + \ldots.) \quad \text{...(II-29)}$$

$H(\xi)$, its derivatives and $\sin(\xi)$ were now substituted into (II-26) and coefficients of equal powers of ξ equated. This resulted in:

$$h_1 = s_1^{1/4} \quad \text{.....(II-30)}$$

$$h_3 = (M\cdot s_3)/(6 + 10M) \quad \text{.....(II-31)}$$

$$h_5 = [M\cdot s_5 - h_3^2(30+36M)]/[20+16M] \quad \text{....(II-32)}$$

etc.

where $s_1 = 1$ .....(II-33)

$s_3 = -1/6$ .....(II-34)

$s_5 = 1/120$ .....(II-35)

$s_{2n+1} = (-1)^n/(2n+1)!$ .....(II-36)

Since the coefficients, h_i, depended on the Prandtl number, the function H would be more properly written as $H(Pr,\xi)$. $H'(\xi)$ and $H(\xi)\cdot H'(\xi)$ are plotted in Figure 25 for various values of Pr.

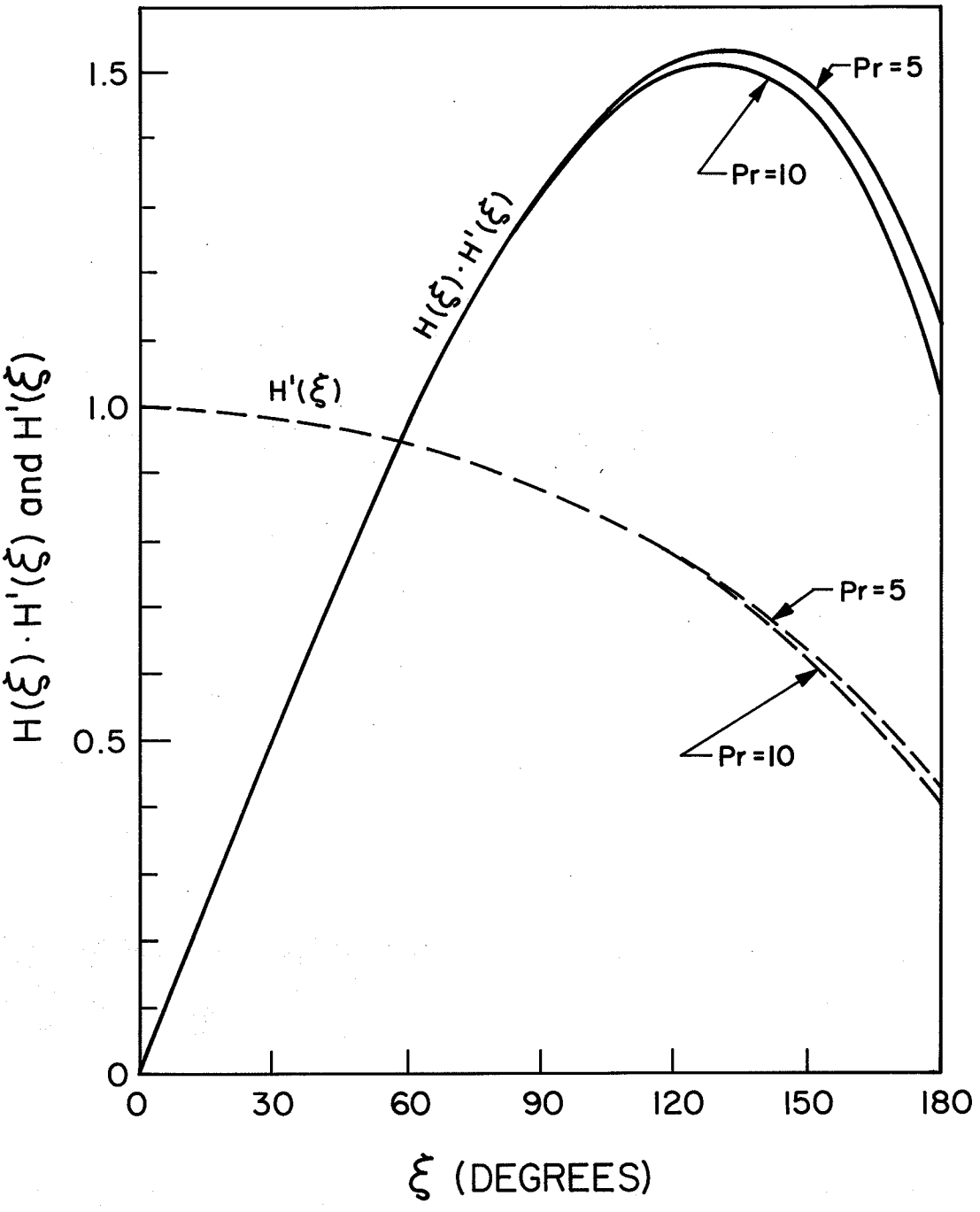

Fig. 25. Merk and Prins' Azimuth Functions, $H'(\xi)$ and $H(\xi)\cdot H'(\xi)$ Versus Angle, ξ

APPENDIX III

PRANDTL NUMBER VARIATION OF HERMANN'S DATA

Hermann's basic heat transfer equations were:

$$Nu(\xi) = -1.189 \cdot g(\xi) \cdot t'(0) \cdot Gr^{1/4} \quad \text{.....(III-1)}$$

$$\overline{Nu} = -0.732 \cdot t'(0) \cdot Gr^{1/4} \quad \text{.....(III-2)}$$

It was assumed that Eckert and Drake's form of the equation for the Nusselt number was correct, i.e.:

$$\overline{Nu} = C \cdot [Pr/(.952+Pr)]^{1/4} \cdot (Gr \cdot Pr)^{1/4} \quad \text{...(III-3)}$$

Equating (III-2) and (III-3):

$$-0.732 \cdot t'(0) = C \cdot [Pr^2/(.952+Pr)]^{1/4} \quad \text{...(III-4)}$$

From which: $$C = -0.732 \cdot t'(0) \cdot [(.952+Pr)/Pr^2]^{1/4} \quad \text{...(III-5)}$$

Hermann's equations were based on a Prandtl number of 0.733 . At this value of Pr, t'(0) = -0.508:

$$\text{Therefore } C = 0.495 \quad \text{.....(III-6)}$$

$$Nu(\xi) = 0.804 \cdot g(\xi) \cdot [Pr/(.952+Pr)]^{1/4} \cdot (Gr \cdot Pr)^{1/4} \quad \text{.....(III-7)}$$

$$\overline{Nu} = 0.495 \cdot [Pr/(.952+Pr)]^{1/4} \cdot (Gr \cdot Pr)^{1/4} \quad \text{.....(III-8)}$$

$$t'(0) = -0.676 \cdot [Pr^2/(.952+Pr)]^{1/4} \quad \text{.....(III-9)}$$

Table 8 compares equation (III-9) with Ostrach's tabulated results for the solution of the differential equations with various values of the Prandtl number. For water, the region of interest is $2 < Pr < 14$. The The agreement between the two is excellent in this Prandtl number range (Figure 26). With the aid of equation (III-9), Hermann's results may be extended to any reasonable Prandtl number.

TABLE 8

COMPARISON OF ANALYTIC AND EMPIRICAL VALUES OF $t'(0)$

	Pr					
	.733	1.0	2.0	10	100	1000
$t'(0)_{Ostrach}$	-0.508	-0.567	-0.717	-1.169	-2.191	-3.966
$t'(0)_{eq'n\ (III-9)}$	-0.508	-0.572	-0.729	-1.175	-2.133	-3.801
Percent error	0.00	+0.85	+1.79	+0.49	-2.65	-4.16

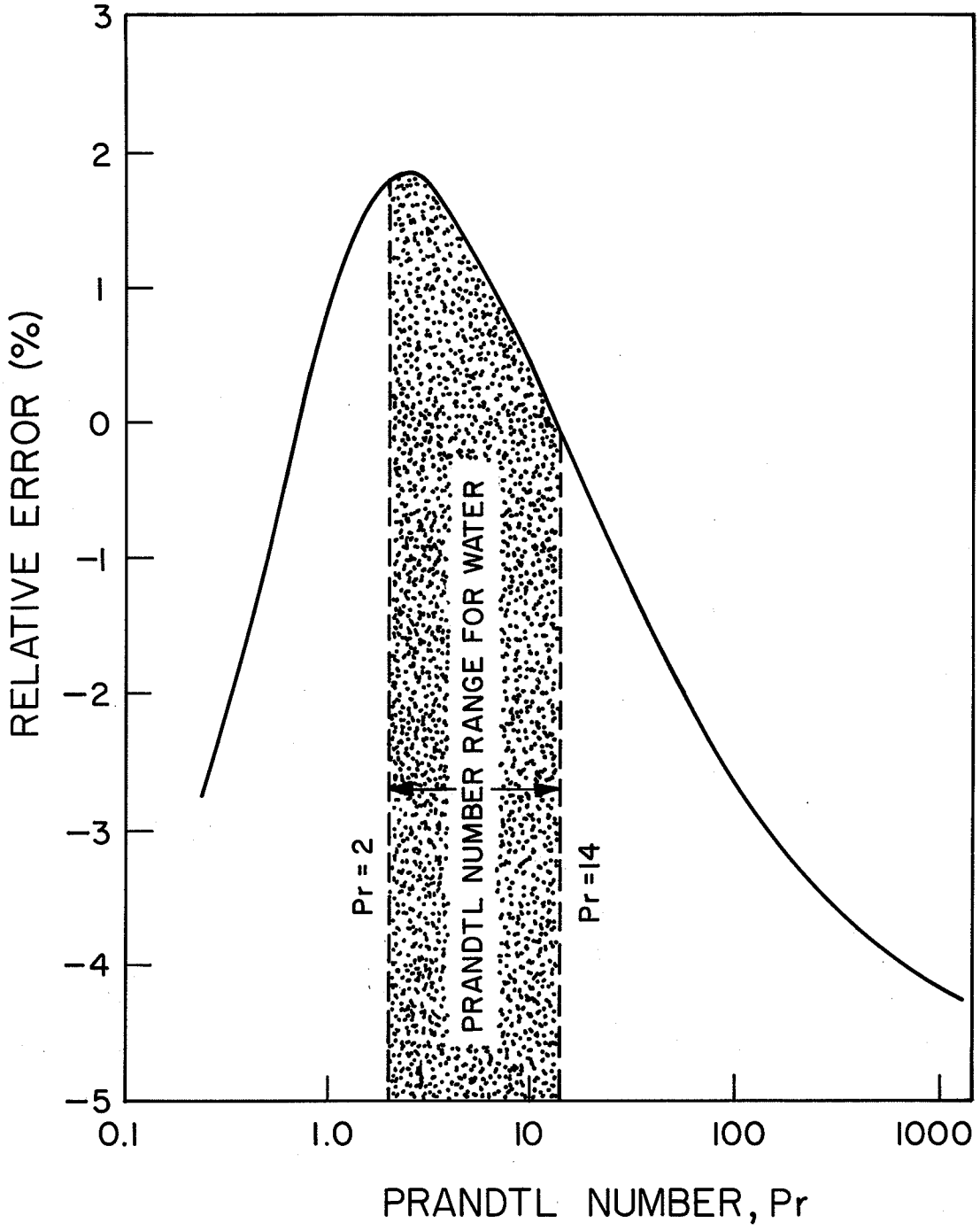

Fig. 26. Error in Using Equation (III−9) to Predict Hermann's Temperature Function at the Surface, $t'(0)$

APPENDIX IV

FLUID PROPERTIES

In this study, four fluid properties were considered to be variable and had to be evaluated as functions of temperature. They were the density ρ, the dynamic viscosity μ, the Prandtl number Pr and the thermal conductivity k.

The variation of density was given by the expression:

$$\rho_o/\rho = 1 + D_1T + D_2T^2 + D_3T^3 \quad \ldots\ldots\ldots\ldots (IV\text{-}1)$$

From Dorsey [6]: ρ_o = density at 0^oC

$= 0.9998676\ gm/cm^3$

Vanier's correlation between 0^oC and 20^oC gave:

$$D_1 = -0.6669167 \times 10^{-4}\ {}^oC^{-1}$$
$$D_2 = \ \ 0.871689 \times 10^{-5}\ {}^oC^{-2}$$
$$D_3 = -0.647664 \times 10^{-7}\ {}^oC^{-3}$$

The standard deviation of the data in this temperature range from equation (IV-1), using the above values of the constants, was 5.4×10^{-7}. For temperatures in excess of 10^oC, Vanier's

correlation of the data between $0^{o}C$ and $35^{o}C$ gave better results:

$$D_1 = -0.6226173 \times 10^{-4}\ {}^{o}C^{-1}$$
$$D_2 = \ 0.807554\ \times 10^{-5}\ {}^{o}C^{-2}$$
$$D_3 = -0.432592\ \times 10^{-7}\ {}^{o}C^{-3}$$

The standard deviation of the data between $0^{o}C$ and $35^{o}C$ from equation (IV-1), using these values of the constants, was 5.7×10^{-5}.

The variation of viscosity was given by the expression:

$$\mu/\mu_o = 1 + V_1T + V_2T^2 + V_3T^3 \ \ldots\ldots\ldots\ldots (IV\text{-}2)$$

From Dorsey's data: μ_o = dynamic viscosity at $0^{o}C$

$= 1.794238 \times 10^{-2}$ gm/cm/sec.

From Yuill's correlation of Dorsey's data between $0^{o}C$ and $37^{o}C$:

$$V_1 = -3.265706 \times 10^{-2}\ {}^{o}C^{-1}$$
$$V_2 = \ 6.698907 \times 10^{-4}\ {}^{o}C^{-2}$$
$$V_3 = -6.425338 \times 10^{-6}\ {}^{o}C^{-3}$$

The standard deviation of μ/μ_o from the tabulated values using the above constants and equation (IV-2) was 1.6×10^{-3}.

The variation of Prandtl number was given by the expression:

$$Pr = P_0 + P_1T + P_2T^2 + P_3T^3 + P_4T^4 \quad .....(IV-3)$$

From Yuill's correlation of Dorsey's data between 0^oC and 37^oC:

$$P_0 = 13.50174$$
$$P_1 = -5.235501 \times 10^{-1}\ {}^oC^{-1}$$
$$P_2 = 1.417347 \times 10^{-2}\ {}^oC^{-2}$$
$$P_3 = -2.439155 \times 10^{-4}\ {}^oC^{-3}$$
$$P_4 = 1.828932 \times 10^{-6}\ {}^oC^{-4}$$

The standard deviation of the Prandtl number data from this equation using the above values of the constants was 1.05×10^{-2}.

Finally, the expression for thermal conductivity was given by Dorsey as:

$$k = [-1390.53 + 15.1937(T_k) - 0.0190398(T_k)^2] \times 4.184 \times 10^{-6} \quad ....(IV-4)$$

where k is in $W/cm/^oC$ and T_k is the absolute temperature in degrees Kelvin (^oK). No estimation of the error in this equation was given but in any event, the variation of thermal conductivity with temperature is very small.

APPENDIX V

DERIVATION OF EXPRESSIONS FOR α, α_i, α_o, T_Σ AND Σ

V-1 Derivation of Expression for α

In conventional analyses, where there are no density maxima or minima, the buoyancy force/unit mass is defined as:

$$B = g\beta\theta_p\tau \quad \text{.....(V-1)}$$

$$\tau = \theta/\theta_p$$

$$= (1 - y/\delta)^2 \quad \text{.....(V-2)}$$

$$= \text{constant}$$

The form of the equation for τ is the one normally used in integral analyses. The mean buoyancy force is given by:

$$\overline{B} = (1/\delta)\int_o^\delta B \cdot dy$$

$$= (1/3)g\beta\theta_p \quad \text{.....(V-3)}$$

The Grashof number is then defined as:

$$Gr = g\beta\theta_p D^3/\nu^2$$

$$= 3\overline{B}D^3/\nu^2 \quad \text{.....(V-4)}$$

For the analysis of water near 4^oC, Yuill [48] has shown that:

$$B = g(\rho_\infty - \rho)/\rho \text{ per unit mass}$$
$$= g\beta_\infty \theta_p (\tau + P\tau^2 + Q\tau^3) \quad \text{.....(V-5)}$$

$$P = [(D_2 + 3D_3 T_\infty)\theta_p / (D_1 + 2D_2 T_\infty + 3D_3 T_\infty^2)] \quad \text{....(V-6)}$$

$$Q = [D_3 \theta_p^2 / (D_1 + 2D_2 T_\infty + 3D_3 T_\infty^2)] \quad \text{.....(V-7)}$$

$$\beta_\infty = [(D_1 + 2D_2 T_\infty + 3D_3 T_\infty^2)/(1 + D_1 T_\infty + D_2 T_\infty^2 + D_3 T_\infty^3)] \quad \text{.....(V-8)}$$

The constants D_1, D_2 and D_3 are defined in Appendix IV.

The mean buoyancy force/unit mass is:

$$\overline{B} = (1/\delta)\int_0^\delta B \cdot dy$$
$$= (1/3 + P/5 + Q/7) g\beta_\infty \theta_p \quad \text{.....(V-9)}$$

Yuill defined the Grashof number as:

$$Gr^* = 3\alpha g \beta_\infty \theta_p D^3 / \nu_f^2 \quad \text{.....(V-10)}$$

But from equation (V-4):

$$Gr^* = 3\overline{B}D^3/\nu_f^2 \quad \text{.....(V-11)}$$

Therefore, the dimensionless boundary layer buoyancy

is defined as:

$$\alpha = 1/3 + P/5 + Q/7 \quad \text{.....(V-12)}$$

which reduces to $\alpha = 1/3$ at a point far enough away from the density maximum.

V-2 Derivation of Expressions for α_i and α_o

In the bidirectional flow region, there will be a point in the boundary layer, Ω, where the density will be the same as that of the bulk fluid. This point marks the division between the inner and outer boundary layers. For the inner boundary layer:

$$\overline{B}_i = (1/\Omega)\int_o^{\Omega} B \cdot dy \quad \text{.....(V-13)}$$

Substituting in (V-2) and (V-5) and integrating:

$$\begin{aligned}\overline{B}_i = g\beta_\infty\theta_p[&(1+P+Q) - (1+2P+3Q)\Sigma \\ &+ (1/3+2P+5Q)\Sigma^2 - (P+5Q)\Sigma^3 \\ &+ (P/5+3Q)\Sigma^4 - (Q)\Sigma^5 + (Q/7)\Sigma^6] \quad \text{.....(V-14)}\end{aligned}$$

$$\Sigma = \Omega/\delta \quad \text{.....(V-15)}$$

If the inner boundary layer Grashof number is defined as:

$$\begin{aligned}Gr_i^* &= 3\overline{B}_i D^3/\nu_{fi}^2 \\ &= 3\alpha_i g\beta_\infty\theta_p D^3/\nu_{fi}^2 \quad \text{.....(V-16)}\end{aligned}$$

$$\text{then } \alpha_i = (1+P+Q) - (1+2P+3Q)\Sigma + (1/3+2P+5Q)\Sigma^2 - (P+5Q)\Sigma^3 + (P/5+3Q)\Sigma^4 - (Q)\Sigma^5 + (Q/7)\Sigma^6 \quad \text{.....(V-17)}$$

The outer boundary layer may be analyzed in a similar manner:

$$\overline{B}_o = [1/(\delta-\Omega)]\int_{\Omega}^{\delta} B \cdot dy = \alpha_o g \beta_\infty \theta_p \quad \text{.....(V-18)}$$

$$Gr_o^* = 3\overline{B}_o D^3/\nu_{fo}^2 = 3\alpha_o g \beta_\infty \theta_p D^3/\nu_{fo}^2 \quad \text{.....(V-19)}$$

$$\alpha_o = [(1/3+P/5+Q/7) - (1+P+Q)\Sigma + (1+2P+3Q)\Sigma^2 - (1/3+2P+5Q)\Sigma^3 + (P+5Q)\Sigma^4 - (P/5+3Q)\Sigma^5 + (Q)\Sigma^6 - (Q/7)\Sigma^7]/(1-\Sigma) \quad \text{.....(V-20)}$$

V-3 Derivation of Expressions for T_Σ and Σ

Rearranging equation (V-5):

$$\rho_\infty - \rho = \rho g \beta_\infty \theta_p (\tau + P\tau^2 + Q\tau^3) \quad \text{.....(V-21)}$$

At a point in the boundary layer, Ω, the densities are

the same and the left hand side of (V-21) becomes zero. Therefore, assuming that equation (V-2) describes the temperature distribution in the boundary layer and knowing that $\tau = 0$ only at the outside of the boundary layer then equation (V-21) can be simplified to:

$$1 + P\tau_{\Sigma} + Q\tau_{\Sigma}^{2} = 0 \quad \text{.....(V-22)}$$

$$\tau_{\Sigma} = [-P - (P^2 - 4Q)^{1/2}]/2Q \quad \text{.....(V-23)}$$

$$T_{\Sigma} = \theta_p \tau_{\Sigma} + T_{\infty} \quad \text{.....(V-24)}$$

The film temperatures of the inner and outer boundary layers are given by:

$$T_{fi} = 0.5(T_p + T_{\Sigma}) \quad \text{.....(V-25)}$$

$$T_{fo} = 0.5(T_{\Sigma} + T_{\infty}) \quad \text{.....(V-26)}$$

Substituting (V-2) and (V-15) into (V-23) and rearranging:

$$\Sigma = 1 - (\tau_{\Sigma})^{1/2}$$

$$= 1 - [(-P - (P^2 - 4Q)^{1/2})/2Q]^{1/2} \quad \text{....(V-27)}$$

All of the above derivations follow the work of Yuill [48].

APPENDIX VI

DETAILS OF CYLINDER

The results of the experimental work depended a great deal on an accurate knowledge of the cylinder diameter, since it was an integral part of both the Grashof and Nusselt numbers. Vernier calipers were used to measure the diameter of the main test section at six different places around the circumference. The average value of the diameter obtained in this manner was 10.254 cm. (4.037 in.). The results are tabulated in Table 9.

TABLE 9

DIAMETER MEASUREMENTS

Reading Taken Between Heaters #	Diameter (cm)
1 & 7	10.254
2 & 8	10.251
3 & 9	10.262
4 & 10	10.249
5 & 11	10.249
6 & 12	10.257

$\overline{D}$ = 10.254 cm.

The most important quality of the assembled test section was that it be as near to being perfectly round as was possible. Surface height profiles were taken around the circumference of the main test section in three places, the centerline and the two ends of the test section. The profiles were performed with a dial guage which was capable of measuring to the nearest .0013 cm. (.0005 in.). The purpose of these profiles was to indicate high or low spots around the periphery of the cylinder, which indeed they did. After hand finishing and polishing the test section, a final set of profiles was taken. The results, which are presented in Figure 27, indicated that the cylinder was round to within .020 cm. (.008 in.).

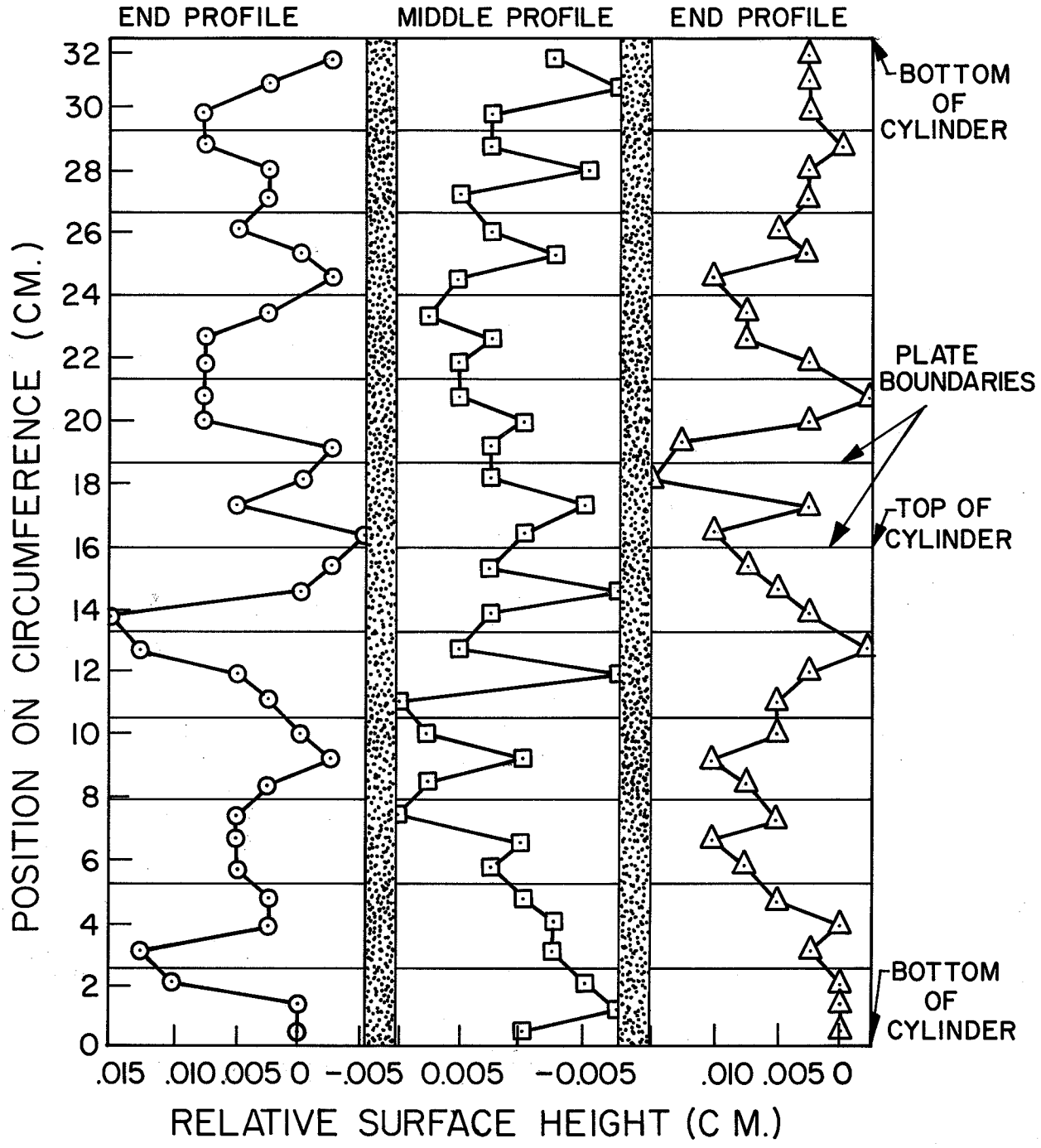

Fig. 27. SURFACE PROFILES ON CYLINDER

APPENDIX VII

BOUNDARY DEFINITIONS

The boundaries between the flow regions were defined by Yuill [48]. A description of the division points for a bulk water temperature of $0^{o}C$, as well as the physical reasons for the differing types of flow, were given in section 1.2. The convergence of the boundaries to the point $T_p = T_\infty = 4^{o}C$ is intuitive, while the symmetrical relationship of the density of water around the point $4^{o}C$ explains why the boundaries are more or less straight lines (i.e. the Ia-Ib boundary occurs when the densities of the water at the cylinder surface and at the outer edge of the boundary layer are the same. This happens at $8^{o}C$ and $0^{o}C$, at $7^{o}C$ and $1^{o}C$, at $6^{o}C$ and $2^{o}C$, etcetera). With the above arguments in mind, the boundaries may be mathematically described as follows:

Adiabatic line : $T_p = T_\infty$ .....(VII-1)

Ia-Ib boundary : $T_p = 8.0 - T_\infty$ .....(VII-2)

I-II boundary : $T_p = 12.4 - 2.1(T_\infty)$ .....(VII-3)

II-III boundary: $T_p = 26.8 - 5.7(T_\infty)$ .....(VII-4)

III-IV boundary: $T_\infty = 4.0$ .....(VII-5)

When the data in region II was analyzed, it was ap-

parent that Yuill's location of the boundary between regions II-N and II-S, the non-separated and separated bidirectional flow regions, at $\phi = -0.6$ did not fit the present data. His location of this border was chosen to fit his data and could not be positively identified with the amount of data that he collected. In any event, the curvature of the cylinrical surface would probably have influenced the position of this boundary. As can be seen in Table 10, the data of the present experiment divided into two groups according to the value of Σ, the dimensionless division point between upflow and downflow in the boundary layer. That is to say, the points in region II-N all had values of Σ above .3430 while the points in region II-S all had values of Σ below .2832. Hence, a value of $\Sigma = .31$ which was midway between these two values of Σ was chosen as the boundary to fit the data of the present experiment.

TABLE 10

Experimental Values of Σ in Region II

Test	Region	Σ	Test	Region	Σ	Test	Region	Σ
1	II-N	.4457	22	II-S	.2555	36	II-S	.2631
8	II-N	.4222	23	II-S	.2536	37	II-S	.2712
9	II-N	.4105	24	II-S	.2527	38	II-S	.2682
11	II-N	.4460	25	II-S	.2594	39	II-S	.2763
12	II-N	.3884	26	II-S	.2524	40	II-S	.2816
13	II-N	.3430	27	II-S	.2176	41	II-S	.2832
14	II-N	.3534	28	II-S	.2605	42	II-S	.2756
15	II-N	.3890	29	II-S	.2443			
16	II-N	.3550	30	II-S	.2566			
17	II-N	.3633	31	II-S	.2534			
18	II-N	.3489	32	II-S	.2583			
19	II-N	.3665	33	II-S	.2550			
20	II-N	.3894	34	II-S	.2532			
21	II-N	.3866	35	II-S	.2653			

The boundary between these two regions was then described by:

II-N - II-S boundary: $T_p = 17.1 - 3.3(T_\infty)$ .....(VII-6)

The boundaries were also described by the values of other variables which have already been defined:

Adiabatic line: $\theta_p = 0^oC$ .....(VII-7)

Ia-Ib boundary: $\Sigma = 0$ .....(VII-8)

I-II boundary: $\alpha \simeq 0.02825$.....(VII-9)

II-N - II-S boundary: $\Sigma \simeq 0.31$ .....(VII-10)

II-III boundary: $\phi = 0^oC$ .....(VII-11)

III-IV boundary: $T_\infty = 4^oC$ .....(VII-12)

APPENDIX VIII

ERROR ANALYSIS

The sources of error discussed in the succeeding sections were divided basically into two parts, extraneous heat losses from the heated surfaces and errors in the values of the measured or calculated variables.

VIII-1 Heat Losses

There were three alternate paths of heat flow from the heated surfaces other than by free convection. They were conduction from the side surface to the paraffin wax and guard heaters, conduction from the rear surface to the plexiglass tubing and fiberglass insulation and finally, conduction through heater leads, voltage taps and thermocouples.

The side losses through the paraffin wax were given by:

$$\dot{Q}_{side} = -kA\Delta T/L \quad \text{.....(VIII-1)}$$

where k = thermal conductivity of paraffin wax

$= 0.001$ W/cm/^{o}C

A = cross-sectional area of paraffin gap

$= 0.142$ cm^2

ΔT = maximum temperature imbalance across gap

$= 0.10$ ^{o}C

L = length of paraffin gap

= 0.145 cm.

The maximum loss was 9.79×10^{-5} W on each side or a total of 1.958×10^{-4} W. The test with the minimum heater power was test #42 which had one heater with a power of 0.345 W. Therefore, the maximum percentage side loss was 0.06%.

The back losses were approximated by assuming that the heat flowing out of the rear surfaces of the heaters then flowed axially along the plexiglass tubing and fiberglass insulation. The problem then became one of one dimensional conduction in concentric cylinders which is described by:

$$\dot{Q}_{back} = -(k_1A_1 + k_2A_2)\theta_p/L \quad \text{.....(VIII-2)}$$

where k_1 = thermal conductivity of plexiglass

$= 1.869 \times 10^{-3}$ W/cm/^{o}C

k_2 = thermal conductivity of fiberglass

$= 0.346 \times 10^{-3}$ W/cm/^{o}C

A_1 = cross-sectional area of plexiglass

$= 1.583$ cm^2

A_2 = cross-sectional area of fiberglass

$= 5.173$ cm^2

L = tubing length in which temperature drop occurs

= 10.16 cm.

For test #1 (θ_p = 14.37°C), $\dot{Q}_{back}$ = 0.007 W. Since heat flows axially from both ends of each heater, the total loss would be twice this amount or 0.014 W. The percentage losses for the different heaters of this test varied from a minimum of 0.15% to a maximum of 0.25%. For test #49 (θ_p = 1.76°C), $\dot{Q}_{back}$ = 0.002 W. The percentage errors ranged from a low of 0.17% to a high of 0.33%. These two tests represented the maximum and minimum temperature differences, θ_p.

The wire losses consisted of three separate items. The heater leads both lost heat by conduction and gained heat by Joule heating. It was desired to design the apparatus so that the leads would be the correct length to balance both of the above processes and leave the temperature gradient in the leads equal to zero at the point where they were connected to the heaters. The formula for the correct lead length was:

$$L = (2k\theta_p/S)^{1/2} \quad \text{.....(VIII-3)}$$

where k = thermal conductivity of copper leads
= 3.893 W/cm/°C

θ_p = maximum expected temperature difference
= 26.8 °C

S = maximum internal heat generation rate of the leads based on a heater power of 25 W.
= 2.131 W/cm^3

The calculated optimum lead length was 9.9 cm. However, the length of the apparatus necessitated a minimum lead length of 25 cm. Therefore, there was a positive temperature gradient in the heater leads at the heaters (i.e. the heaters were gaining heat from the heater leads). The heat gain was given by:

$$\dot{Q}_{leads} = (SAL/2) - (kA\theta_p/L) \quad \text{.....(VIII-4)}$$

where A = cross-sectional area of heater leads
$= 3.243 \times 10^{-3}$ cm^2
L = heater lead length
= 25 cm.

For a temperature difference of 26.8^{o}C and a heater power of 25 W, this gain turned out to be 0.073 W. The total heat gain was twice this amount, or 0.146 W, since each heater had two leads attached to it. The loss in the voltage tap leads was given by:

$$\dot{Q}_{V.T.} = -kA\theta_p/L \quad \text{.....(VIII-5)}$$

where k = 3.893 W/cm/^{o}C
$A = 3.243 \times 10^{-3}$ cm^2
$\theta_p = 26.8^{o}$C
L = 25 cm.

This loss was 0.014 W for each voltage tap or 0.028 W for each heater. The losses in the thermocouples were given by:

$$\dot{Q}_{T/C} = -(k_1+k_2)A\theta_p/L \quad \text{.....(VIII-6)}$$

where k_1 = thermal conductivity of copper wire

= 3.893 W/cm/^{o}C

k_2 = thermal conductivity of constantan

= 0.214 W/cm/^{o}C

A = cross-sectional area of thermocouples

= 5.067×10^{-4} cm^2

L = length of thermocouples in cylinder

= 25 cm.

The loss in each thermocouple worked out to be 0.002 W. Each main heater used in the calculations had two thermocouples mounted on its surface (in fact, some had three). Therefore, the total thermocouple loss was 0.004 W. The total wire heat gain was:

$$\dot{Q}_{wire} = \dot{Q}_{leads} + \dot{Q}_{V.T.} + \dot{Q}_{T/C}$$

$$= 0.146 - 0.028 - 0.004$$

$$= 0.114 \text{ W} \quad \text{.....(VIII-7)}$$

Assuming the same heater power as that used to calculate S

(25 W), the percentage gain was 0.46%. This percentage would be relatively constant for other heater powers since all three components of the total loss depended on the heater power and consequently on the temperature difference, θ_p.

VIII-2 Measurement Errors

The current in each circuit was calculated using a standard resistor of known resistance. These resistors were not calibrated before use in the present experimental work. The tolerance listed by the manufacturer was 1% of the stated resistance and was believed to be a fairly reliable estimate of error since these resistors exceeded military specification MIL-R-18546 which is the specification for housed chassis-mounted power resistors.

The resistance change due to heat buildup was neglected for two reasons. First, all tests were conducted far below the rated power of 50 W. For instance, the highest average power through the standard resistor, which occurred in test #1, was 1.653 W or 3.31% of the rated load while the minimum average power (test #11) was 0.109 W or 0.22% of the rated load. Second, the standard resistors were immersed in a constant temperature mineral oil bath to insure that heat did not build up in the resistors housings.

The voltages were measured on a Keithley model 160 digital multimeter which had a claimed accuracy of ±0.1% of full scale or one unit, whichever was the greater. The lowest

readings taken in any one voltage range were about 18% of full scale. The maximum error would therefore be expected to be in the range of 0.56%.

The surface temperatures used in all of the calculations were actually averages of the experimental data and hence, were subject to a certain degree of error. Table 11 shows the deviations from isothermal conditions of each of the fifty-six tests conducted. The average root mean square percentage deviation of the temperature data was 1.54%. The measurements of the bulk water temperature were more accurate. The three thermopiles usually agreed to within $0.01^{o}C$, which would translate into an error between 0.06% and 0.93%. In most tests, the water temperature was between 2 and $3^{o}C$, giving an error in the order of 0.33% to 0.50%.

The thermocouple wire was not calibrated before beginning the experimental work. Yuill [48] had calibrated his wire and found that it agreed almost exactly with the tabulated values for copper-constantan wire published by the U.S.National Bureau of Standards. Therefore, his voltage-temperature relationship was used in the present work. It was:

$$T = [0.00832 + 46.90503(e/1000) - 1.314565(e/1000)^{2} + 0.001818864(e/1000)^{3}]/1.8 \quad \text{.....(VIII-8)}$$

TABLE 11

Deviations From An Isothermal Cylinder

Test No.	Region	Bulk Temp. (°C)	Surface Temp. (°C)	Temp. Diff. (°C)	Max. Error (°C)	Max. Error (%)	R.M.S. Error (%)
1	II-N	1.82	16.18	14.37	0.71	4.92	2.85
2	III	2.98	14.56	11.59	-0.64	-5.51	2.16
3	III	3.74	10.68	6.94	-0.27	-3.88	2.02
4	III	3.32	12.21	8.89	-0.26	-2.90	1.57
5	III	2.65	13.09	10.44	-0.25	-2.36	1.25
6	III	3.35	11.28	7.93	-0.26	-3.23	1.64
7	III	3.58	10.62	7.05	0.21	2.98	1.42
8	II-N	2.79	10.08	7.29	-0.13	-1.78	0.96
9	II-N	3.02	8.71	5.69	-0.12	-2.10	1.23
10	III	3.29	8.16	4.86	0.09	1.89	1.23
11	II-N	3.66	5.93	2.27	-0.08	-3.68	1.76
12	II-N	3.51	6.17	2.66	-0.07	-2.74	1.50
13	II-N	2.75	8.59	5.84	0.14	2.44	0.86
14	II-N	2.50	9.73	7.23	-0.12	-1.65	0.97
15	II-N	2.14	12.21	10.08	-0.23	-2.31	0.99
16	II-N	2.30	10.54	8.23	0.33	3.97	1.70
17	II-N	2.68	9.25	6.57	0.21	3.27	1.37
18	II-N	2.94	7.98	5.03	0.09	1.82	0.99
19	II-N	3.09	7.65	4.56	-0.18	-3.98	2.41
20	II-N	3.23	7.38	4.15	0.09	2.06	0.96
21	II-N	3.35	6.83	3.48	-0.06	-1.60	0.86
22	II-S	2.10	9.02	6.92	0.14	2.06	0.87
23	II-S	1.73	9.97	8.24	0.22	2.71	1.09
24	II-S	1.56	10.40	8.84	0.40	4.49	2.26
25	II-S	1.54	10.61	9.07	-0.23	-2.55	1.32
26	II-S	1.63	10.21	8.58	0.18	2.06	0.82
27	II-S	1.66	9.39	7.73	0.33	4.24	1.68
28	II-S	1.87	9.73	7.86	0.13	1.70	1.14

TABLE 11 (continued)

Deviations From an Isothermal Cylinder

Test No.	Region	Bulk Temp. (°C)	Surface Temp. (°C)	Temp. Diff. (°C)	Max. Error (°C)	Max. Error (%)	R.M.S. Error (%)
29	II-S	1.97	9.16	7.20	-0.10	-1.42	0.69
30	II-S	2.15	8.90	6.75	0.12	1.80	1.04
31	II-S	2.26	8.56	6.30	0.11	1.76	0.79
32	II-S	2.36	8.38	6.02	0.11	1.81	0.83
33	II-S	2.43	8.14	5.71	0.10	1.79	1.23
34	II-S	2.53	7.84	5.31	-0.09	-1.77	1.13
35	II-S	2.65	7.70	5.05	0.07	1.44	0.79
36	II-S	2.74	7.41	4.67	0.09	2.01	1.07
37	II-S	2.85	7.21	4.36	0.07	1.62	0.69
38	II-S	2.92	6.97	4.05	0.09	2.22	0.99
39	II-S	3.02	6.80	3.78	0.07	1.87	0.79
40	II-S	3.09	6.66	3.57	-0.05	-1.32	0.84
41	II-S	3.17	6.43	3.26	-0.04	-1.38	0.92
42	II-S	3.23	6.18	2.94	-0.04	-1.31	1.02
43	I	1.69	4.64	2.95	-0.16	-5.32	4.07
44	I	1.07	7.24	6.16	-0.21	-3.43	2.27
45	I	1.31	5.99	4.69	-0.10	-2.06	1.28
46	IV	9.58	17.08	7.50	-0.51	-6.80	4.93
47	IV	12.20	16.32	4.12	-0.19	-4.58	2.43
48	IV	15.79	17.57	1.78	0.08	4.57	2.25
49	IV	16.18	17.94	1.76	0.08	4.38	2.84
50	IV	13.42	15.73	2.31	0.12	5.27	2.60
51	IV	12.20	15.14	2.94	0.09	3.00	2.04
52	IV	13.97	16.77	2.80	0.12	4.10	2.14
53	IV	11.17	14.56	3.39	0.12	3.47	1.77
54	IV	9.71	13.92	4.21	-0.09	-2.15	1.43
55	IV	8.33	13.01	4.68	0.13	2.79	1.92
56	IV	6.73	11.69	4.96	0.16	3.24	1.81

where T = temperature (^{o}C)

e = thermocouple voltage (μV)

The National Bureau of Standards stated that all commercial thermocouple wire sent in to be tested agreed to within ±2.5% of these values. This figure would seem to represent the order of magnitude of error in the thermocouple calibration.

The final possible source of error in temperature was through the copper surface itself. The thermocouples actually measured the temperature on the back side of the copper plates. The temperature change through the thickness of copper is given by:

$$\Delta T = -h\theta_p L/k \quad \text{.....(VIII-9)}$$

where h = surface conductance ($W/cm^2/^{o}C$)

θ_p = temperature difference, $T_p - T_\infty$, (^{o}C)

L = thickness of copper plate

= 0.056 cm.

k = thermal conductivity of copper

= 3.893 $W/cm/^{o}C$

The maximum surface conductance measured was in test #1, where h = 0.021124 $W/cm^2/^{o}C$ and where θ_p = 14.37^{o}C, Therefore, the maximum temperature difference across the copper

was -0.004°C and the maximum percentage error was 0.02%.

The only other physical property which was measured was the diameter of the cylinder, D. From an inspection of Table 9 (Appendix VI), the root mean square deviation of the six measurements taken was 0.005 cm. or roughly 0.05%. The last source of error was in the equations for the fluid properties given by Yuill [48] and by Dorsey [6]. These errors, however, were extremely small and insignificant when compared to others, most notably the error due to the deviation from isothermal conditions and from the National Bureau of Standards thermocouple correlation.

In conclusion, a detailed error analysis was not performed because the associated measureable experimental errors were much smaller than the deviation of the average heat transfer results from the correlations. The greater part of these errors were attributed to random phenomena such as vibrations from the fan motor, convective air currents on the free surface produced by the fan itself or convective currents set up in the water, all of which were undetectable and impossible to measure quantitatively.